In search of the phosphorus legacy: merging hydrological and biogeochemical approaches to understand phosphorus dynamics in streams.

A DISSERTATION

SUBMITTED TO THE FACULTY OF THE

UNIVERSITY OF MINNESOTA

BY

Ethan David Pawlowski

IN PARTIAL FULFILLMENT OF THE REQUIREMENTS

FOR THE DEGREE OF

DOCTOR OF PHILOSOPHY

Advised by Dr. Diana L. Karwan

September 2022

Acknowledgements

This thesis has been a long road and I could not have completed it without all of the funding I received during graduate school. I would like to thank my advisor, Dr. Diana Karwan for helping me navigate and balancing graduate school, parenting, and a pandemic while still moving forward with my research. I know that I struggle at times with letting things go (especially my writing) so I have greatly appreciated your patience and also your encouragement to just let go. You have been a great advisor and mentor! I would also like to thank my committee members, Drs Randy Kolka, Stephen Sebestyen, and Jacques Finlay. I appreciate all of your insights and willingness to help me throughout my time in graduate school. I have learned a lot from all of you! Over the years I have had the pleasure of working with amazing collaborators and members of our lab group. Thank you Faith, James, Sarah, Audrey, Hannah, Mark, Tatem, Nicole, Kevin, Hudson, and Ryan. You all helped in big and small ways! I would like to also thank Lucy and Zac for the thought provoking discussions and advice over the years. A big thank you also needs to go out to my brother Zach. Without your image wizardry a workable thesis would not have been possible!

I would like to acknowledge the friends that I have made while attending the University of Minnesota. Although not directly involved, I do not think I could have completed this thesis without your friendship and the balance you provided. Thank you!

I would also like to thank my family especially my children. You each brighten and enrich every day I get to spend with you. I have been in graduate school for your entire lives and I look forward to entering this next phase of my life with you. This thesis and my degree would have never reached completion without the love and support of my wife. Thank you for sticking it out all of this time! I cannot even put into words how lucky I have been to have you with me throughout this process. I look forward to seeing where life takes us next! Finally I would like to thank and dedicate this thesis to God for without whom this thesis would not have been possible. Thank you for my path and helping me find you again.

Abstract

Nutrient and sediment pollution of surface waters remains a critical challenge for improving water quality. Phosphorus and sediment export to lakes and rivers has resulted in diminished water quality placing drinking water supplies, human health, recreation opportunities, and aquatic ecosystems at risk. Understanding both biogeochemical processing and transport of phosphorus and fine sediments (a major sorbent of phosphorus) in stream channels is required to understand the legacy effects of agricultural land management decisions and the effects of mitigation strategies. I focused my thesis on sediment and phosphorus dynamics in Midwestern USA watersheds by examining three parts: (1) using the Nutrient Tracking Tool (NTT) with physical site characteristics to target areas for revegetation, and to compare this field-scale tool with watershed export data; (2) a combination of tracer experiments with transient-storage modeling and biogeochemical assessment to understand phosphorus and sediment dynamics at base flow within Plum Creek, WI; and (3) the inventory and assessment of fallout radionuclides as a potential sediment fingerprint in the upper Midwest.

To assess potential load reductions using revegetation, the nutrient tracking tool (NTT) was used with a scoring system to identify areas where vegetation mitigation could be implemented within three selected Fox River, WI sub-watersheds. A corn-soybean rotation, an implementation of a 10-m vegetated buffer, a full forest conversion, and tiling were modeled and assessed. The corn-soybean results were aggregated and compared to watershed level

gauge data in two sub-watersheds. Edge of field data was compared to modeled results using multiple parameterization schemes. The agricultural areas that scored higher and were untiled showed greater potential nutrient and sediment export reduction when vegetation mitigation was implemented in the model. Aggregated watershed results showed disparities between modeled and measured phosphorus exports but modeled sediment export fell within observed gauge data ranges. Field specific parameter adjustments resulted in more accurate modeled results compared to measured edge of field data, but needed further refinement. Targeted mitigation using vegetation based on the scoring system was shown to be a helpful tool for nutrient and sediment reductions when modeled. Using a field scale model aggregated to the watershed scale presents tradeoffs regarding processes found beyond the edge of field.

To understand in-channel processes, a fluorescent fine particle surrogate, bromide, and phosphate were injected and sampled under base flow conditions within two stream reaches that are representative of the lower and upper Plum Creek, WI, watershed. Grab samples were analyzed and breakthrough curves were modeled utilizing the one-dimensional transport with inflow and storage (OTIS) model. Sediment and stream water samples were analyzed for equilibrium phosphate concentration determination to gain a better understanding of phosphorus dynamics and the potential time lags associated with phosphorus delivery from agricultural fields to downstream water bodies when used in conjunction with transport parameters determined by OTIS. Results indicate

sediments within Plum Creek have a large potential to sorb dissolved phosphorus entering the stream channel and reduce dissolved loads at the individual reach scale. These results suggest a large potential for discrepancies between mitigation implementation and noticeable water quality improvements when considering base flow transport and storage metrics.

Fallout radionuclides beryllium-7 and lead-210 were measured at the St. Paul Weather Station, MN and at the Marcell Experimental Forest by collecting bulk deposition. Event-based sampling was completed in St. Paul whereas weekly sampling was done at the Marcell Experimental Forest in order to compare results with data from the National Atmospheric Deposition Program. Results showed that neither beryllium-7 nor lead-210 were correlated with precipitation inputs, but showed seasonal patterns with peak deposition occurring during the summer months. Beryllium-7 was weakly correlated with precipitation at the Marcell Experimental Forest and showed some correlation with sulfate and chloride deposition but the correlation was not strong enough that either sulfate or chloride could be used as a predictor of beryllium-7 deposition. Cumulative deposition followed a linear trend and could be useful for predicting deposition or filling data gaps in areas with scant depositional records or in remote settings.

Table of Contents

List of Tables

List of Figures

Chapter 1: Introduction

Water quality issues are on the rise throughout the world and in particular from the threat of hypoxia and the proliferation of algal blooms that often produce toxins that make freshwater unfit for recreation and consumption (Dodds et al., 2009; Selman et al., 2008). This issue is of particular importance in the Laurentian Great Lakes in the Midwestern United States where 35 million people rely on its water for drinking (Michigan Report 2019) which is in conflict with a region where agriculture is a multi-billion dollar industry (Dodds et al., 2009). The proclivity of agricultural producers to over fertilize over decades has led to a challenging dynamic where nutrients and sediment transported to large relatively dilute Great Lakes results in large harmful algal blooms. Even when nutrients are reduced, the long term nutrient buildup or “legacy” stores from historic management can influence downstream waterbodies for decades (Inamdar et al., 2020; Andrew Sharpley et al., 2013).

Sediment and fine sediment (clay and silt-sized particles) in particular play an important environmental role, especially in the phosphorus cycle. Charged particle surfaces are capable of binding heavy metals, nutrients, and other pollutants that can negatively affect downstream water bodies when environmental conditions stimulate the release of pollutants (Civan et al., 2018; Lü et al., 2016; Naden, 2010; Tye et al., 2004, 2016). Binding to sediment surfaces can also play an important ecosystem service that can promote water quality by acting as a net sink for those metals, pollutants, and nutrients

(Boedecker et al., 2020). The interplay between fine sediment and phosphorus changes from field to stream and upon final delivery to large fresh- or saltwater environments due to the changes in background water chemistry that promotes chemical and biotic changes along different transport pathways. Although this issue has been ongoing for decades, many processes that effect this interplay between phosphorus and sediment remain poorly understood

I address knowledge gaps surrounding in-stream phosphorus distribution by focusing on phosphorus movement through streams and rivers in two phases – dissolved and on the surface of fine sediment. The components are designed to inform watershed-wide water quality management strategies by investigating processes at stream reach and watershed scales. Following this introductory chapter, I divided my dissertation into three additional chapters that **(1)** based on existing datasets and a field scale model, highlight areas where conservation practice implementation will reduce sediment and phosphorus delivery at the regional scale. I then zoom in to stream scale processes; through a series of experiments I **(2)** measure and model phosphorus and fine particle transport and storage within a representative Midwestern agricultural stream; and **(3)** develop an understanding of a tool used to trace fine sediment by investigating climate patterns that affect the wet deposition of naturally occurring fallout radionuclides.

For chapter one I utilized existing datasets and a field scale model to identify key areas where conservation practice implementation may reduce sediment and phosphorus delivery to streams. Conserving and restoring natural

vegetation are common and well-studied conservation practices that enhance and/or restore water quality (Asbjornsen et al., 2014; Dodd & Sharpley, 2016; Kovacic et al., 2006; Schulte et al., 2017). To get a landscape, level view, I used a scoring system to identify areas in row crop agriculture within the Fox River Basin, WI that could benefit from targeted revegetation efforts to reduce harmful algal blooms (Keller & Fox, 2019). Scores were assigned to 10-m grid cells based on slope and hydrologic soil group; the hydrologic soil group describes a soils infiltration capacity or rate of water transmission. Grid cells that had both high slopes and poor infiltration were classified as high priority; mid-priority areas were classified as having either a high slope or poorly draining soil; and a low priority areas had low slopes and good drainage characteristics. Grid cells that were spatially adjacent were aggregated into “fields” and subsequently modeled to assess potential water quality benefits predicted with reforestation (Chapter 2). The modeled scenarios were a corn soybean rotation, the addition of a 10-m vegetated buffer (barrier between fields and streams), and a conversion to a red pine plantation. Fields that had tile drainage were also included and incorporated in the scenarios. Cumulative aggregated field results for two watersheds were compared with two watershed outlet gauge datasets and individual modeled field scale results were contrasted with available water quality data.

Phosphorus export was underestimated by one to two orders of magnitude but sediment export was the same order of magnitude as measured watershed scale data. On an individual basis, the model could be further

adjusted to specific cropping systems and likely improve phosphorus export results. The NTT underestimated surface and subsurface discharge for the individual field which lowered nutrient and sediment export estimates below what were measured. However, when a longer training period was used similar to the watershed scale and high priority area export analysis, nutrient and sediment export were closer to measured values. The NTT results of high priority areas showed significant export reductions following targeted reforestation without tile drainage compared common row-crop agricultural management. These results show that land managers can use simple physical characteristics to target revegetation efforts and user friendly models can successfully reproduce export reductions. The results also provide a useful contribution to work comparing models and datasets to different spatial scales. However, the underestimation of phosphorus export elucidates a missing process related to phosphorus transport and storage in the watersheds.

Stream channel phosphorus transport and storage processes may be the missing piece behind the watershed scale exports and the aggregated field export for the watersheds. Inorganic phosphorus is transported either in a dissolved form or associated with sediment (Dolph et al., 2019; Withers & Jarvie, 2008). Fine sediment in particular, clay- and silt-sized particles, act as reactive sticky traps capable of catching dissolved phosphorus and transporting further downstream depending on environmental conditions (Withers & Jarvie, 2008). Those conditions change between the active flowing stream channel and areas

of delayed transport or transient-storage zones. In-stream fine sediment transport and storage is a critical piece to understanding phosphorus delivery and understudied in the glaciated landscapes of the upper Midwest (Boano et al., 2014). Even rarer are studies assessing both fine particles and phosphorus transport dynamics in stream channels (Boano et al., 2014; Minshall et al., 2000; Newbold et al., 1983).

In chapter three I measured and modeled phosphorus and fine particle transport and storage within a Midwestern agricultural stream to address disparities between field scale export and watershed scale export data by examining channel processes. I accomplish this by conducting a series of experiments whereby I introduced a series of tracers including: a fine sediment surrogate (fluorescent clay-sized pigment), a non-reactive dissolved salt, and dissolved phosphorus into Plum Creek, WI, a tributary of the Lower Fox River. These tracers and the sampling design effectively captured the various ways phosphorus is transported and stored within the stream channel. Plum Creek drains a typical agricultural Midwestern landscape but the sediment export is composed of a high percentage of fine sediment (Fitzpatrick et al., 2019) which is a shared feature of other Environmental Protection Agency (EPA) priority watersheds (drainage areas that export excess nutrients and sediment to waterbodies with targeted mitigation). Basic transport and storage questions related to phosphorus transport upon entering stream channels were answered through the experimentation and modeling. To compliment the tracer tests, a

biogeochemical method was employed that utilized sediment from the tracer experiment reaches; the equilibrium phosphorus concentrations (EPC_0) and related metrics of a variety of sediment were determined throughout the Plum Creek drainage area. The EPC_0 measurement is indicative of the likelihood a sediment will release phosphorus to the water column or if it will act like a sponge and remove it from the water.

The results provided specific information relating hydrologic, sediment, and phosphorus transport dynamics to address basic knowledge gaps (Boano et al., 2014) and relate to the chapter 2 result disparities. Base flow advection of all tracers was slow during every tracer test; to travel 10-km under similar stream conditions as the tracer tests were completed in would take non-reactive solutes 25 to 72 d in the downstream reach and 1.5 y in the upstream reach and even longer for particles and phosphorus. Loss from the water column to storage zones for both particles and phosphorus was observed and apparent in the modeling efforts despite high model parameter uncertainties. This is in agreement with the biogeochemical results which indicate the sediments in the stream have a high capacity for removing phosphorus from the water column. This removal mechanism likely mitigates and stores high concentrations phosphorus within the stream channel eroded or leached into the stream channel from upland sources. When paired with high water column phosphorus concentrations, the channel phosphorus storage and the observed advective transport timescales suggest the channel represents a massive phosphorus

reservoir in this system. This further explains the dissimilarity between the NTT modeled results when aggregated to a watershed scale and the measured watershed scale export estimates at USGS stream gages. Without accounting for the channel storage, aggregating the field exports only explains the continued phosphorus and sediment supply to the channel and not the built up storage within the channel.

Channel storage represents a missing storage reservoir that bridges the disconnect between field scale mitigation and modeling efforts with watershed scale export datasets and mitigation goals. This phosphorus loading and storage presents challenges for land managers that need to continue promoting sediment and SRP retention on agricultural fields to mitigate the effects of downstream transport of SRP and SRP laden sediment to Green Bay in Lake Michigan. By understanding the capacity of sediment to release phosphorus, land managers will be able to understand what happens in the stream channel and what mechanisms may delay water quality improvements despite successful sediment and phosphorus reductions through mitigation at the field scale. In-stream storage results from the tracer experiment provided insight on the possible processes changing phosphorus forms in stream networks from a hydrodynamic perspective and the NTT modeling efforts show that field scale modeling is a useful tool for implementing mitigation measures at that scale but need to be used together to effectively reduce nutrient and sediment loads. These techniques and pairing will enable managers to target areas within the stream

and/or on the farm fields for phosphorus reduction practices, as well as anticipate a long lag time required for the benefits of field mitigation techniques to be measurable downstream.

By better understanding fine sediment and phosphorus dynamics, the broader goal of chapters 2 and 3 is to help protect aquatic environments from the large nutrient imbalances that negatively affect water quality and aquatic environments in the Great Lakes Region. Although my results look at a small piece of this highly complex issue, I hope that they will help propel the science forward and eventually lead to water quality improvements for future generations.

Chapter 4 is related to these water quality challenges but deviates from understanding watershed, reach, and field scale processes and focuses on developing an understanding of a fine sediment tracer for use in the upper Midwest. The transport of fine sediment essential to understanding phosphorus dynamics in streams (Kleinman et al., 2011; Reid et al., 2018) but is understudied in stream channels (Boano et al., 2014). In the absence of a surrogate tracer, fine sediment transport is often tracked using chemical tracers (Collins et al., 2017; Owens et al., 2016; Walling, 2005). Beryllium-7 and excess lead-210 are two fallout radionuclides or atoms undergoing radioactive decay deposited from the atmosphere to the land surface that easily attach to sediment surfaces and may be transported along with the sediment. Each radionuclide has a different decay rate that allows for the determination of sediment ages and provides a means of possible sediment source identification to and within stream

channels. This enables land managers to determine if a sediment source is surface erosion (“younger”) or resurfaced after deeper burial (“older”). Relative aging helps to pinpoint sediment sources and relevant mitigation strategies to reduce sediment and sediment bound phosphorus exported to waterbodies (Collins et al., 2017; Walling, 2005). The decay rates of beryllium-7 and lead-210 allow for sediment source discrimination at an event (rainstorm) timescale but the beryllium-7 decay rate minimizes the number of samples that can be analyzed before the decay becomes undetectable. This has resulted in a scarcity of depositional data, especially in the upper Midwest and other mid-continental climate locations. In chapter 4 I examined 4 years of deposition patterns to gain a better understanding and build a bulk depositional dataset for these two fallout radionuclides in Minnesota. I found that peak deposition occurs during the summer in Minnesota for both radionuclides and that cumulative deposition is largely linear, but the linear pattern is shifted seasonally. Beryllium-7 deposition often showed an inverse relationship with lead-210 deposition and neither radionuclide showed strong correlation with precipitation inputs. By understanding deposition rates and patterns, the utility of fallout radionuclides as sediment tracers may be expanded and reduce the need to sample deposition. A better understanding of deposition patterns will enhance fallout radionuclides as a tool to further environmental phosphorus understanding.

As a whole, I focused my thesis on nutrient and sediment transport while using and developing a variety of tools and datasets to understand this

challenging problem. I first used a field scale model to assess if vegetation mitigate sediment and nutrient export on areas of high slope and poor infiltration capacity. These results and the model parameters were checked against measured field scale exports and then aggregated modeled results are checked against measured watershed scale exports. Field scale modeling could be further improved, but watershed wide aggregation showed that phosphorus loads observed at watershed outlets far exceed the modeled inputs from agricultural fields. After conducting reach scale tracer and biogeochemical tests, the channel was found to be a large phosphorus reservoir for the studied system and explained the differences between modeled exports and observed exports. I then focused on understanding fallout radionuclide deposition patterns to help further develop this sediment fingerprinting tool for use in the upper Midwest. My results show that sediment and phosphorus transport and storage is a complex issue and one that will be present for a long time into the future, but my research provides a basis to propel future research on this topic.

Chapter 2: Assessing nutrient and sediment load reduction potential of vegetation at the field and watershed scale in a Great Lakes Priority Watershed

1.0 Introduction

Soil and water degradation from agriculture remains an important concern for sustainable agriculture and global food security. This degradation has a negative impact on crop yields and poses concerns to communities beyond the field. Continued intensification and reliance on chemicals to meet demand places stress on the health and availability of soil and water resources (Tilman et al., 2002, 2011). Chemical fertilizer use paired with common agricultural practices have created large nutrient imbalances in agricultural soils that can be transported from the field in soluble and particulate forms to downstream waterbodies (Alexander et al., 2008; Thompson et al., 2011). Eutrophication caused from the excess delivery of phosphorus (P), nitrogen (N), and sediment loads are particularly detrimental to aquatic ecosystem health, drinking water supplies, and outdoor recreation. These eutrophic areas are expected to increase globally and throughout the Great Lakes (Dodds et al., 2009; Selman et al., 2008).

Revegetation provides an effective mitigation strategy to reduce non-point source nutrient and sediment loads from agricultural areas (Keller & Fox, 2019; Powers et al., 2012; Reddy et al., 1999a; Schulte et al., 2017). Revegetation in

this work is defined as the process of replanting and rebuilding the soil in disturbed sites. Additional vegetation promotes increasing biodiversity both above and below the soil surface along with the accumulation of organic matter which aids in aggregate and macropore formation. These features improve water infiltration rates and storage that reduce nutrient and sediment loads stemming from overland flow. The soil aggregates are less likely to erode and increases in nutrient use efficiency by an intact network of plant, microbial, and mycelium further retain nutrients and sediment within agricultural fields (Rubin & Görres, 2021; Schulte et al., 2017; Tilman et al., 2002). The key to obtaining these benefits is through strategic and targeted implementation that utilize physical characteristics of individual fields such as contours, soil erodibility, areas of marginal production, and drainage characteristics to efficiently place vegetation to intercept sediment and nutrients (Asbjornsen et al., 2014; Carstensen et al., 2020; Jiang et al., 2020; Lenhart et al., 2018; Prosser et al., 2020; Schilling & Jacobson, 2014; Schulte et al., 2017). These benefits are achievable through the incorporation of a wide range of different vegetative species (Prosser et al., 2020); to narrow this scope I focus on native forest and prairie plant communities but other vegetative management is considered later in the discussion. There are added benefits to using native plant communities besides reducing sediment and nutrient erosion; the Science-based Trials with Row-crops Integrated with Prairie Strips (STRIPS) experiment in Iowa showed that using native prairie communities had significantly greater benefits to native insect, pollinator, and bird

species abundance than non-native species planted with less biodiversity such as in some cover cropping systems (Schulte et al., 2017). Even with using native species, a targeted approach that matches physical site characteristics with plant species that will thrive in those conditions is pivotal for successful sediment and nutrient reduction (Prosser et al., 2020). A major caveat to using native vegetation is the acreage for crop production is reduced. However, studies have shown that even modest land conversions of 10% have significantly greater benefits on water quality and soil health with further increases in biodiversity following native perennial vegetation establishment (Schulte et al., 2017). Thus, the assessment and identification of areas where the conservation of, or land conversion to, native vegetation is important for water quality management (Dodds et al., 2009; Selman et al., 2008).

Utilizing physical characteristics is pivotal to identifying areas for revegetation of native plant communities. Using the landscape slope and hydrologic drainage class provides a critical first step in identifying areas at high risk of nutrient and sediment loss under traditional row cropping rotations. Hydrologic drainage class divides soils into four main groups (A, B, C, and D) based on runoff potential and infiltration capacity. Landscape slope and hydrologic drainage class form the basis for the USDA Soil Vulnerability Index (SVI; Lohani et al., 2020) and the GIS-based Agricultural Conservation Policy Framework (ACPF; Porter et al., 2016), two tools that were designed to identify areas susceptible to nutrient and sediment losses in agricultural settings. The

SVI additionally incorporates the soil erodibility K-factor using coarse fragment and organic carbon percentage which improved the index site differentiability in areas with heterogeneous slopes and soils but are less important than slope and hydrologic drainage class in areas with greater homogeneity (Lohani et al., 2020). The ACPF identifies areas of probable overland flow using hydrologic routing (based on soils and slopes) and notes that proper validation of the slope and drainage characteristics are vital to proper on-site mitigation planning (Porter et al., 2016). Beyond these tools designed to target mitigation areas, common models that predict nutrient and sediment export often rely on the curve number approach (Neitsch et al., 2002; Texas A&M AgriLife Research, 2017) which is an empirical approach that uses slope, hydrologic drainage class, and land cover characteristics (Ponce & Hawkins, 1996). These examples use a host of physical characteristics to elucidate and estimate sediment and nutrient export processes but the common and key piece between all of them is the utilization of slope and drainage characteristics to effectively model and identify those processes.

Models have been shown to simulate conservation practice implementation effectiveness at reducing nutrient and sediment export (US Environmental Protection Agency, 2018). These models work at varying scales from watersheds to individual agricultural fields and have vastly differing data requirements, treatments of hydrologic routing, incorporation of management decisions, and ease of use (US Environmental Protection Agency, 2018). Focusing on agricultural revegetation of native species an appropriate model

must be able to incorporate vegetative changes, agricultural practices, as well as model nitrogen, phosphorus and sediment. The Soil-Water Assessment Tool (SWAT) and the Agricultural Policy Environmental eXtender Model (APEX) are two models that satisfy these requirements, but at differing scales (Texas A&M AgriLife Research, 2017; USDA ARS Grassland Soil and Water Research Laboratory & Texas A&M AgriLife Research, 2018). The APEX is a field-scale model whereas SWAT is a watershed scale model. A field is an area of open land usually bounded by property boundaries and individual land owner management systems. A watershed is an area of land surface whose hydrology drains to a single point. Models designed for a specific spatial scale may have difficulty simulating results relevant to another because the key processes could differ or processes may even be absent at different spatial scales. Conservation practices are often applied and implemented to achieve field scale results based on individual management decisions; making field scale models appropriate for simulating those decisions at a local scale (A. N. Sharpley et al., 2009; Tomer & Locke, 2011) but those practices are often evaluated at the watershed scale (Tomer & Locke, 2011). I focused on using a field scale model for this research because conservation practices are implemented within individual agricultural fields. The Agricultural Policy Environmental eXtender (APEX) model was designed to simulate N and P interactions with varying crops, conservation practices, and hydrologic events such that field scale exports can be computed for various land management scenarios (Gassman et al., 2009). The APEX

model has been applied and evaluated across the globe and shown to be an effective field scale model for estimating the export of nutrients and sediment (Keller & Fox, 2019 and references within). The Nutrient Tracking Tool (NTT) provides a user-friendly web-based graphical user interface to run the Agricultural Policy Environmental eXtender (APEX; Texas A&M AgriLife Research, 2017) model paired with U.S. Department of Agriculture (USDA) soil property databases with online simulations. Just like APEX, the NTT is designed to evaluate the effectiveness of several conservation practices, including reforestation, on nutrient export from fields to surface waters (Ali Saleh et al., 2015). One downside to the NTT is that reforestation options available within the model are currently limited to red pine plantations which may not be suitable for all locations (A. Saleh et al., 2011). Nutrient Tracking Tool results have primarily been verified in watersheds flowing into Lake Erie (Ali Saleh et al., 2015), but the model is in various stages of verification across the United States. Despite limited validation, using a user-friendly model was a key attribute in deciding to move forward with using the NTT. Conservation practice implementation and investment from private landowners is increased when the process and benefits are openly communicated and easy to understand with input contributed from both the private landowner and the conservationist practitioner (Brant, 2003; D. C. Rose et al., 2018; Walsh et al., 2019). Although not a part of this research, the NTT provides a way for landowners to be actively involved in the modeling

process in the future resulting in reduced barriers to conservation practice implementation (Brant, 2003).

In this study, I evaluated the NTT prediction of field scale nutrient and sediment load reductions due to revegetation efforts in select sub-watersheds within the Lower Fox River Watershed (FRW), WI. I perform preliminary analysis to focus revegetation implementation on agricultural lands with low infiltration capacity and high slopes, following the framework developed by Fox & Keller (2019). These lands are generally less productive and more suitable to target for conservation practice implementation. Upon identification of areas with high slope and poor drainage, the NTT was used to simulate and evaluate the load reductions resulting from the addition of buffer strips between agricultural crops and adjacent waterways, conversion to forest, and the effects of tiling on load reductions. Model outputs utilizing traditional and observed cropping systems were juxtaposed with measured edge of field and watershed gage export data. Considerations for widespread NTT application in the Lower FRW and other Great Lakes Priority Watersheds are also discussed.

2.0 Methods

2.1 Site Description

The FRW is 1,701,397-ha in size and located in Northeast WI (Figure 1-1). According to the 2016 National Land Cover Dataset (NLCD) the primary land uses are approximately 36% cultivated cropland, 40% undeveloped land, and 8% urban/suburban (MRLCC, 2016). The climate is temperate with average high

temperatures around 27˚C in July and August, and an average high of -5˚C in January. In Green Bay, WI, at the FRW outlet, the average annual precipitation is 750 mm with an average annual snowfall deposition of 1,295 mm (as snow) during the colder months; the monthly rainfall peaks in June with 99 mm (*Climate Green Bay, Wisconsin*, 2021). Peak river discharge correlates with the snowmelt period each spring (Graczyk et al., 2011; Jacobson, 2012). Past glaciation is reflected in the watershed topography, soils, and geomorphic features (Hadley & Pelham, 1976; Luczaj, 2011, 2013). Glacial features range from outwash plains to lacustrine plain deposits but ground and end moraines are predominant. The Niagara Escarpment forms the eastern boundary to the watershed (Luczaj, 2013). Glacial tills are common with particles ranging from boulder to clay sized. Various loams are commonly found throughout the watershed with greater percentages of clay and silt sized particles chiefly located in the eastern part of the watershed and more sand sized particles located in the western part of the watershed. Drainage characteristics range from well drained in the sandy outwash plains to very poorly drained in the lacustrine deposits common near the watershed outlet (Natural Resources Conservation Service, 2008a, 2008b; Provost et al., 2001; Santy et al., 2001). Tile drainage is largely unknown in the greater watershed, but attempts have been made to quantify tiling in areas with excessive nutrient and sediment pollution (S. Kussow, personal communication, 08/04/2020).

The Lower FRW has been designated an USEPA priority watershed and has been in the Total Maximum Daily Load (TMDL) program since 2012 for excessive P and sediment loads. Three sub-watersheds, the Lower East River (LER), Plum Creek (PC), and White Lake Creek-Wolf River (WLCWR) were used for the nutrient and sediment load quantification using the NTT (Figure 1-1). Plum Creek and the LER have been identified as major contributors to the P and sediment loads impairing the Lower FRW. Cultivated crop land covers 76% of the 9,030-ha PC watershed, with the remainder comprised of 9% developed land and 10% as vegetated land uses such as forests and wetlands. Agricultural and developed land uses cover 50% and 36%, respectively, of the 11,600-ha LER sub-watershed (MRLCC, 2016). Both sub-watersheds are situated in an area defined by glacial lacustrine deposits (Hadley & Pelham, 1976) with lower infiltration rates and high erodibility relative to other soils in the watershed (Soil Survey Staff, 2020). The WLCWR sub-watershed is located outside of these deposits and 84% of its land cover is in forested, shrubby, or wetland vegetation. The WLCWR was included as a stark contrast to compare NTT results from the more developed landscapes found in the LER and PC.

2.2 Priority Scoring Areas for Revegetation

The entire FRW was scored to identify areas where revegetation, such as reforestation, could improve water quality based on soil and slope properties (Figure 1-2; Keller & Fox, 2019). Soils with lower infiltration capacity based on their hydrologic group rating as published in the USDA Soil Survey Geographic

database (SSURGO) were assigned a greater component, or priority score for each 10-m grid cell (Table 1-1). Although other soil properties may have been useful, infiltration capacity paired with slope are essential components of other vulnerability tools (Lohani et al., 2020; Porter et al., 2016) and thus provide a simple but effective way to identify soils vulnerable to nutrient and sediment export. Slope was calculated between grid cells using a 10-m U.S. Geological Survey DEM (U.S. Geological Survey, 2018). Higher slopes were assigned a higher component score (Table 1-1). The total priority score was computed as the sum of the soil and slope component scores for each 10-m grid cell over the FRW. My approach has been modified from Keller and Fox (2019) to accommodate a greater range in slope properties.

2.3 Modeling Approach and Field Data Evaluation

2.3.1 Modeled nutrient and sediment load reductions utilizing the Nutrient Tracking Tool

The NTT was used to evaluate potential nutrient load reduction to waterways from agricultural fields and forested land within targeted FRW sub-watersheds. Developed land, such as urban/suburban land use, was not included in this analysis. Areas in agricultural land use according to the most recent NLCD (MRLCC, 2016) with a total priority score greater than or equal to 6 (section 2.1) that met all of the following criteria were identified as high priority for revegetation and modeled within the NTT:

- in a row crop land use per the 2016 NLCD,

- within 100-m of stream channels,
- aggregated scoring area greater than 0.4-ha (40 grid cells) in size,

Untiled areas meeting the above criteria were identified and evaluated separately from tiled areas. Untiled areas were aggregated based on scoring and grid cell adjacency within the raster file such that high priority areas could encompass a subsection of a larger field whereas entire tiled fields adjacent to streams were included regardless of prioritization score. These sets of aggregated grid cells were converted to a shapefile for upload into NTT. An agricultural field may be composed of 10-m grid cells with varying priority scores (high, mid-, and low priority). Tiles were treated separately because the tiles may connect the sub-surface drainage areas of varying scores, so the whole field was treated as one hydrologically connected unit because tile extent within fields was unknown. Tiled fields were mapped as a shapefile using GIS software by Outagamie County Land Conservation Department by identifying fields with tile inlets based on aerial imagery (S. Kussow, personal communication, 08/04/2020), hence tile presence was known, but tile network connection and condition within individual fields were unknown.

Upon selection based on scoring and location, field shapefiles for both tiled and untiled areas (referred to as fields hereafter) were uploaded and identified within the spatial interface of NTT and a field list was created. The NTT subsequently incorporated the USDA SSURGO database to obtain soil properties for each individual field. The USDA SSURGO database is the same

database and uses the same spatial extent used to score the land area. Four main scenarios were then set up in the NTT:

- (Scenario 1) a corn-soybean rotation (the business-as-usual case),
- (Scenario 2) a corn-soybean rotation with 10-m vegetated buffer along waterways,
- (Scenario 3) conversion to a red pine plantation (currently the only forest option within the NTT), and
- (Scenario 4) elimination of tiling where present.

Tillage, fertilization, planting, and harvesting practices were incorporated into these scenarios as described in Keller & Fox (2019). Tillage consisted of chisel plowing in the spring, field cultivating prior to planting, and disking post-harvest. Fertilizer was applied in the spring; planting occurred in early May for corn and mid-May for soybeans with harvests set for October. The tiled fields used the same scenarios with the addition of tiling specified for each field in the NTT. A subset of forested land within the WLCWR watershed was simulated with the NTT to simulate the conversion of forested land to row crop agriculture using the scenarios listed above. Results are labeled as low priority because the most recent NLCD dataset classifies the land cover as forested, shrubby, or wetlands. The NTT simulated annual field export of total nitrogen (TN), total phosphorus (TP), and sediment over a 35-year period. Model results break the TN into runoff N, tile drain N, organic N, and subsurface N components. TP is separated into organic, soluble reactive P (orthophosphate), and tile drain P loads. Each of the

individual components makes up the total N or P values. Sediment export is defined as surface erosion and not broken down into other components. NTT generated results by incorporating PRISM weather data (PRISM Climate Group, 2004) to model field runoff and water quality constituent export within NTT. PRISM combines spatial climate knowledge with point data from weather stations, digital elevation models, and other spatial datasets with regression to generate annual, monthly, daily, and event-based climatic estimates are interpolated at an approximately 800-m grid cell size (PRISM Climate Group, 2004). The interpolated climatic values of each 800-m grid are assigned to the NTT fields based on the spatial overlap.

A randomly-selected subset totaling 15 fields of tiled, high priority, and mid-priority area (score of 4 and 5 that met criteria listed above) P export results from the main branch of PC were tested for sensitivity or dependence to the NTT P model parameters utilizing the corn-soybean rotation scenario. Mid-priority areas were added to the analysis in order to complete the watershed scale evaluation (described below) and were added to the sensitivity analysis after completing that evaluation. A mid-priority area is one that may have a relatively steep slope or low infiltration capacity that resulted in a score of 4 or 5 but did not represent combination of both low infiltration and steep slopes such as the areas ranked as high priority that resulted in scores of 6 or greater. The soluble P runoff coefficient and the P enrichment ratio coefficient for routing were left at the default values of 20 (0.1 $m^3 Mg^{-1}$) and 0.78 respectively. Other parameters that

were included in the sensitivity analysis were the soluble P runoff exponent, the P enrichment ratio exponent for routing, and the soluble P leaching equilibrium dissociation constant value. These parameters are used in the NTT model equations to generate the nutrient export results. Parameters were adjusted to maximize P export from NTT simulations, which were at the field scale. Using the changed parameter values, the NTT simulated new export values for the chosen fields that were compared to the original values. The sensitivity analysis was used to check if unadjusted parameter settings caused the large discrepancy between the high priority and mid-priority aggregated modeled NTT exports and the sub-watershed data used during the watershed scale evaluation (described below). Nitrogen was excluded from this exercise because TN watershed export data is unavailable for PC.

2.3.2 Evaluation of NTT Output at the Watershed and Field Scale

Verifying the modeled results with export data at both the field- and watershed-scale acts as an effective way to evaluate the NTT model at both scales and also serves as a proof of concept that any modeled reductions from revegetation mitigation using the NTT may be an effective mitigation strategy for the FRW. The comparison between NTT modeled field exports and published watershed loads additionally checks the magnitude of the NTT model results against the measured data. Field scale data was recently published (Komiskey et al., 2021), and the main branch of PC and the LER have annual sediment and P export estimates at the watershed scale in association with U.S. Geological

Survey Gauges (040851378 & 04084911) from 2012 to 2017 and 2004 to 2006 (Graczyk et al., 2011; Jacobson, 2012; U.S. Geological Survey, 2016a, 2016b). The data collection period for these studies is significantly shorter than the average annual sediment and nutrient exports estimated from the NTT over the 35-year simulation period. Published watershed export values were compared against NTT simulated sediment and P results in the tiled and high priority areas under the corn-soybean rotation scenario (business as usual) with the addition of mid-priority areas (score of 4 and 5), which represented the remainder of the agricultural area in row crops within the watershed.

For the field scale evaluation, NTT parameters were adjusted along with the cropping system to better match the field scale characteristics and management practices. The comparison was completed on a single edge of field monitoring site (ESW3) that had both surface and tile drain datasets that were collected from 2014 to 2019 (Komiskey et al., 2021). The NTT was run separately for the surface and sub-surface export from the field because the tiled portion drains approximately 10-ha and the surface drains approximately 2.8-ha. The parameters were changed based on previous work using the ArcAPEX model (Kalk, 2018) and involved adjusting settings to resemble the cropping and soil systems found in the field along with incorporating a 5-yr training or model warm up period prior to the 2014 to 2019. Just like how the NTT runs APEX with a web-based interface, ArcAPEX runs the APEX model within GIS software; the underlying parameters are the same, but the user interacts with the model on a

different platform. The NTT was also ran with the parameter values used for the watershed evaluation of the NTT output but used the shortened timescale so that the model results could be compared to Kalk (2018) in addition to the measured data. Nash Sutcliffe Efficiency (NSE) was calculated for the discharge and phosphorus values based on annual variation between modeled and observed values.

3.0 Results

3.1 Priority Scoring

The 10-m grid cell scores based on slope and hydrologic drainage class were totaled for the FRW. Scoring resulted in 208,093-ha or 12% of the watershed classed as high priority areas (score ≥6), 700,420-ha or 41% of the watershed area as mid-priority areas (score equal to 4 or 5), and 672,888-ha, or 40% of the watershed area as low priority (score equal to 2 or 3; Figure 1-2). Within the FRW, a total of 51,865-ha or 3% of the watershed area were both scored high priority in this analysis and were classified as cultivated cropland in the 2016 NLCD.

3.2 Results of NTT Field Scale Simulations

3.2.1 Lower East River

The LER encompasses approximately 11,300-ha of which 43% is in row crop agriculture. Of the land in row crop agriculture, tiled fields account for 28% and an additional 12% was determined to be high priority and untiled using the scoring system, and 3% were scored as less than high priority. Tiled fields in a

corn-soybean rotation showed an average annual loss of (34.56 ± 14.31) $x10^{-3}$ Mg ha^{-1} TN, (1.13 ± 0.32) $x10^{-3}$ Mg ha^{-1} TP, and 0.97 ± 0.55 Mg ha^{-1} sediment (Figure 1-3). The conversion of tiled lands to a red pine plantation decreased loads the greatest. The forest conversion resulted in 85.7, 94.7, and 89.2% reductions for TN, TP, and sediment, respectively. The untiled high priority fields showed a similar trend with forest conversion corresponding to 85.3% TN, 91.8% TP, and 80.9% sediment reductions. Buffer strips did provide nutrient reductions with the greatest modeled reduction occurring for sediment compared to the nutrients. The buffer strips in high priority untiled fields reduced TN, TP, and sediment by 8.9, 22.9, and 57.6%. Tiled systems reduced TN, TP, and sediment by reductions 0.5, 6.0, and 41.5% respectively (Figure 1-3).

3.2.2 Plum Creek main branch

The agricultural land in Plum Creek is 31% tiled and 2% scored as high priority. The corn-soybean rotation in tiled fields were projected to yield (32.70 ± 14.07) $x10^{-3}$ Mg ha^{-1} TN, (1.05 ± 0.30) $x10^{-3}$ Mg ha^{-1} TP, and 0.93 ± 0.55 Mg ha^{-1} sediment in annual losses. The corn-soybean rotation in the high priority fields resulted in (39.79 ± 17.04) $x10^{-3}$ Mg ha^{-1} TN, (2.25 ± 0.72) $x10^{-3}$ Mg ha^{-1} TP, and 5.50 ± 2.48 Mg ha^{-1} sediment losses on an annual basis. Similar to the LER, tile removal and conversion to forest resulted in the greatest nutrient and sediment reductions with 85.4, 95.2, and 86.2% reductions for TN, TP, and sediment, respectively (Figure 1-3). Forest conversion in the non-tiled high priority areas showed similar results with 87.2% TN, 92.9% TP, and 86.2% sediment

reductions. Buffer effectiveness is limited when tile drainage systems remain functional within fields by increasing TN and TP loads by 27.2% and 6.7% versus those fields with tiles removed. Sediment export was reduced by 18.8% in the tiled scenario versus when tiles were removed (Figure 1-3).

3.2.3 White Lake Creek - Wolf River

The WLCWR has 84% of the 10,522-ha in forested and wetland vegetation. The modeled forested landscapes in the WLCWR result in less nutrient and sediment losses to streams compared to conversion to row crop agriculture. Converting forested land uses to a corn-soybean rotation resulted in 803%, 9800%, and 3767% increases in TN, TP, and sediment exports to waterbodies with modeled fluxes changing from $(4.87 \pm 1.82)x10^{-3}$ Mg ha^{-1} TN, $(0.02 \pm 0.02)x10^{-3}$ Mg ha^{-1} TP, and 0.13 ± 0.09 Mg ha^{-1} sediment to $(44.05 \pm 17.05)x10^{-3}$ Mg ha^{-1} TN, $(2.22 \pm 0.76)x10^{-3}$ Mg ha^{-1} TP, and 5.25 ± 2.06 Mg ha^{-1} sediment exported annually (Figure 1-3).

3.3 Watershed and Field Scale Evaluation of NTT

According to the NTT simulations, the LER tiled and high priority fields exported 2.739 ± 0.846 Mg yr^{-1} of TP and $3,981 \pm 2,159$ Mg yr^{-1} of sediment (Table 1-2). TN was not measured at the watershed outlet so it was excluded from the evaluation. From 2004-2006, the measured annual TP export reported at the LER U.S. Geological Survey gaging station (Gauge number 040851378) averaged 35.11 Mg yr^{-1} and ranged from 17.28 to 62.60 Mg yr^{-1} (Graczyk et al., 2011; U.S. Geological Survey, 2016a). The Lower East River measured

sediment export (Table 1-2) from the same timespan averaged 9,350 Mg yr^{-1} and ranged from 2,422 to 20,593 Mg yr^{-1} (Graczyk et al., 2011; U.S. Geological Survey, 2016b). Comparing the NTT field export to the watershed yield indicates the cumulative modeled field sediment export is on the same order of magnitude as the measured yield at the watershed outlet; however, annual variation in the watershed outlet is considerable, as the annual average has a standard deviation of 9,824 Mg yr^{-1}, or 105%. Comparison of the TP values indicates the NTT 35 y average annual field export is well under the TP yield measured at the watershed outlet, with the NTT field export prediction approximately one order of magnitude lower than the annual average measured at the watershed outlet over 2004-2006.

In PC, the tiled, high priority, and mid-priority fields combined were predicted to annually export 6.23 ± 1.89 Mg yr^{-1} of TP and 8,051 ± 4,433 Mg yr^{-1} of sediment based on NTT simulations (Table 1-2). Both the TP and sediment modeled field export fell within the ranges of observed exports at the PC gauge from 2012 to 2017 (U.S. Geological Survey gauge 04084911): 6.12 to 18.69 Mg yr^{-1} TP and 3,157 to 11,649 Mg yr^{-1} of sediment (U.S. Geological Survey, 2016b).

The measured surface and tile drain discharge, TN, TP and sediment export from the edge of field ESW3 location were checked against the NTT model output. The observed tile drainage had an annual average discharge of 17,169 m^3 and tile export of 527 x 10^{-3} Mg TN, 3.72 x 10^{-3} Mg TP, and 477 x 10^{-3} Mg sediment along with an annual average surface runoff discharge measured at

5,131 m^3 and an annual surface export of 83.0 x 10^{-3} Mg TN, 20.6 x 10^{-3} Mg TP, and 7.73 Mg of sediment between 2014 and 2019 (Komiskey et al., 2021). Using NTT model parameter values from the watershed wide comparison (referred to as default values), the average annual surface runoff was estimated at 3,237 m^3 and 3,400 m^3 using the adjusted parameter values from Kalk et. al. (2018). The surface hydrologic output had an NSE value of -0.05 and 0.04 respectively. When the model training period was increased from 5 y to 14 y using the default parameters the NSE increased by 56% to 0.09. The average tile drainage using the adjusted parameter values was 17,268 m^3 and 14,980 m^3 using the default parameters. The tile drainage using the adjusted parameter values had an NSE of -1.26 and -1.47 using the watershed wide parameter settings. TN surface and tile exports were undervalued by the default and updated parameter changes and parameters need further refinement. The parameters were not explicitly changed for N export and NSE values reflected that with -4.77 and -4.78 for the default and adjusted parameters for the surface export. The organic N values in surface exports were improved from -1.92 for the default parameters to -1.75 using adjusted parameter values and were further improved using the default settings with a longer training period (NSE -1.10). TP showed similar trends as TN. There were no changes in NSE values between the tile exports using either the default or adjusted parameter settings (NSE of -3.84). However, the adjusted parameters increased the NSE by 7% compared to the default settings for surface exports from -2.02 to -1.89. Using a longer training period increased the

NSE by 87% to -0.25. NSE results were also improved by 4% when the soil P value was manually adjusted based on soil P test results (Kalk, 2018). Although TP results were poor in terms of the NSE, using default parameter settings with a long training period resulted in a NSE of 0.32 for soluble reactive phosphorus (SRP). Sediment export yielded a NSE value of -1.14 and -1.54 with the default and adjusted parameters respectively. Values below 0 for the NSE suggest that the observed mean does a better job of predicting discharge or export than the model.

3.5 Sensitivity to Model Parameters

Adjusting model parameters to maximize TP export and limit the discrepancy with the measured watershed data resulted in minimal changes within the high priority and mid-priority sites in PC. When parameters were changed to maximize P export in tiled fields, the tile drain P export averaged an increase of 867% and increased the TP export between 19 to 74% with an average increase of 48% across all tiled PC fields when P parameters were changed. Even when a 48% increase in TP export is used to compare the aggregated modeled results with the gauge data for PC, the modeled results are still on the lower end of the range observed at the gauge. Despite these parameter changes and the resultant increases the nutrient and sediment export were within the original parameter setting margin of error.

4.0 Discussion

4.1 Field vs Watershed Scale discrepancies

The field scale results were poor compared to the observed U.S. Geological Survey edge of field location at ESW3 and other work using ArcAPEX at this site. Kalk (2018) used three edge of field locations for model calibration (including ESW3) and found a NSE value of 0.67 for discharge after calibration at the ESW3 location with a value over 0.5 deemed acceptable for the calibration. Despite that success when using the same parameter values in this study the NSE value for discharge was significantly lower (NSE 0.04). The U.S. Geological Survey dataset was collected on an event basis following edge of field sampling protocols (Komiskey et al., 2021). Having adjusted for differences in time scales, a key difference between the NTT and ArcAPEX research was that the NTT used PRISM data for the weather modeling whereas the work using ArcAPEX used rain gauge data collected at the field location. PRISM precipitation estimates are derived from weather station data that informs 800-m grid cells that may vary from localized data collected at the ESW3 location and could have resulted in some of the discrepancies in modeled water volumes. Precipitation can vary significantly from what was observed at a weather station and a field a few kilometers away. If hydrologic differences exist or are inaccurate, then the nutrient and sediment export cannot be calibrated appropriately within the NTT model. Kalk's calibrated ArcAPEX model did lose performance in the subsequent years and locations, and the Kalk noted a number of discrepancies (Kalk, 2018). At ESW3, 95% of TP was sediment bound and APEX overestimated the sediment load by 18% (Kalk, 2018) which was similar to the results from NTT in

my study where almost no DP or tile drain P was shown in the NTT model outputs. This lack of partitioning has dramatic effects on DP and P lost through tile drains. Across all six locations evaluated from within the Lower FRB in Kalk (2018), they found DP and tile drained P were quite different than measured values despite calibrating the model to the surface and tile hydrologic volumes. Similarly, tile drained P was essentially estimated at zero by the NTT in this study. One change that did make TP export more accurate in both this study and Kalk (2018) was the inclusion of measured P from field soil samples. APEX will automatically set this value based on the soil characteristics and farming management scenarios and in the case of Kalk (2018) the soil P was estimated at roughly half the value as the measured P at the site. Therefore, APEX and the NTT are undervaluing TP stored and/or historically applied in these systems. Even with the default soil P settings, the TP values had better NSE scores when using a longer model training period and should be utilized in future modeling efforts in the FRB. One other large challenge in the calibration is how to handle the presence of tiling in the NTT and underlying APEX system. The surface drainage area was approximately 2.8-ha whereas the estimated tile drainage area was approximately 10-ha. Kalk (2018) also noted that the APEX model had a difficult time predicting the influence of snowmelt during their calibration because APEX uses solar radiation to predict snowmelt which is a simplification of the melting process. Relying solely on solar radiation to simulate snowmelt may not work well in the upper Midwest where snowmelt produces some of the

largest nutrient and sediment loads (Dolph et al., 2019; Huisman et al., 2013). Overall, APEX and the NTT need further refinement to accurately model field scale exports within the Lower FRB, including but not limited to field data to inform model calibration and assess model output.

At the watershed scale, aggregating field scale results, with their associated discrepancies, could compound into the large discrepancies observed for TP at PC and the LER. If APEX is undervaluing the DP and tile drain export, aggregating those results to the watershed scale could drastically reduce the estimated nutrient loads at the watershed outlets. Even in ESW3 with the primary TP flux being sediment bound, Kalk (2018) found that soil P was estimated by APEX at approximately 50% of the actual value which was similar to this study. Additionally, when aggregating to an entire watershed one shortcoming of using field scale models is the lack of accounting for storage and transport processes within the stream channel. Phosphorus in particular can be held in varying sediment fractions with differing capacities to release SRP to the water column (Lannergård et al., 2020). Associations with iron and manganese oxides may be reduced by microbiota in anoxic conditions and release P. In systems with high calcium concentrations, secondary mineral formation of apatite which binds calcium and P in a mineral structure, may essentially eliminate any possible SRP release because the mineral has low solubility. Additionally, biological processes paired with hydrologic fluxes may lengthen the time both P and sediment are stored within the stream channel (Dolph et al., 2019). However, aggregated

results for sediment were within observed ranges at the watershed scale despite having NSE values below zero (an indication that the observed mean predicted sediment export better than the modeled results at the field scale) indicating that modeled values were close to actual field scale exports but not a replacement for actual field data. The discrepancies between the field and watershed scale results emphasizes tradeoffs between field scale accuracy and the accuracy needed for a generalized watershed scale aggregation when a model cannot be finely tuned to every field within a watershed due to lack of site knowledge and resources.

Despite these results the NTT, and the underlying APEX model, has been found to be an effective model in agricultural systems at the field scale (Gassman et al., 2009; Ali Saleh et al., 2015) and is an excellent model for developing conservation practices with individual landowners (A. Saleh et al., 2011). The more a model is calibrated to an individual farming system the more likely it is to accurately predict nutrient and sediment losses. Shortcomings can arise when model parameters are applied across varying sites and when applying a field scale model at the larger watershed spatial scale. The NTT was not designed to account for hydrologic, sediment, and nutrient dynamics beyond the field. In particular, channel processes and hydrogeological routing are absent and could be a source of disparities between aggregated field-scale model results and watershed outlet data particularly in systems with legacy P. Other models that include better subsurface hydrologic routing, nutrient and sediment storage

parameters, channel processes, and incorporate land uses other than agriculture may be more effective at modeling nutrient and sediment export at larger scales and in more diverse landscapes. The USEPA summarizes 30 different models ranging from simple to difficult and two modeling systems that can be used for watershed protection (USEPA 2018). Some of these models, such as the NTT, address the field scale and require moderate knowledge of the field system, whereas others only work at the watershed scale (e.g. SPAtially Referenced Regression On Watershed attributes or SPARROW). Other models are capable of modeling at both scales such as SWAT (Soil & Water Assessment Tool).

The greatest benefit of the NTT is the intuitive and easy-to-use interface. Even though limitations exist, it is a more accessible model to a variety of users (e.g. landowners and local conservation district employees) versus a more sophisticated model such as SWAT which requires advanced training. Moving forward, utilizing the NTT APEX output or using APEX to model mitigation strategies at the field scale in conjunction with agricultural management systems as an input to a model such as SWAT for watershed assessments could be an effective way to model and refine water quality goals (Wang et al., 2011). Model choice should also take the availability of data for validation into consideration. Data found for this study encompassed a spatial extent beyond what is found at the field scale. Although the aggregated data comparison for PC and the LER fell within measured ranges observed at U.S. Geological Survey gage locations for

sediment, in-channel and watershed scale processes are absent from the modeling effort and could be a source of error in PC, the LER, and other sub-watersheds. These potential sources of error bring to question the suitability of using the NTT, or other field-scale planning tools, in future work to model nutrient and sediment export at the watershed or larger spatial scale. Despite a lack of field scale data, the goal to assess potential benefits of revegetation as a mitigation strategy was able to be accomplished using the NTT and existing datasets.

As a field scale model, the NTT is an excellent tool for understanding the interplay between agriculture and conservation practices that can be tailored to individual farming systems. To aggregate data over a broad spatial extent, such as a watershed, meant that individual fields were simplified (Fox and Keller, 2019) by making assumptions about the cropping systems to complete the analysis because specific management characteristics were unknown. Future work with the NTT could be improved by diversifying farm management practices and adding complexity (e.g. including manure application, no-till) and tailoring model parameters to individual fields. Tailoring model parameters would likely reduce disparities between results and field-scale observational data.

4.2 Management Considerations

4.2.1 Incorporating Vegetation

The addition of buffers decreased the modeled N, P, and sediment loads from the fields versus the typical corn-soybean rotation. My ability to modify

buffers based on individual field physical characteristics such as topography and landscape setting is another limitation of the NTT but could provide further load reductions. Within the NTT a buffer width may be specified but the user interface does not allow for the modification or the addition of multiple buffers on a field. Buffer design that varies buffers with topography and drainage characteristics such that areas where the majority of nutrients and sediment are being exported from the field surface (i.e. areas of convergent overland flow) are proven to be more effective at reducing nutrient and sediment loads (Dosskey et al., 2002; Helmers et al., 2011; Jiang et al., 2020; Schulte et al., 2017; Zhou et al., 2014). Total buffer area can also be spread out into multiple strips within a field and still yield reductions as long as the design allows for the greatest contact between the buffer and the flow bearing nutrients and sediment from the field (Hernandez-Santana et al., 2013). Buffers are a commonly used best management practice so field scale designs are paramount to their success. If landowners are unwilling to break up a field using vegetated strips, conservation practices may still be optimized by placing vegetated features near the channel (Hansen et al., 2021). Placing vegetation between the fields and the stream would further delay routing and be pivotal in reducing nutrient and sediment loads entering the stream channel (Kreiling et al., 2021). Nutrient and sediment storm event data from PC shows hysteresis patterns where transport to streams is delayed in the upper portion of the watershed suggesting mobilization from fields (L. A. Rose & Karwan, 2021) and provides evidence that vegetation could further delay and

largely reduce delivery to the stream channel. Despite many positives, buffers are not able to reduce 100% of all nutrients and sediment being exported from fields. The buffers can act as nutrient sources especially in cold climates (Vanrobaeys et al., 2019). Buffers may also increase the available soil P pool. Deep rooted perennial plants have been shown to increase labile P previously immobilized in soils (Stutter et al., 2009). Harvesting buffers could help offset these negatives by physically removing nutrients tied up in biomass. Removal of one kind of vegetation within a buffer at a time (e.g. a buffer with trees and grasses where only the trees or grass is removed) can also be used to minimize reduced nutrient and sediment capture efficiency stemming from vegetation loss (Jiang et al., 2020; Liu et al., 2021).

Being able to assess different vegetation communities for both buffer and forest conversion management scenarios would be an improvement to the current NTT model framework. Evaluation of nutrient losses following agricultural land conversion to forest or other regionally appropriate vegetation could be more reasonable with a broader variety of forest and endemic vegetation cover types. Specifically, the conversion of agricultural land to red pine plantation may not be as beneficial to nutrient and sediment export as other forest types or forested wetlands historically found in the area. In many locations within the Great Lakes region, red pine may not be a suitable species. Within the NTT, the fields are assumed to be managed for agricultural products and the NTT was not designed to simulate land conversion between agriculture and specific forest or

wetland vegetation communities. In these forested systems, the NTT might not fully parameterize the nutrient and water quality tradeoffs under the full range of other forest and wetland vegetation types. Incorporating vegetation suitability from soil survey databases into the scoring system may be one alternative to work around these limitations in the future. If the forest conversion scenario were expanded to include open or forested wetlands, the field scale results have the potential to yield more realistic results at the watershed scale from a mitigation standpoint. Both upland forests and forested wetlands retain nutrients, may provide a means for economic income through tree harvesting, and these landscape features dampen the effects of extreme hydrologic events by lowering the magnitude and increasing the duration of elevated discharge observed in stream networks (Grant et al., 2008; Kovacic et al., 2006; Salemi et al., 2012; Zhu et al., 2020). Future work assessing the strategic placement of vegetated areas could have a dramatic effect on nutrient and sediment loads observed in the stream channel. An example of vegetated systems strategically placed on a large scale are the Everglades Stormwater Treatment Areas (STAs) which were created to intercept and slow the nutrient and sediment loads flowing from agricultural areas to the Everglades. These wetlands have succeeded in reducing nutrients and sediment in addition to providing flood mitigation (Mitsch et al., 2015; Moustafa et al., 2012; Pietro & Ivanoff, 2015). A similar scenario could work as a long-term mitigation strategy within the FRW if perennial upland forest, prairie, or wetland vegetation is implemented at a larger scale.

The NTT does allow for the simultaneous incorporation of other management practices despite limitations on complexity such as with buffer design. The scenarios that I tested were buffer installation and land conversion to a forested plantation system. Buffer installation combined with other conservation practices such as implementation of no-till or the use of cover crops could further reduce nutrient and sediment loads and increase buffer effectiveness. These practices behave relatively similar to buffers where carbon storage, water infiltration, water storage, nutrient retention, and erosion protection are field characteristics that are generally improved with adoption along with improvements to overall soil health and biodiversity (Kaspar & Singer, 2011; Myers et al., 2019; Poeplau & Don, 2015). Cover crops in particular reduce farm costs when combined with other cropping practices and provide many economic benefits to the landowner (Myers et al., 2019). On the other side of the spectrum, the conversion of cropped fields to forests or wetland vegetation, albeit an effective way to reduce nutrient and sediment loads, is unlikely to be implemented as a management option without further economic incentives. In spite of the simplification to not incorporate other practices to compare aggregated modeled results to the loads observed at the PC and LER watersheds, future work incorporating more specific cropping systems will likely improve model results and close the gap between the observed P export and the modeled export.

4.2.2 Tile Drainage

One benefit of working in the LER and PC watersheds was the inclusion of tile drainage in the management scenarios for the Lower FRW. Future work in larger watersheds will need to overcome data limitations regarding tile drainage extent. No large scale records exist of tile networks because they are implemented on private property. Available data did not allow for the validation of the modeled tile exports in the LER and PC watersheds, however the NTT sensitivity analysis indicated weaknesses to the model and/or the scenario in these watersheds. By changing parameters affecting P loads, the tile drain P increased from an average of about 5% to upwards of 34 to 51% of the TP load which is consistent with other studies following similar fertilization scenarios (Williams, King, Baker, et al., 2016). However, those increases were within the margin of error for the scenario outcomes using the original model parameter values. Even if all fields within PC and the LER watersheds were assumed to be tiled, a 50% increase in the TP load would bring the modeled estimates for the LER to 4,090 kg yr^{-1} P and PC to around 9,090 kg yr^{-1}. The estimate would bring PC to within 50% of the maximum observed export based on the gage data (U.S. Geological Survey gauge 04084911, US Geological Survey, 2016b), but the model result for LER is still 15 Mg y^{-1} lower than the minimum measured (U.S. Geological Survey, 2016a).

Despite the dissimilarity between the gauge data and the model, the model results show that the inclusion of tile drainage reduces the effects of vegetation as a nutrient and sediment mitigation strategy and increases nutrient

export which is in general agreement with the literature (Carstensen et al., 2020; Hanrahan et al., 2021; Klaiber et al., 2020; Royer et al., 2006; Schilling et al., 2020; Thalmann, 2021). Tile drains tend to increase dissolved N and P losses from fields, but in comparison to undrained fields increased surface losses may have a net zero effect on TP export depending on the agricultural management practices used in the field (Klaiber et al., 2020; Royer et al., 2006; Thalmann, 2021). The presence of tile drains allows for targeted mitigation of the drainage systems (Schilling et al., 2020). Terminating tile drains prior to reaching buffers or rerouting drainage so that tile effluent must flow through vegetated buffers, wetlands, or bioreactors are common mitigation strategies that yield nutrient and sediment reductions despite the presence of subsurface drainage (Carstensen et al., 2020; Gordon et al., 2021; Jaynes & Isenhart, 2014; Mendes, 2020). Thus, when planning mitigation using vegetation, knowledge of subsurface drainage is critical to the mitigation effectiveness from a load reduction viewpoint.

5.0 Conclusion

The NTT was used to successfully simulate nutrient and sediment export from three sub-watersheds within the FRW. The modeling demonstrated that conversion or conservation of vegetated areas within watersheds is an effective management strategy to reduce nutrient and sediment export from fields and that the targeted placement of vegetation can have a dramatic effect on load reductions. By using slope and hydrologic drainage class, conservation measures in high priority areas were shown to have greater sediment, TN, and

TP reductions than mid-priority scoring areas within the PC watershed when buffer and forest conversion scenarios were compared to the corn-soybean rotation. The NTT model is effective and accessible for land managers to use which could allow for the addition of greater complexity to the modeled scenarios resulting in increased accuracy and precision of modeled results at the field scale.

Future work will be needed to build datasets to further validate NTT results at both the field and watershed scales to meet load reduction requirements of particular watersheds in the FRW. Modeled field hydrologic discharge along with nutrient and sediment export were not accurate compared to measured field-scale means. The field scale modeling exercise showed that field scale data is pivotal to accurately modeling field exports with the NTT. When scaling up to watershed exports, aggregated values of TP were undervalued compared to sediment which fell within ranges observed at gauge sampling locations. The discrepancies between using a field scale model for watershed scale exports comes from many caveats and model tradeoffs. The omission of in-stream and channel transport and storage processes may be a critical piece missing from the aggregated results especially when considering the complexity of phosphorus cycling and fractionation within the environment.

Chapter 3: Phosphorus and Fine Sediment Reach Scale Transport in Plum Creek, WI

1.0 Introduction

Phosphorus (P) is an essential component of all living things. The element makes up a large part of DNA, bones, cell structures, and is primary to the metabolic process. However, a conundrum has developed because P is an essential nutrient (Jarvie et al., 2015) yet the depletion of mined phosphate reserves and the inefficient use and redistribution of P across landscapes has led to deficiencies and excess that are unsustainable and environmentally harmful to aquatic ecosystems (Andrew Sharpley et al., 2018). Excess and inefficient use is the main driver behind ecological imbalances found in eutrophic streams, rivers, lakes, estuaries, and seas worldwide. Eutrophication effects more than 400 coastal communities (Selman et al., 2008) and countless freshwater bodies worldwide. In the United States, P loading is on the rise across the country (Stoddard et al., 2016) resulting in harmful algal blooms and hypoxic events (Ho & Michalak, 2015). In the upper Midwest a notable example is Lake Erie, a part of the Laurentian Great Lakes and one of the largest freshwater lakes in the world, which has had algal blooms of increasing frequency, duration, and magnitude (Dodds et al., 2009; Ho & Michalak, 2015; Stoddard et al., 2016). One cyanobacteria bloom of note led to a drinking water ban for 500,000 residents of Toledo, Ohio in August 2014 (Ho & Michalak, 2015).

Despite mitigation efforts, phosphorus is often transported in excess to downstream water bodies. The increase in P reservoirs due to past and current land management has created chronic-long term loading to downstream waterbodies and is known as “legacy” effects (Jarvie et al., 2013; Powers et al., 2016; Andrew Sharpley et al., 2013). Phosphorus binds readily to sediment surfaces and initial mitigation efforts focused on reducing sediment loads to streams from agricultural lands utilizing practices such as conservation tillage and buffer strips (Helmers et al., 2005; Kaspar & Singer, 2011; Moustafa et al., 2012; Robinson et al., 1996). When these practices were implemented, particle load reductions occurred, but in some cases, watershed export of soluble reactive phosphorus (SRP) increased due to historical loading and the quick flow pathways of tile drainage systems that transport SRP away from fields and into water bodies. Dolph et al. (2019) found that across 22 sites encompassing a large spatial extent of western, central, and southern Minnesota that average total P loads were made up of 53% (ranging up to 74%) SRP and 47% (ranging up to 71%) particulate P. In another study from Minnesota SRP ranged from 7% to nearly 100% of the TP load (Boardman et al., 2019). SRP is considered the most biologically available P form and poses a grave ecological threat to not only downstream waterbodies but is often found above water quality standards (Jarvie et al., 2017; Shore et al., 2017). To understand the loading that may occur and the effects of legacy sediment many different biogeochemical techniques have been employed to estimate the forms (e.g. organic, inorganic, sediment bound) and amounts of phosphorus reaching downstream waterbodies (Cheesman et

al., 2014; Jarvie et al., 2002; Kinsman-Costello et al., 2014; Paludan & Jensen, 1995; Ruban et al., 2001; U.S. Environmental Protection Agency, 1978; C. Wang et al., 2013).

Even though particulate P and SRP are chemically linked, loading to downstream waterbodies is influenced by hydrologic conditions. The greatest P loads to downstream waterbodies occur during stormflow for both dissolved and particulate P (Boardman et al., 2019; Dolph et al., 2019; Jordan et al., 2012; Shore et al., 2017). Dolph et al. (2019) found that greater than 70% of total phosphorus export occurred when stream discharge was greater than 90% exceedance probability and an additional 15% of the total phosphorus export occurred when discharge was between 90 and 75% exceedance probability. Mobilization of particulate P and SRP as well as the potential to be transported increase as runoff and connected quick flow paths, such as tile, ditch, and storm water drainage, expand (Kast et al., 2021; Royer et al., 2006; Thalmann, 2021; Williams, King, Ford, et al., 2016). During events, flashy streams send large quantities of phosphorus downstream (Jordan et al., 2012; Shore et al., 2017). The fluvial transport of particulate P is more dependent on flow than SRP because the flow must be able to entrain and transport the particle associated P downstream. These interactions between flow stream particles, and shear velocity can lead to scouring of particles in some areas and their deposition in others such as in a floodplain (Verhoff et al., 1979). Fine sediment (< 0.0625 mm) is particularly important to this process. The loss of fine sediment from channel margins, topsoil, gulleys, and rills. has been associated with the transport of

metals, pollutants, organics, and nutrients sorbed to sediment surfaces (Ongley, 1996). Equilibrium phosphorus concentration (EPC_0) experiments have shown a greater proportion of sediment bound P associated with fine sediment (Palmer-Felgate et al., 2009) and stream sediment often has the capacity to bind more P (Agudelo et al., 2011; Inamdar et al., 2020; Palmer-Felgate et al., 2009).

Downstream transport of particulate P and SRP largely depends on hydraulic regimes (high flows account for the majority of the loading) as well as reactive and storage time scales for water, solute, colloidal, and particulate transport. The P form (solute, particle bound, organic, etc.) influences interactions with sediment, other chemicals found in the water column, and biota – all of which are processes that can bind or convert SRP to less bioavailable forms reducing the immediate eutrophication risk. Specific mechanisms that control bioavailability include advection and diffusion (Casey & Farr, 1982; Reddy et al., 1999a), sorption and desorption reactions (Froelich, 1988; Reddy, Kadlec, Flaig, & Gale, 1999; A. Sharpley, Richards, Herron, & Baker, 2012), mineral precipitation and dissolution (William A. House, 2003; Pierzynski et al., 2005), organic P mineralization (Li et al., 2016), fertilizer application (Boardman et al., 2019), and uptake by primary producers and microorganisms (McLaren et al., 2015; Richardson & Simpson, 2011).

There is an opportunity to advance biogeochemical understanding of in-channel phosphorus cycling by utilizing techniques developed to parameterize reach scale hydrologic transport. A majority of in-stream phosphorus experimentation revolves around the biogeochemical processing or watershed

monitoring efforts. In-stream tracer experiments and related data modeling can parameterize reach scale transport processes, such as advection, dispersion, transient-storage exchange, degradation, etc., by incorporating transient-storage modeling. Most transient-storage modeling has been used conservative or reactive solutes (Boano et al., 2014). Using multiple tracers is advantageous because a conservative solute will help bound the reactive parameters while the reactive parameters yield a better understanding of more complex in stream processes (Boano et al., 2014). Transient-storage models allow for the parameterization of reactive tracers which can be used to understand the short term SRP uptake and loss to the channel via biogeochemical processing based on the reach scale loss observed. Despite the use of tracer injection experiments to further mechanistic and process understanding of transient-storage zones and modeling advances, there is a lack of experimentation involving the co-injection of fine particle and reactive solute tracers within the literature (Boano et al., 2014). Co-injecting solutes and particles allows for a deeper system understanding because particle transport is affected by different storage mechanisms such as burial and requires specific flow conditions to become mobile. By measuring the transport and storage of solutes and particles the phosphorus cycling mechanisms can be paired with and constrained by hydrodynamics.

I aim to address the following primary hypotheses relevant to the watershed cycling of phosphorus and fine sediment within the study reaches.

1) If base flow conditions increase transient storage and delay the downstream hydrologic transport of fine particles, then ambient concentrations of sediment-bound phosphorus deposits will increase with storage time on less than annual timescales.
2) Fine sediment reactivity and abundance will increase phosphorus storage within the stream channel and delay its downstream transport because fine sediment transport is delayed relative to the soluble form.

To address the hypotheses a set of tracer injection experiments were conducted to measure the transport and storage parameters of SRP and fine particles in agricultural reaches within the upper Midwest, USA. In this study, particles play an important role modulating phosphorus within stream channels. By using fine particles during base flow conditions, a better understanding of that short term storage (e.g. where particles may be deposited within the channel and later mobilized at the next storm flow event) is gained. The fate of particles co-injected with dissolved P in a stream network would be a step towards mimicking fine particle and reactive solute dynamics that are found in stream channels (Withers & Jarvie, 2008) and parameterizing that transport will lead to a better understanding of legacy P stores. I then pair this technique with classical equilibrium phosphorus methods to gain a better understanding of in-stream phosphorus storage and the associated barriers to water quality improvements at the watershed scale.

2.0 Methods

2.1 Site Description

Plum Creek is a tributary to the Lower Fox River located in east central Wisconsin, USA (44.31˚N, 88.17˚W NAD27; Figure 1-1). The Lower Fox River and Green Bay, Wisconsin receive excessive sediment loads that fuel algal blooms of increasing frequency. Plum Creek was originally listed as impaired by the USEPA in 1998 and due to basin wide impairments a total maximum daily load (TMDL) was approved for the Lower Fox River and its tributaries in 2012. This TMDL lists Plum Creek as a major contributor of sediment and phosphorus and calls for greater than 70% reductions for both impairments.

The watershed and surrounding area were last glaciated about 10,000 y ago and lie within the Eastern Ridges and Lowlands geographical province in Wisconsin. Glacial features include moraine, outwash, and lake plains. Soils are composed of loam, silt loam, and clay loam (Soil Survey Staff, 2020). Soils in the Plum Creek Watershed generally have low water infiltration that generate high runoff volumes and soil erosion. This part of Wisconsin has a northern latitude temperate continental climate affected by Lake Michigan The average annual high temperature is 12 ˚C ranging from 27 ˚C in July to -4.3 ˚C in January and a mean annual low temperature of 1.6 ˚C ranging from -13 ˚C to 15 ˚C as measured in nearby Appleton, WI (*Climate Appleton- Wisconsin*, 2020). The average annual precipitation is 750 mm falling predominantly as rain during the warmer months. The annual average snowfall is 1300 mm measured as snow depth and is deposited from November through April (*Climate Appleton-Wisconsin*, 2020).

At the outlet gage, Plum Creek has a 54.9 km^2 drainage area and approximately 31 km of stream length. The watershed was primarily composed of forests and wetlands prior to European settlement and was subsequently cleared and drained during the conversion to agricultural lands which cover 75% of the watershed area (45% cultivated crops and 32% hay and pasture) (“Nonpoint Source Implementation Plan for the Plum and Kankapot Creek Watersheds,” 2014). Most of the agricultural land follows a typical dairy crop rotation of corn and alfalfa or row crop rotations of continuous corn or corn soybean rotations. Agriculture has been identified as a primary contributor to the excessive sediment and phosphorus loads discharged into the Lower Fox River (“Nonpoint Source Implementation Plan for the Plum and Kankapot Creek Watersheds,” 2014). The watershed is composed of two primary sections (Figure 2-1). The upper portion of the watershed is composed of three primary tributaries that are impacted by the surrounding land use where relatively greater slopes and lack of conservation practices results in dynamic sediment transport from upland areas into the stream network. The stream reaches are coarser in texture with visually observable transient-storage zones such as pools and areas of slower moving water connected to the relatively faster moving channel. The lower portion of the watershed is comprised of an entrenched valley. The narrow floodplain and valley slopes are forested with a decrease in stream slope compared to the upper stream sections but the stream bed is primarily a hard packed clay that results in fast transport of sediment during high discharge storm events. At base flow and low flow conditions the stream channel transforms into a series of slow

to stagnant pools connected by shallow riffles. Upper sections can oftentimes have intermittent flow conditions.

2.2.1 In-stream Transport Study

Tracer was added at two sites (Figure 2-1). Site one was located just above U.S. Geological Survey gauge 04084911 (44.31˚N 88.17˚W), east/upstream of the County D bridge, within the lower watershed and is denoted as Lower Plum Creek. Gauge data provided discharge measurements (U.S. Geological Survey, 2016b). Injections took place through a riffle pool system approximately 100-m in length. Site two was located in the upper portion of the watershed west of Cemetery Road (44.24˚N 88.15 ˚W; Figure 2-1) and is denoted as Upper Plum Creek. Injections took place on June 23, 2021 and November 9, 2021 at the Lower site and on November 2, 2021 for the Upper site. Upper Plum Creek only had one tracer test due to drought conditions in Northeast Wisconsin during the spring, summer, and early fall of 2021 that eliminated flow in the upper watershed. Discharge was estimated using the injection data and checked with a USGS rating curve developed for the site. Samples were collected 10-m and 60-m downstream of the injection site.

Tracer additions were performed at base flow conditions using bromide (Br^-as sodium bromide (NaBr); VWR International >99% purity; CAS: 7647-15-6) as the conservative tracer, orthophosphate (PO_4^{3-} as potassium phosphate monobasic (KH_2PO_4); Fisher Scientific >99% purity; CAS: 7778-77-0), and Dayglo Aurora Fluorescent AX pigment as a particle surrogate (Drummond et al., 2014). The particles have a density of 1.36 g cm^{-3} and range in size from 1 to 10

μm diameter with an average size of 4 μm (Drummond et al., 2014). This particle surrogate covers the clay and smaller silt sized particles, but has a lighter specific gravity closer to that of fine particulate organic carbon (Brady & Weil, 2007). By using a fluorescent particle the particle concentrations can be directly measured. During the June 23 injection at Lower Plum Creek, all analytes were mixed in a single reservoir with a 10 L addition of 5 g L^{-1} of sodium hexametaphosphate (SHMP $(NaPO_3)_6$; J.T. Baker lab grade; CAS: 10124-56-8) as a dispersant to keep the slightly hydrophobic particles in suspension following methods outlined by Drummond (2018). The salts were dissolved in 10 L of ultrapure water (ThermoFisher E-Pure) water the day prior to the injection and added to the reservoir with stream water composing the remaining volume (110 L in total). The particles and SHMP solution were mixed approximately 1.5 h prior to the start of the injection to adequately disperse the particles for the injection. The reservoir was continuously mixed throughout the injection and pumped into the stream at a rate of 0.02 L s^{-1} for 85 min with a peristaltic pump (Masterflex). The tubing was split using nylon T connections so injectate was pumped into the stream at multiple points across a single stream cross section.

After the initial analysis, modifications were made for the second and third injections. The Br^- and PO_4^{3-} salts were kept in and pumped from separate reservoirs into the stream. A diffuser was built using PVC piping to distribute analytes more evenly into the stream. The diffuser was kept submerged for the full duration of tracer additions. Sodium bromide (0.047 kg) and KH_2PO_4 (0.049 kg) were dissolved in 14 L of ultrapure water and pumped at a rate of 0.0025 L s^-

[1]. The SHMP solution (10 L) was added to 60 L of stream water to yield a SHMP and particle concentrations of 7 and 5 g L^{-1} respectively; the solution was continuously mixed and pumped into the stream at 0.0094 L s^{-1}. The pumps were on for 61 min during the second injection at the Lower Plum Creek site and 105 min at the Upper Plum Creek site

Grab samples were collected at each sampling locations from the water column. Sample collection timing was informed using a conductivity probe at the furthest downstream location to monitor the conservative solute plume transport. Due to the hard-packed nature of the bed, hyporheic sampling was not conducted during any of the injections. Samples were collected into 125-mL high density polyethylene (HDPE) bottles and a 20-mL sub-sample for Br^- and SRP analysis was syringe filtered through a 0.45-µm polyethersulfone (PES) filter at the time of collection. Samples were stored chilled and in the dark prior to analysis. SRP was analyzed using colorimetric methods EPA 365.3 with a UV/Vis spectrophotometer (ThermoScientific Geneys 180; lower detection limit 0.01 mg P L^{-1}; U.S. Environmental Protection Agency, 1978) and bromide was measured using and ISE meter with a bromide specific probe (ORION Bromide Electrode 9435BN; lower detection limit 1 mg Br^- L^{-1}) with a calibration range of 1 to 79 mg L^{-1}. The particle concentrations were measured using a fluorescent spectrophotometer (Horiba Aqualog; 650 to 24 nm excitation) to generate emission-excitation-matrices (EEMs). A calibration curve was used to measure the particle concentration in each sample. The resulting EEMs were corrected for inner filter effects, blanks and scattering. The greatest peak was selected

(excitation 263 nm and emission at 569 nm) using the eemR package (Massicotte, 2019). After examining the calibration data, the excitation range was shortened to speed processing time and the peak wavelengths were selected because the wavelengths had the greatest peak that did not overlap with peaks found in the stream water.

2.2.2 1-D Hydrodynamic Model

Time series tracer concentration data, or breakthrough curves, were fit using the One-Dimensional Transport with Inflow and Storage (OTIS) model, a mathematical transport simulation for streams and rivers (Runkel 1998, 2000). The model is based on the 1-D advection-dispersion equation with terms to account for transient storage which is represented as a mass transfer between the water column and a well-mixed storage zone. The OTIS equations are:

1. $\frac{\partial C}{\partial t} = \frac{-Q}{A}\frac{\partial C}{\partial x} + \frac{1}{A}\frac{\partial}{\partial x}\left(AD\frac{\partial C}{\partial x}\right) + \frac{q_{Lin}}{A}(C_L - C) + \alpha(C_s - C)$
2. $\frac{\partial C}{\partial t} = \alpha\frac{A}{A_s}(C - C_s)$

Where t is time (s); x is downstream distance (m); C, C_L, and C_s are the solute concentrations in the main channel, lateral inflow, and storage zone respectively (g m^{-3}); D is the dispersion coefficient (m^2 s^{-1}); α water exchange coefficient between the water column and storage zone (s^{-1}); A_s, the storage zone cross sectional area (m^2). Additional terms were added for reactive (non-conservative) tracers to account for kinetic sorption and first-order decay when necessary with the phosphate and particle data from the Upper Plum Creek injection (Runkel, 1998):

3. $\frac{\partial C}{\partial t} = L(C) + \rho\lambda_3(C_{sed} - K_d C) - \lambda_1 C$

4. $\frac{\partial C_s}{\partial t} = S(C_s) + \lambda_4(C_{sb} - C_s) - \lambda_2 C_s$

Where C_{sb} is the background storage zone solute concentration (g m^{-3}); C_{sed} is the sorbate concentration on the streambed sediment (g/g); K_d is the distribution coefficient (m^3 g^{-1}); λ_1 is the main channel first-order decay coefficient (h^{-1}); λ_2 is the storage zone first-order decay coefficient (h^{-1}); λ_3 is the main channel sorption rate coefficient (h^{-1}); λ_4 is the storage zone sorption rate coefficient (h^{-1}); ρ is the mass of accessible sediment per volume water (g m^{-3}); and L (C) and S(C_s) represent the physical processes in the main channel and storage zones (Equations 1 and 2). The model was fit using a combination of OTIS-P which uses inverse modeling to obtain parameter estimates through an iterative process and manual adjustments with OTIS. Due to the dual usage of OTIS and OTIS-P, the combination approach will be referred to as OTIS from this point forward unless specific mention is necessary. OTIS was chosen because it is more influenced by hydraulics (which fit Plum Creek characteristics) than stochastic transient-storage models which tend to be influenced by channel morphology (Drummond et al., 2016). Sensitivity analysis was performed using the methodology laid out by Wagner and Harvey (1997) using Damkohler number:

5. $DaI = \frac{\alpha\left(1+\frac{A}{A_S}\right)L}{u}$

Where L is the experimental stream reach length (m) and u is the average stream water velocity (m s^{-1}) over the reach. The transport parameters determined by OTIS best-fits were then used to provide a crude time estimate of

transport of particles and solutes from the Upper Plum Creek site to the Lower Plum Creek site at base flow.

2.3 Sediment and water column phosphorus characteristics

Streambed, channel bar, and bank sediment samples were collected from both study reaches on September 30, 2021. Stream water samples were also collected and immediately filtered through 0.45 µm PES syringe filters into HDPE bottles, chilled, and stored in the dark for SRP analysis. Additionally, surface sediment was collected from an agricultural field (denoted Edge of Field in Figure 2-1; 44.23˚N 88.16˚W). Sediment bank, bar deposit, and streambed samples were collected by scraping and homogenizing surface sediment (< 5 cm depth) using a hand trowel to collect representative samples. Samples were collected in zip top polyethylene bags. Bank sediments were split into multiple samples based on observable differences in texture and color along the vertical profile. Samples were stored chilled (<4˚C) in the dark until analysis. Water samples were analyzed for SRP using EPA method 365.3 (U.S. EPA, 1978) less than 48 h after sample collection using the same UV/VIS spectrophotometer described in section 2.2.1. Sediments were ground and sieved through a 2-mm mesh to remove organic debris and small rocks prior to proceeding with calculation of equilibrium phosphorus concentration (EPC_0; mg L^{-1}; Inamdar et al., 2020), phosphorus exchange potential (PEP; log (mg L^{-1}); Simpson et al., 2021), and the phosphorus sorption index (PSI; mg kg^{-1}; Inamdar et al., 2020).

2.3.1 Equilibrium Phosphorus Concentration and Phosphorus Exchange Potential

Six solutions of SRP were created (0, 0.1, 0.5, 1, 5, 10 mg P L^{-1}) by dissolving KH_2PO_4 (same as described in 2.2.1) in ultrapure water. Calcium chloride dihydrate (($CaCl_2$)-2(H_2O); Fisher Scientific >99% purity; CAS: 10035-04-8) was used as a background electrolyte at a concentration of 100 mg Ca L^{-1} for all samples to match stream water chemistry. Each of different SRP and $CaCl_2$ solutions was mixed with each of the sediment samples in duplicate at a rate of about 1 g sediment (exact weight noted) per 20 mL solution. Samples were shaken in the dark for 20 h at 21 ± 2°C. After 20 h the supernatant was centrifuged at 2000 rpm for 15 min and then syringe filtered through 0.45 µm PES filters. The filtered solution samples were analyzed for SRP using standard colorimetric EPA method 365.3 (U.S. Environmental Protection Agency, 1978) on the same UV/Vis spectrophotometer as the other samples. The P sorbed on the sediment phase (q; in units of mg g^{-1}) after the 20 h of shaking was calculated using the equation:

6. $q = \frac{(C_0 - C_f)\,V}{m}$

Where C_0 (mg L^{-1}) is the initial P concentration prior to mixing, C_f (mg L^{-1}) is the final P concentration after 20 h of mixing, V is the solution volume (L), and m is the sediment mass (kg). q (y-axis) was plotted against C_f (x-axis). The equilibrium phosphorus concentration (EPC_0) is the value of C_f where q equals zero based on the range of values that produced a linear fit isotherm (W. A. House & Denison, 2000; Inamdar et al., 2020).

The phosphate exchange potential (PEP) is calculated as:

7. $PEP = \log_{10} EPC_0 - \log_{10} SRP$

When the EPC_0 is greater than SRP the sediment will release SRP and when EPC_0 is less than SRP the sediment will sorb SRP. Phosphorus exchange potential is a similar concept except it is scaled to be more comparative between sites and represents a potential with negative values indicating that sediment may remove phosphorus given proper conditions and release SRP given a positive value (Simpson et al., 2021).

2.3.2 Phosphorus Sorption Index (PSI)

The phosphorus sorption index (PSI) is a measure of the maximum sorption capacity of sediment (Inamdar et al., 2020). All sediment were treated in duplicate with a 73 mg P L^{-1} and 100 mg Ca L^{-1} solution created by dissolving KH_2PO_4 and $CaCl_2$ as a background electrolyte in ultrapure water (Inamdar et al., 2020). About 1 g of sediment was added to with 20 mL of the sorption solution in HDPE bottles and shaken in the dark for 20 h at 21 ± 2°C. After 20 h the supernatant was centrifuged at 2000 rpm for 15 min and then syringed filtered through 0.45 µm PES filters. The filtered solution samples were analyzed for SRP using EPA-365.3 method on the same UV/Vis spectrophotometer. The PSI (mg kg^{-1}) was determined using the equation found in Inamdar (2020):

8. $$PSI = \frac{(73\ mg\ P\ L^{-1} - C)\ V}{m}$$

Where C is the equilibrium P solution concentration (mg L^{-1}) after 18 h, V is the volume of solution (L), and m is the sediment mass (kg).

3.0 Results

3.1 Breakthrough Curve and 1-D Transport Model

Flow conditions were steady with discharges of $2.33x10^{-2}$, $4.34x10^{-4}$, and $2.78x10^{-2}$ m^3s^{-1} for the June Lower Plum Creek, November Upper Plum Creek, and November Lower Plum Creek tracer tests, respectively (Table 2-1). Peak tracer concentrations occurred simultaneously for all of the tracers (Figure 2-2a, 2-2b, 2-2c, 2-3a, 2-3b, 2-3c, 2-4a, 2-4b, and 2-4c). The SRP breakthrough curve from the June Lower Plum Creek was unusable due to particle SRP interaction and sorption that likely occurred in the mixing barrel (Benefiel, 2022) which prompted the methodological change noted in the previous section. Variability at the peaks of the Br^- and particles for June Lower Plum Creek injection (Figure 2-2a and 2-2b) resulted in modeled breakthrough curves peaks that were lower than measured data. The variability is decreased after the methodological changes and is visually observed when comparing the breakthrough curves of all three tracer tests (Figure 2-2a, 2-2b, 2-2c, 2-3a, 2-3b, 2-3c, 2-4a, 2-4b, and 2-4c). OTIS failed to parameterize the Upper Plum Creek data for the particles and PO_4^{3-} due to singular convergence errors (Figure 2-3b and 2-3c). Generally, to successfully parameterize the injections the effective channel area (A) and storage zone area (A_s) needed to increase for both particles and SRP compared to Br^- (Table 2-1). The dispersion coefficient and storage zone coefficients were of similar magnitudes across individual injections. The particles in tracer tests at Lower Plum Creek did not need to have reactive components (Eq 4 and 5) in order to successfully model the measured data. The Upper Plum Creek site needed first order decay components to model the breakthrough curve. Soluble reactive phosphorus needed every reactive parameter to be successfully

modeled. The Damkohler numbers (Eq 5) were not consistent across solutes and were calculated at $9.97x10^{1}$, 3.1, $8.78x10^{9}$, $1.19x10^{11}$, $1.92x10^{11}$, 7.0, 0.6, 0.4 for tracer tests 1, 2, and 3 along with solutes Br^{-}, particles, and SRP, respectively (Table 2-1).

3.1 Sediment and water column phosphorus characteristics

Equilibrium phosphorus concentrations varied between the two stream reaches. Lower Plum Creek generally had greater EPC_0 values than the upstream site (Table 2-2). At the upper site the bed sediment had the lowest EPC_0 value ($8.47x10^{-3}$ mg L^{-1}) followed by the side bank ($9.5x10^{-3}$ mg L^{-1}) and bar deposit ($1.26x10^{-2}$ mg L^{-1}) respectively (Table 2-2). At the lower site the lower side bank had the lowest EPC_0 value ($5.87x10^{-3}$ mg L^{-1}) and the upper side bank and stream bed had the same values ($1.21x10^{-2}$ mg L^{-1}; Table 2-2). The field sample from the edge of field site was the highest with an EPC_0 of $3.83x10^{-2}$ mg L^{-1}. The upper site had a lower SRP concentration ($3.35x10^{-1}$ mg L^{-1}) than the upper site (1.38 mg L^{-1}). At both sites, the PSI values greater than $1.3x10^{3}$ mg kg^{-1} in all sediment except the Upper Plum Creek side bank sample ($1.02x10^{3}$ mg kg^{-1}; Table 2-2). The PEP was negative for all samples suggesting a potential net uptake by the streambed (Table 2-2).

4.0 Discussion

4.1 Legacy phosphorus and the fine sediment cascade

Sediment in Plum Creek provides a storage mechanism for P in the stream channel that increases in the downstream direction. This in channel storage is reinforced by the longitudinal transport trends and the EPC_0 and PEP

results. The agricultural field (Edge of Field) location that was sampled had the largest sediment bound P of any of the sampled sediment (EPC_0 3.83 $x10^{-2}$ mg L^{-1}) and the PEP value closest to zero (-0.94 log (mg L^{-1}) (Table 2-2). Positive PEP values mean that sediment has a greater potential to release SRP to the surrounding water column and negative values indicate that SRP removal from the water column is more likely. Sediment loss from agricultural fields could explain why the Upper Plum Creek bar sample has a greater EPC_0 by an order of magnitude than the bank and bed samples; the bar sample is likely a combination of upland sourced sediment along with sediment derived from near channel sources. This is in agreement with other studies completed in the watershed. A geochemical fingerprinting study in Plum Creek found that sediment bound P represented 73% of the TP loads exported from the watershed at the Lower Plum Creek site (Fitzpatrick et al., 2019). The suspended sediment was composed of over 80% silt and clay sized particles with most of that sediment originating from bank erosion (44-51%) with gullies (24-25%) and ditches (11-22%) comprising the next largest sources of sediment over the course of the study (Fitzpatrick et al., 2019). Geochemical fingerprinting relies on unique sediment chemical characteristics to distinguish sources. Fitzpatrick et al. (2019) note that the ditch and some of the gully sediment sources may represent a combination of sediment being eroded from upland sources such as crop fields. Mixed geochemical fingerprints implies that cropland is likely to be contributing more than the 3 to 6% of the sediment loads as calculated in the study but the cropland was not chemically distinct enough to differentiate from native ditch

sediment (Fitzpatrick et al., 2019). In Lower Plum Creek, upland sources may also be diluted by the large amount of bank erosion located in the lower portion of the watershed that was indicated by the geomorphic assessment (Fitzpatrick et al., 2019). Patterns in event-scale TSS and SRP hysteresis and flushing indicated that in the upper watershed TSS and SRP sources were distal from the stream whereas the lower watershed had patterns that largely indicated near-channel contributions (L. A. Rose & Karwan, 2021) which agreed with the sediment source apportionment from the geochemical fingerprinting study by Fitzpatrick et al. (2019). Despite this influx of bank sediment (EPC_0 of 5.87 $x10^{-3}$ mg L^{-1}) the measured P in the bed sediment (EPC_0 of 1.20 $x10^{-2}$ mg L^{-1}) and water column (1.38 mg SRP L^{-1}) is greater than in the upper watershed suggesting increased P storage in the downstream direction.

The capacity of a sediment to bind phosphorus is critically important to overall P transport and processing within a stream. Although the field sediment sampled in Plum Creek had a negative PEP value, this is not the case in watersheds where agricultural P inputs create huge imbalances in the P distribution within a watershed. Agudelo et al. (2011) found that SRP patterns following storm events indicated that field sediment release SRP to stream water after sediment mobilizing precipitation events that was based on sediment sampling and EPC_0 evaluations. In that system, the fields represent a large store of phosphorus built up by a legacy of agricultural inputs. Stream sediment in this same system sorbed excess SRP, especially when discharge returned to base flow. Soluble reactive phosphorus removal by channel sediment, observed by

Agudelo and others, is similar to Plum Creek where bed and bank samples had EPC_0 values less than the field sampled location. The difference in Plum Creek is based on the water SRP concentrations; even if the field sediment are deposited into Plum Creek, high SRP levels in the stream water still favor SRP sorption to sediment rather than release to the water column. The PSI value of the Plum Creek sediment is high compared to other values in the literature (135 to 2564 mg kg^{-1}; Inamdar et al., 2020) which is likely due to the higher percentages of silt and clay sized particles due to the glacial history of the area (Fitzpatrick et al., 2019). The large sorption capacity of the sediment creates a circular loop where upland sediment sources are continually eroded into the stream channel and continue to build up P stores on the sediment due to the high SRP values in the water column. The sediments do not have an opportunity to lower these stores other than through biological uptake or removal from the channel. The elevated EPC_0 stream bed value from the lower watershed is probably a result of the accumulation of SRP-laden sediment that increases as SRP and sediment are transported downstream.

Injecting SRP through tracer tests provides another boundary on P transport within Plum Creek because of the importance of SRP to sediment-P interactions at base flow. Particles and SRP are mixing throughout transport events so tracking both SRP and particles during downstream transport is critically important to understanding channel processes relative to watershed scale mitigation. Based on the discharge and main channel cross sectional area parameters a conservative solute would take 541 d, or approximately one and a

half years, to reach the Lower Plum Creek site from the location of the Upper Plum Creek tracer test, should the average channel velocity remain constant between the Upper Plum Creek and Lower Plum Creek sites. Although flow increases during storms and with downstream distance (discharge at the USGS gauge near the Lower Plum Creek site varies from 0.2 to over 2000 m^3s^{-1}; U.S. Geological Survey, 2016), at base flow the water velocity is slow. Base flow is the primary flow condition observed in Plum Creek (L. A. Rose & Karwan, 2021), hence the slow velocity coupled with the high sorption capacity of the stream sediments promote P storage in the channel. This slow flow becomes important when considering the loss of SRP and particles to storage areas within the stream reaches at both the upper and lower sites. Lower Plum Creek tracer tests in June and November raised stream concentrations to 1.65 and 3.77 mg SRP L^{-1} along with 5.1 and 1.73 mg L^{-1} of particles. Within the 100-m reach span those concentrations were reduced to 0.58 and 1.24 mg SRP L^{-1} and 4.21 and 1.21 mg particles L^{-1}. At the Upper Plum Creek site, the tracer test raised stream concentrations to 14 mg SRP L^{-1} and 75 mg particles L^{-1}. These concentrations reduced to 3.95 and 4.23 mg L^{-1} of SRP and particles respectively at the sampling location 53-m downstream of the tracer test upper boundary. Some of the SRP loss could be attributed to sorption to the fine particles (Benefiel, 2022), but represents a common scenario where sediment and SRP are actively mixing during transport while at the same time sediment may be retained by biota, captured by channel features or simply fall from suspension. The rapid loss of particles and SRP at these base flow conditions aligns well with the literature that

indicates annual load is dominated by storm events, but base flow is a critical time for storage, retention, and biological uptake processes within the stream channels (Dolph et al., 2019; Jordan et al., 2012). The reactivity during base flow time periods, combined with the EPC_0 and PSI measurements taken within the watershed indicates fine sediment in Plum Creek serves as a sink for SRP under base flow conditions.

Stream geomorphology may further control the SRP-sediment interactions in the channel. Plum Creek discharge has a flashy response to precipitation inputs from storms with recession from peak flow occurring quickly at both the upper and lower portions of the watershed (L. A. Rose & Karwan, 2021). At base flow the channel has a step pool morphology where flow is minimal and sometimes stagnant through large pools that spill through riffles into the next pool. This pattern was found in nearly all of the reaches measured during the USGS rapid geomorphic assessment (Fitzpatrick et al., 2019). Slow flow promotes increased contact time between SRP from the water column and bed sediment that is likely allowing sorption to the sediment as indicated by the high PSI values (Table 2-2). Side banks that are above the typical base flow water level lack the nutrient inputs supplied by fertilization at upland agricultural sources and only have contact with nutrient rich water during high flow events. Thus stream banks tend to be lower in P stores than the channel and upland sources (Agudelo et al., 2011; Inamdar et al., 2020). Removal of sediment via floodplain storage could be an important part of this longer storage process and may provide long term P storage in the watershed. Despite flowing through a

narrow and entrenched valley, the upper bank sediment at the more downstream site had a greater EPC_0 value than the lower bank (Table 2-2) suggesting that P enriched sediment may have been deposited in the past and may be acting as a legacy P store. These deposits could be colluvial, from the surrounding hillslopes, or a combination of colluvial and fluvial. Currently, I do not have the data to determine the deposit origin.

4.2 Management considerations

Base flow transport experiment and sediment characterization results indicate that Plum Creek has the capacity to store large quantities of P within the watershed. My results largely agree with other research that has taken place in the watershed (Fitzpatrick et al., 2019; L. A. Rose & Karwan, 2021). Erosion of fine sediment with high P concentrations and high base flow SRP concentrations found within Plum Creek do not align with written water quality goals in the Plum Creek Watershed ("Nonpoint Source Implementation Plan for the Plum and Kankapot Creek Watersheds," 2014). Conservation practices that reduce sediment transport to streams are critical to reducing SRP in the channel. Keeping agricultural sediment retained on the fields and adjusting P fertilizer timing and input quantity will help keep P located within the upland source fields. Conservation tillage, filter strips, stream side buffers, cover crops, retention wetlands, and bioreactors are effective methods to reduce P and sediment loading to streams (Carstensen et al., 2020; Prosser et al., 2020; Ramesh et al., 2021; Schulte et al., 2017). Tile effluent discharged into a treatment wetland or filter strip would reduce sediment and SRP export directly to local ditches

(Hansen et al., 2021). Phosphorus drawdown techniques designed to remove P from a watershed through biomass removal without additional P fertilization has also been shown to reduce sediment P stores in agricultural fields and may be another method that could be employed in the watershed (Zhang et al., 2020).

Sediment and P transport could also be mitigated by promoting water retention within the watershed. Wetlands, increased vegetative cover, and slowing ditch flow through the use of swales or dams could help reduce peak flows and increase storm flow duration within Plum Creek (Davis et al., 2006; Jefferson et al., 2017; Winston et al., 2016). These water retention strategies lower the erosive capacity of storm events. Although water retention may be beneficial for reducing sediment erosion within stream channels (e.g. bank erosion), and the promotion of infiltration should allow SRP to sorb to available sediment within the soil profile, lowering SRP concentrations during base flow should also be a priority. The capacity of Plum Creek sediments to retain nutrients likely buffers the SRP entering the channel from sewage treatment plants, septic systems, riparian zones, base flow tile effluent, and manure along with the SRP being lost from agricultural fields during precipitation events (Withers & Jarvie, 2008). Ideally conditions need to promote SRP drawdown within the channel itself to eliminate stored P which could further buffer the effects of any upland nutrient and sediment sources entering the stream channel. Without further SRP source reductions, Plum Creek sediment will continue to bind SRP from the water column and continue building legacy P stores. If SRP reductions are unachievable, physical removal of P laden sediment could be

another mitigation strategy. The lower EPC_0 of the lower side bank suggests that sediment removal could expose sediments without elevated P concentrations. Although Plum Creek is finding equilibrium within its own channel, this fails to meet the water quality goals outlined in the FRW TMDL (“Nonpoint Source Implementation Plan for the Plum and Kankapot Creek Watersheds,” 2014).

4.3 Future modeling considerations

Modeling these reaches brought to light certain challenges when trying to mimic the export of sediment and nutrients within Plum Creek. Within reaches, the Damkohler numbers varied with solute with greater variation associated with Br^-. Low values could be due to short reach lengths or long exchange timescales because only a small amount of tracer may be interacting with the storage zone (Wagner & Harvey, 1997). High Damkohler numbers could mean solute exchange rates are fast which could be the case in the lower watershed where storage zones likely encompass area within water column eddies. Pool and eddy storage could also be high within these pools and are represented by the first order decay coefficients. These discrepancies could be due to the geomorphic nature of the stream, conditions during each tracer test, and from calculating these values for SRP and fine particles which are typically non-conservative or undergo other processes that may enhance retention within a stream reach. Future work could involve different transient-storage models or different parameter optimization methods to reduce parameter uncertainty (Kelleher et al., 2019; Ward et al., 2017).

Even though some of the Damkohler number values are high indicating uncertain parameter estimates, this work could be used in future modeling efforts. SWAT modeling performed on Plum Creek estimated that 95% of the sediment and sediment bound P stemmed from agricultural sources (Cadmus Group, 2012) which was contradicted by the geochemical fingerprinting study (Fitzpatrick et al., 2019). Previous model discrepancies along with the reach scale and biogeochemical assessment results from this study highlights the need to continue collecting field data to inform these modeling efforts. A reach scale model such as OTIS and the EPC_0, PEP, and PSI results from Plum Creek could be used to further parameterize watershed or field scale modeling efforts with any larger field or watershed scale model that incorporates stream dynamics into its framework.

5.0 Conclusions

This study paired a 1-D hydrologic model with biogeochemical laboratory methods to gain an understanding of the transport and storage processes within a highly impaired agricultural stream. Modeling efforts indicated that at base flow conditions transport is relatively slow, especially within the upper watershed and that even within the short study reaches fine particle and SRP loss occurs despite parameter uncertainty. Advection was slow at both the Upper and Lower Plum Creek sites. To travel 10 km a conservative solute would take 1.5 y, 72 and 25 d based on the advection of the Upper site and Lower site in June and November respectively. The EPC_0 and PSI values indicate that the sediment within the reach have a high capacity for removing SRP from the water column

and likely mitigate high SRP concentrations observed during the tracer tests and during water sampling for the biogeochemical portion of this study. The field location had the greatest level of sediment bound P compared to the within stream locations. This phosphorus loading presents challenges for land managers that need to continue promoting sediment and SRP retention on agricultural fields to mitigate the effects of downstream transport of SRP and SRP laden sediment to Green Bay in Lake Michigan.

Chapter 4: Beryllium-7 and Lead-210 Deposition Patterns at Mid-continental Locations, USA

1.0 Introduction

Sediment is a source of water quality degradation around the world when transported in excessive amounts for both drinking water supplies and aquatic ecosystems. Besides causing physical changes to streams and waterbodies (Naden, 2010; Wood & Armitage, 1997), sediments also transport chemical pollutants that sorb to the sediment surface. Sorbed pollutants can negatively affect downstream waterbodies, particularly if those pollutants are not retained by the sediment surface (Cappuyns et al., 2006; Richards et al., 2009). In particular fine sediment (clay and silt-sized particles) have been shown to sorb greater quantities of chemicals than larger sized particles due to increased reactive surface area (Du Laing et al., 2009; Huisman et al., 2013; Revelli & Ridolfi, 2003). The transport of these materials can lead to water quality degradation through the eutrophication in lakes, reduction of light transmission, smothering of aquatic vegetation, and the silting of streambed material that can negatively affect trout species, benthic organisms, and macroinvertebrates (Walling 2013, Brady 2007, Dodds et al 2008, Gooddy 2016, Sweka and Hartman 2001, Wood and Armitage 1997). Sediment delivery is a necessary geomorphic process,(Boedecker et al., 2020; Naden, 2010), however, when that delivery is excessive or facilitates the transport of chemical pollutants, negative consequences for aquatic ecosystems arise. The potential negative effects of

fine sediment delivery to aquatic ecosystems makes the study of particle movement a priority for land managers concerned with water quality.

Sediment provenance is difficult to track in the stream environment where sediment from a variety of sources may be present. Tracking sediment often requires using chemical signatures or fingerprints unique to those sources to tease apart the transport processes from the surrounding landscape (Walling, 2013). Chemical signatures or tracers, may be unique to the sediment themselves from their formation and parent materials or from anthropogenic influences that may mark sediment with excessive phosphorus, heavy metals, pesticides, or organic pollutants (Belmont et al., 2014; Brady & Weil, 2007; Gellis et al., 2016; Koiter et al., 2013; Walling, 2013). Zhang (2001) describes the ideal tracer as something that is strongly bound or incorporated into sediments, not used for biological processes, inexpensive, and easily measured. There is no universal tracer that meets these criteria perfectly or works well in every watershed. Several chemical tracers have been established in watersheds worldwide, including: fallout radionuclides (Mambit and Walling 2008, Blake et al 2009), sediment color (Martinez-Carreras et al 2010), stable isotopes (Fox and Papanicolaou 2007, Onstad et al 2000), plant pollen (Brown et al 2008), compound-specific stable isotopes associated with plant fatty acids (Gibbs 2008, Blake et al 2012, Hancock and Revill 2013), rare earth element oxides (Kimmoto et al 2005, Liu et al 2016), fluorescent dyes (Flurry and Wai 2002), and magnetic beads (Collins et al 2013).

Beryllium-7 (^{7}Be) and excess lead-210 ($^{210}Pb_{xs}$) are two short-lived fallout radionuclides that are used in the sediment fingerprinting community to determine the relative ages of sediment transported within a watershed (Mabit et al., 2014; Taylor et al., 2013; Walling, 2005). Both nuclides readily bind to sediment particle surfaces (Minning et al., 2015; Pawlowski & Karwan, 2019; Ryken et al., 2018; Taylor et al., 2012; Yang et al., 2015) when they come into contact, hence provides a way to distinguish surface from deeper sediment sources. Sediments near the surface, presumably in contact with precipitation, are considered relatively young and show higher levels of ^{7}Be and $^{210}Pb_{xs}$. Relatively young sediment is often a sign of sediment delivery from a surface erosion processes whereas relatively old sediment indicates delivery of sediment from deeper in the profile and/or previously buried sediment such as through gulley formation. Beryllium-7 (half-life ~53 d) is a cosmogenic radionuclide created by cosmic ray spallation of nitrogen and oxygen molecules in the upper atmosphere (Dunai & Lifton, 2014; Kaste et al., 2002). Production of ^{7}Be varies with the ~ 11 y solar cycle with production changing with cosmic ray delivery to the atmosphere. Large scale atmospheric processes also create seasonal deposition patterns (Belmont et al., 2014; A. P. Leppänen et al., 2010; Ari Pekka Leppänen & Paatero, 2013). The greatest deposition typically occurs during the spring through down welling of stratospheric air into the troposphere (D. M. Koch et al., 1996; D. Koch & Rind, 1998). The stratosphere is the primary ^{7}Be reservoir with minor production occurring in the upper troposphere (Dunai & Lifton, 2014). Lead-210 (half-life 22 y) is a product of the uranium-238 decay chain and is

found in the atmosphere and within the Earth surface (Noller, 2000). Lead-210 excess ($^{210}Pb_{ex}$) is created in the atmosphere when radon off-gasses from the soil surface the subsequent decay produces $^{210}Pb_{ex}$ or dust carrying the nuclide is transported by atmospheric processes and is later deposited to the surface of the Earth. Beryllium and lead are considered to be reactive and readily adsorbed by aerosols and sediment but there are uncertainties associated with their spatial distribution and input rates that are both typically assumed to be uniform (D. M. Koch et al., 1996; X. C. Zhang et al., 2001).

This assumption is often not valid because deposition varies spatially and temporally due to a variety of atmospheric processes. Precipitation “scavenges” aerosols from the atmosphere such that wet deposition makes up the majority of bulk deposition for both radionuclides and the atmospheric stores are often depleted or “washed” out at the beginning of precipitation events (Ali et al., 2011; Balkanski et al., 1993; Ishikawa, 2014). Inter-storm mixing can have a dramatic influence on the deposition patterns especially for ^{7}Be which is transported from the upper atmosphere versus $^{210}Pb_{ex}$ which ultimately has geogenic origins. Large storms with vertical mixing can mine ^{7}Be stores in the upper troposphere. In the mid-latitudes, mechanisms such as strong radiative cooling near the tropopause (Zierl & Wirth, 1997), gravity wave breaks (Land & Feichter, 2003), diabatic processes in convective and stratiform clouds (Poulida et al., 1996), and shear instability due to turbulence (Shapiro, 1980) promote stratosphere troposphere exchange and folding which can lead to storms enriched with ^{7}Be derived from the stratosphere. Sprenger et al. (2007) was able to show that at

potential temperatures between 290 and 350 K, Rossby waves account for about 70% of all stratosphere troposphere exchange. The timing of these exchanges does vary within storms and seasonally. Greater intensity cyclones and convective updrafts are more likely to promote and lengthen stratosphere troposphere exchange (Jaeglé et al., 2017) and events with higher cloud top height have been associated with greater ^{7}Be deposition (Karwan et al., 2016). Seasonally, the mid-latitudes see greater stratosphere to troposphere transport in the winter and spring at the peak of stratosphere circulation and larger troposphere to stratosphere transport has been observed in mid to late summer as convective updrafts build in the troposphere and reach the stratosphere (Gettelman et al., 2011; Stohl et al., 2003).

Although mechanisms for atmospheric deposition of ^{7}Be and $^{210}Pb_{ex}$ are largely known, due to sampling and measurement constraints these radionuclides are not commonly measured particularly at event timescales, which limits their broad usage by the sediment fingerprinting community (Mabit et al., 2014; Taylor et al., 2013). Both radionuclides emit low levels of gamma radiation during decay and because the radionuclides are not found in great abundance, researchers must make tradeoffs between sample size, sample frequency, and measurement constraints in terms of both cost per sample, detector availability, and the time required for measurement. Beryllium-7 in particular is limited by its short half-life which requires a large enough sample to be measureable in addition to requiring fast sample processing times so that it may be counted before no longer existing within a sample. This can have a direct influence on the

sampling frequency and requires the sampling location to be easily accessible. These tradeoffs may make the use ^{7}Be and $^{210}Pb_{ex}$ as sediment fingerprints prohibitive to researchers.

Due to these limitations, there have been a sparse number of published studies measuring both ^{7}Be and $^{210}Pb_{ex}$ in mid-continental locations within North America. I evaluated the bulk deposition patterns of ^{7}Be and $^{210}Pb_{ex}$ in Minnesota, a mid-continental location, from July of 2016 to February of 2020 and compare results with patterns expected from the literature. If ^{7}Be atmospheric deposition is seasonally effected by large scale atmospheric processes and annually effected by the solar cycle as indicated by the literature then ^{7}Be deposition will peak in the winter and spring when the troposphere receives down-welling air from the stratosphere and the annual deposition will decrease as the solar cycle moves towards its maximum. If $^{210}Pb_{ex}$ is seasonally effected then deposition should be limited or non-existent during the winter months when soils are frozen in Minnesota. At the precipitation event scale, I expect there to be a weak correlation between precipitation and fallout radionuclide deposition. Partway through the study period sampling was expanded to a second location with additional atmospheric chemistry data for a single season. Based on the literature I expect there to be a correlation between ^{7}Be and sulfate deposition along with a correlation between $^{210}Pb_{ex}$ and other geogenically derived atmospheric deposits. These results will add to the limited knowledge of fallout radionuclide deposition patterns in the upper Midwest and expand their utility as a sediment fingerprinting tool to the scientific community.

2.0 Methods

The St. Paul Weather Station (44.99°N 93.18°W) is a climate observatory located on the University of Minnesota St. Paul campus (Figure 3-1) that is close to laboratory space and analytical equipment required for ^{7}Be and $^{210}Pb_{ex}$ measurement. The site is surrounded by experimental agricultural fields primarily planted with corn and soybeans approximately 30-m away from the sampling site. The climate is continental with an annual average temperature of 13 ˚C with the highest monthly average temperature occurring in July (29 ˚C) and the lowest monthly average temperature occurring in January (-13 ˚C). The average annual precipitation is 793 mm with an annual snow depth of 1371 mm (*Minneapolis/St. Paul Climate Data*, 2022). The summer months receive the most precipitation during the year creating warm and humid summers; winters typically receive snowfall from November through March and are relatively dry and cold.

A second sampling location at the Marcell Experimental Forest was added for a single season at the National Atmospheric Deposition Program (NADP) sampling site. The additional sampling location presented an opportunity to try to link other atmospheric chemistry deposits with the fallout radionuclide deposition. The NADP site (47.53 N, 93.47 W) was established in July 1978. The climate at Marcell is continental with moist warm summers and dry cold winters similar to St. Paul, MN. From 1961 to 2019, the mean annual precipitation averages 787 mm (414-1105 mm)with snow typically present from November through March or April (Sebestyen et al., 2021). Absolute minimum and maximum daily air

temperatures range from -46 ˚C to +38 ˚C with a mean annual temperature of 3.5 ˚C.

Beryllium-7 and lead-210 samples were collected at the St. Paul Weather Station during individual precipitation events from July 2016 to December 2019 and at the Marcell Experimental Forest NADP site during the summer and fall of 2018 following the process detailed in Karwan et al. (2016). Acid-washed high density polyethylene bottles with 20.3-cm diameter funnels were placed on platforms approximately 1.5-m above the ground surface and away from any vegetation that could influence sample collection. Samples were collected after the conclusion of a storm event within 24 to 48 h. Sample collection at the Marcell Experimental Forest coincided with NADP sampling weekly around 9 AM every Tuesday. After retrieval the funnels were rinsed with dilute trace-metal grade hydrochloric acid and the rinse was added to the sample. Snow sampling occurred at a separate, sheltered location beginning in 2018 approximately 2.7 km away from the St. Paul Weather Station to avoid deposited snow from being entrained off the ground and deposited back into the sample. Samples that occurred during winter months prior to 2018 were rain events. Snow was collected in low density polyethylene bags set within a 0.22-m^2 HDPE container and was collected if there was 2.5 cm of snowfall. During select large snow events, multiple snowfall samples were collected and processed as separate samples provided the melted sample accounted for greater than 100 mL of liquid. If the samples did not contain at least 100 mL the bottle was combined with another sample. Once melted, the samples were acidified in acid-washed HDPE

bottles similar to the rain samples collected at the St. Paul Weather Station and the Marcell Experimental Forest.

The radionuclides were extracted from the acidified precipitation using cation and anion ion-exchange resins (Karwan et al., 2016; Komura et al., 2006). POWDEX-PCH (cation) is a sulfonated copolymer of styrene and divinylbenzene in the hydrogen form and POWDEX–PAO (anion) is a trimethylamine functionalized copolymer of styrene and divinylbenzene in the hydroxinde form. Both POWDEX resins contain 4.8 meq g^{-1} of exchange capacity. Approximately 6 g of each resin was added for each liter of precipitation to ensure the removal of all ions from the samples including the ^{7}Be and $^{210}Pb_{ex}$. Due to the sample acidification, both radionuclides are assumed to be in divalent soluble forms. Prior to the addition of the exchange resins a spike of stable Be and Pb ICP-MS standards were added to each sample in order to evaluate the recovery on the exchange resins (Canuel et al., 1990). Upon resin addition the samples were shaken vigorously for 10 min and left to settle overnight (16-24 h). A 15-mL supernatant aliquot was kept and analyzed by an ICP-MS (Perkin Elmer, Elan DRC-e; detection limit 1 µg L^{-1}) to ensure full removal. The balance of the Be and Pb not measured in the aliquot was assumed to be bound to the exchange resin; resin recovery averaged 99% on the subset of 34 samples that were analyzed. Stable Be and Pb were used to check the ^{7}Be and $^{210}Pb_{ex}$ recovery because the binding activity of the isotopes has been found equivalent to the stable counterparts (Mabit et al., 2014; Taylor et al., 2012).

The resins and the remainder of the supernatant were then oven dried (< 60˚C) and sealed in 95.7 mL (6.38 cm diameter, 3.0 cm height) acrylic jars for analysis on high-purity germanium gamma ray spectrometers (Canberra GX4018 Coaxial Detector and a Canberra Model BEGe 3825 Broad Energy Germanium Detectors). Each sample was counted for 48 h and attempts were made to analyze samples within 108 days (two ^{7}Be half-lives) of rainfall collection for ^{7}Be activity (Karwan et al., 2016). Blank subtraction was performed using an empty jar prior to peak area calculations which were computed using multi-channel peaks and the neighboring 5 channels bracketing each peak as background. Counting statistics, minimum detectable area (MDA), and counting limit were calculated using methods in Gilmore (2008). Beryllium-7 was centered at 477.7 keV with efficiency interpolation between ^{210}Pb at 46.5 keV, Americium-241 at 59.5 keV, Cadmium-109 at 88.0 keV, Cobalt-57 at 122.1 keV, and Cesium-137 at 661.7 keV using a mixed isotope standard (Eckert & Ziegler Analytics, Atlanta, GA). ^{210}Pb was centered at 46.5 keV with efficiency calculated using the same mixed isotope standard as used for ^{7}Be. Calculations and statistics used the same methods as for ^{7}Be. Minimum detectable area for a large number of samples was not met so further work will be needed to verify the utility of the samples and to check the MDA values.

The depositional time series was plotted for both ^{7}Be and $^{210}Pb_{ex}$ using examples found in Taylor et al. (2016) and included: a complete time series, aggregated seasonal patterns, ^{7}Be to $^{210}Pb_{ex}$, radionuclide deposition to precipitation depth, and the cumulative deposition of the radionuclides over the

sampling period from July 2016 to February 2020. The percent of each event deposition contribution to the cumulative deposition was divided by the percent of each event rainfall depth contribution to the cumulative rainfall and presented as a ratio as found in Taylor et. al. (2016). These analyses were chosen due to the exploratory nature of the project and the lack of published literature on the deposition patterns at a mid-continental location. All precipitation depths are listed as liquid water depths. Seasons were defined as summer (June-August), autumn (September-November), winter (December-February), and spring (March-May). Results from Marcell were compared to NADP datasets by utilizing paired scatterplots and principal component analysis (PCA). Paired scatterplots were chosen to quickly assess correlation with any other atmospherically deposited chemicals and either ^{7}Be or $^{210}Pb_{ex}$. The PCA was used in a similar manner; because PCA seeks to reduce the dimensionality of a dataset by finding orthogonal fits, biplots showcasing each variable contribution as a vector to the PCA is another way to check if any of the other variables are correlated to ^{7}Be or $^{210}Pb_{ex}$. If the vector direction and magnitude is similar to that of another chemical, that is indicative of correlation. Prior to running the PCA the data was centered by taking each sample value, subtracting the mean, and dividing by the standard deviation (Jollife & Cadima, 2016).

3.0 Results

3.1 St. Paul Weather Station

Event total precipitation depths averaged 16 mm (standard deviation (SD) 11 mm) over the sampling period and ranged from 1 mm to 56 mm for single

events between the 125 samples collected (Table 3-1, Figure 3-2a). Total precipitation was 1903 mm with 166 mm in 2016, 614 mm in 2017, 630 mm in 2018, and 492 mm in 2019.The season with the lowest precipitation (as liquid water) was winter with a mean depth of 12 mm (SD 8 mm) and ranged from 1 to 31 mm (Table 3-1, Figure 3-2 Figure 3-2a). Summer, spring, and autumn all had an average precipitation depth of 16 mm with SD of 10, 11, and 13 mm, respectively (Table 3-1). Summer accounted for the smallest range (3 to 35 mm) per precipitation event but accounted for the season with the most total precipitation and greatest number of precipitation events in all years except 2019 (Table 3-1, Figure 3-2a). Spring storms ranged from 3 to 46 mm of precipitation (Table 3-1, Figure 3-2a). Spring accounted for the second least number of events in all but the 2019 season and accounted for the season with the greatest precipitation in 2019. Autumn had the greatest range (3 to 56 mm) and the largest recorded precipitation event and the second most quantity of precipitation events of the sampling period (Table 3-1, Figure 3-2a).

Beryllium-7 averaged 1.14 (SD 1.68) +- 0.20 (SD 0.33) Bq L^{-1} and ranged from 0 to 9.97 Bq L^{-1} over the entire sampling period (Table 3-1). Seasonally, summer had the greatest input with an average of 1.42 (SD 2.18) +- 0.31 (SD 0.43) Bq L^{-1} that ranged from 0 to 9.97 Bq L^{-1} (Table 3-1). Autumn averaged 1.16 (SD 1.24) +- 0.14 (SD 0.21) Bq L^{-1} and ranged from 0 to 5.27 Bq L^{-1}(Table 3-1). Winter and spring event total inputs averaged 0.62 (SD 0.78) +- 0.10 (SD 0.26) and 0.87 (SD 1.26) +- 0.11 (SD 0.15) Bq L^{-1} respectively. Winter had the smallest range from 0 to 2.76 Bq L^{-1} whereas spring ranged from 0 to 4.58 Bq L^{-1}(Table 3-

1). Besides seasonal variations, ^{7}Be varied annually with deposition increasing in the spring/summer of 2018 (Figures 3-2b and 3-3b). That increase in deposition persisted through 2019 and resulted in precipitation events that were enriched with ^{7}Be with the proportion of deposition to precipitation depth values greater than 1 in the autumn of 2018 along with all 2019 seasons (Figures 3-4, 3-5).

Lead-210 excess also displayed annual variation with enrichment occurring from the start of sampling through winter 2017 (Figures 3-4, 3-5). Enrichment is defined as greater deposition relative to the precipitation depth across precipitation events and is quantified as the ratio between percent of cumulative deposition to percent of cumulative rainfall for single events. Enrichment did not occur again until the summer and autumn of 2019. Lead-210 inputs were more consistent than with an overall mean of 1.39 (SD 2.27) and an uncertainty of +- 0.78 (SD 1.15) Bq L^{-1} and seasonal means of 1.50 (SD 2.31) +- 1.09 (SD 1.30), 1.56 (SD 2.47) +- 0.74 (SD 1.17), 0.63 (SD 0.88) +- 0.38 (SD 0.89), and 1.35 (SD 2.31) +- 0.49 (SD 0.77) Bq L^{-1} for summer, autumn, winter, and spring, respectively (Table 3-1, Figure 3-2b). Overall the $^{210}Pb_{ex}$ ranged from 0 to 11.63 Bq L^{-1} with similar ranges in summer, autumn, and spring seasons. Winter had the narrowest range (0 to 2.81 Bq L^{-1}; Table 3-1).

3.2 Marcell Experimental Forest

Precipitation collected weekly over the summer and autumn of 2018 averaged 22 (SD 19) mm during the entire collection season with summer averaging 26 (SD 23) mm and autumn averaging 18 (SD 13) mm. Precipitation ranged from 2 to 66 mm (*National Atmospheric Deposition Program (NRSP-3)*, 2022). Summer and

autumn precipitation ranged from 5 to 66 mm and 2 to 38 mm respectively (Table 3-2; *National Atmospheric Deposition Program (NRSP-3)*, 2022).

Only two of the sampled weeks contained measurable $^{210}Pb_{ex}$ (Table 3-2) so it was excluded from any other analysis. Beryllium-7 averaged 2.20 (SD 1.33) +- 0.14 (SD 0.17) Bq L^{-1} and ranged from 0 to 5.67 Bq L^{-1}. Summer averaged 2.73 (SD 1.49) +- 0.17 (SD 0.18) with a range of 0.57 to 5.67 Bq L^{-1}. Autumn averaged 1.74 (SD 0.94) +- 0.10 (SD 0.15) with a range of 0 to 3.50 Bq L^{-1}. 59% of samples were enriched with ^{7}Be; of the 7 samples that had a ratio below 1, 5 of the samples were split between the beginning and the end of the sampling period such that the enrichment was greatest during the mid to late summer and early autumn seasons. Both Marcell and the St. Paul Weather Station showed similar seasonal patterns with greater deposition occurring in the summer compared to autumn. Marcell had slightly greater ^{7}Be deposition than the St. Paul Weather Station (2.20 +- 0.14 Bq L^{-1} versus 1.52 +- 0.20 Bq L^{-1}).

The NADP data was used to evaluate correlations with ^{7}Be using pairwise plots and PCA analysis (Figures 3-6, 3-7a, 3-7b, 3-7c, 3-8, 3-9; *National Atmospheric Deposition Program (NRSP-3)*, 2022). According to the pairwise plot, ^{7}Be was correlated with sulfate (SO_4^{3-}) and chloride (Cl^-; p-value < 0.1; Figure 3-6). When assessing the PCA analysis the first five principal components were able to account for 95% of the data variability. A criteria of 95% was used for the inclusion of principle components. Beryllium-7 contributed the most to components 3 and 5; sulfate and chloride were also both positively related to principal component 3 showing similar magnitudes. The pairwise plot showed a

similar correlation (Figure 3-6). In the biplot with principal components 1 and 2 (Figure 3-7a), ^{7}Be plots directly in-line with magnesium (Mg) but has less magnitude. Magnesium was not significantly correlated with ^{7}Be (correlation coefficient 0.303).

4.0 Discussion

A large number of variables affect the deposition of fallout radionuclides to the surface. Production of ^{7}Be is highly dependent on the galactic cosmic-ray flux which is dependent on the ~11 y solar cycle (Kulan et al., 2006; Lal et al., 1958; Masarik & Beer, 2009). This process results in about 67% of the ^{7}Be produced in the stratosphere and 33% produced in the upper troposphere (Kulan et al., 2006); this is in contrast to $^{210}Pb_{ex}$ which is dependent on the ^{238}U already present in soils and the off gassing of its daughter products to the atmosphere. Off gassing from the soil surface is highly contingent on soil moisture and the pore structure of the soils and sediment from which it originates (Noller, 2000). These processes represent two separate reservoirs at opposite ends of the troposphere and likely explains why ^{7}Be and $^{210}Pb_{ex}$ were found to be uncorrelated (Figure 3-8) at the St. Paul weather station and why the collection at Marcell yielded no detectable $^{210}Pb_{ex}$ but did contain ^{7}Be. Unless vertical mixing encompasses upwards movement from the ground surface and downward movement from the upper troposphere the radionuclides should not be correlated. Residence time in the atmosphere can be as short as 4 d but can average 10 d with sufficient vertical air mixing (Semertzidou et al., 2016). Few precipitation events showed any correlation between the radionuclides (Figure 3-

8). Instead, one radionuclide had greater measured activity than the other which resulted in most of the points falling near the x and y axis (Figure 3-8). The lack of correlation between ^{7}Be and $^{210}Pb_{ex}$ is emblematic and informative about the nature of precipitation events near the sampling location. Prior to 2018, the precipitation may have been more frontal in nature resulting in less intense precipitation over greater durations. The precipitation events with higher ^{7}Be during the summer of 2018 and over the course of 2019 may have been composed of more convective systems that were able to reach and remove the ^{7}Be from the reservoirs in the upper troposphere and lower stratosphere. Greater cloud top height is one metric that has been shown to be correlated with increased ^{7}Be deposition (Karwan et al., 2016) and may signal vertical mixing that reaches the upper troposphere and possibly beyond (Jagercikova et al., 2014; D. M. Koch et al., 1996; D. Koch & Rind, 1998). Greater intensity cyclones and convective updrafts are more likely to promote and lengthen stratosphere troposphere exchange in either direction (Jaeglé et al., 2017). Without these exchange events, stratosphere to troposphere exchange usually takes 1 to 2 years, far beyond the half-life of ^{7}Be. One interesting feature of the deposition dataset is that the winter samples of both 2018 and 2019 showed elevated ^{7}Be activity relative to previous samples suggesting that snow may scavenge ^{7}Be more efficiently than rain based on the winter rain samples collected in 2016 and 2017. This deposition pattern could be indicative of a longer term change in production based on the solar cycle or showcase the potential differences between snow and raindrop scavenging efficiency.

Besides the two-year variation cycle between the ^{7}Be and $^{210}Pb_{ex}$ the deposition varied seasonally as well. As a mid-continental location, Minnesota should receive greater stratosphere to troposphere transport in the winter and spring when stratosphere circulation is at its peak; the data suggests that increases in deposition do occur with ^{7}Be deposition increasing in the spring and building up to its peak in the summer. Larger troposphere to stratosphere transport has been observed in mid to late summer as convective updrafts build in the troposphere and reach the stratosphere (Gettelman et al., 2011; Stohl et al., 2003). While convective updrafts do provide a mechanism for upwards mobility within a storm that upward convection results in significant downward air mass movement and likely explains why ^{7}Be deposition commonly peaked in summer. Autumn and spring also had large influxes observed at the St. Paul weather station (Figure 3-2b) but there was greater deposition earlier during autumn and later during the spring. Lead-210 excess exhibited a similar pattern to ^{7}Be with the greatest deposition occurring in the summer. The shoulder seasons, spring and autumn, showed much greater variation between samples. Due to its need to be entrained after leaving the soil surface, soil conditions likely play a role in the observed variability during these times. Elevated soil moisture and frequent precipitation events could restrict off-gassing from the soil surface whereas precipitation that occurs after a period of drying may actually lead to greater loss due to impact with the soil surface (Joung & Buie, 2015). The lead isotopes lowest deposition occurred in the winter and is likely due to frozen soils

and snow cover reducing the vertical mixing and entrainment by air masses of $^{210}Pb_{ex}$ and its sister isotopes.

Even with changes in vertical and horizontal movement found within a storm the air movement does not guarantee a sample will be enriched with either ^{7}Be or $^{210}Pb_{ex}$ because of other factors that alter deposition. By calculating the proportion of radionuclide from a singular event to the cumulative total over the sampling period and the precipitation event rainfall depth divided by the cumulative rainfall total, a ratio can be found by dividing the ^{7}Be fraction by the precipitation fraction. That ratio shows the temporal variation of the radionuclide activity (Figure 3-4, 3-5). A value greater than 1 means the sample is enriched or not depleted for the given precipitation event. The enrichment is largely due to within storm processes related to precipitation scavenging which is simply the capacity of precipitation to capture aerosols and deposit them on the Earth surface. Low-intensity precipitation is highly efficient at removing large amounts of aerosols (Chate & Devara, 2005; Mohan et al., 2019; Taylor et al., 2016). Enrichment could indicate a couple of other scenarios such as a medium intensity storm that scavenges aerosols with relatively low activity. Values less than 1 may signify that a precipitation event lost or washed out of all of its radionuclide inventory prior to arrival at the sampling location, that there was simply low activity to begin with, or the precipitation intensity was so great that dilution occurred.

Studies that observed rainfall scavenging (Chate & Devara, 2005; Ishikawa, 2014; Mohan et al., 2019) are fairly rare but generally show support of

the idea that scavenging removes aerosols and delivers the bulk of the deposition early on during a precipitation event. Besides rainfall, snowfall and its crystalline makeup provide an ideal surface to sorb and remove aerosols from the atmosphere (Ishikawa, 2014). At the snow sampling location, five snowfall events were able to be collected to yield some idea about snowfall scavenging during the winters of 2018 and 2019. Of those five samples, four of the samples showed depletion between the first and second collected sample. One sample had the opposite effect where the radionuclide activity increased throughout the snowstorm. Eight other sample pairs were taken within 24 h of the first bottle collection which also provided a look at aerosol scavenging. This timeframe should still capture scavenging albeit not as effectively as intra-storm sampling (Balkanski et al., 1993; Mohan et al., 2019). Of those eight samples, six of the pairs began with a higher measured radionuclide activity that lessened upon collection of the second bottle. Two samples showed increases after the first bottle was collected, contradicting the idea of washout (Mohan et al., 2019). This shows that scavenging and reservoir depletion does not always occur. At most, depletion could last for five to twelve days which is the estimated residence time of aerosols within the troposphere (Balkanski et al., 1993; Papastefanou, 2009). However, realized depletion in near surface air is likely shorter than this considering that even within precipitation events the deposition is uneven similar to rainfall. Despite washout being well documented the relationship between deposition and precipitation was nearly non-existent and uncorrelated (Figure 3-9 and 3-10) in this study.

Even though within event deposition is highly variable, the cumulative deposition plots indicate the temporal and spatial variations suggest actual deposition may be predictable (Figure 3-11). The plots show that deposition patterns result in largely linear accumulation except at certain times where the line shifts horizontally or follows a different slope. The inflection points (change in slope) tend to correspond to a reduction in slope that appears to occur during the winter months for both ^{7}Be and $^{210}Pb_{ex}$. This seasonal change in deposition makes physical sense because frozen soils should limit $^{210}Pb_{ex}$ development from radon off gassing from the soil surface and even though snowfall is highly effective at scavenging aerosols from the atmosphere, St. Paul received relatively little winter precipitation in terms of both water yield and the sheer number of precipitation events compared to other seasons. Bulk deposition was collected in this study, however when split between wet and dry, the majority of aerosol deposition is delivered with precipitation (Kaste et al., 2002; Noller, 2000; Olsen, 1985; Papastefanou, 2009). If the inflection points or the processes and timing behind the inflection points could be identified, the linear relationship could be utilized to predict the ^{7}Be and $^{210}Pb_{ex}$ deposition patterns reducing the need for event-based sampling frequency; enough samples would be needed to establish the linear relationship with a focus on capturing the shifts that occur as deposition drops off during the shoulder season. Another option could be to try to use predictive modeling approaches such as a Kalman filter (Chatfield, 2000) which is able to predict time series based on limited samples with high uncertainty.

The samples from the Marcell Experimental Forest showed similar patterns to those found in St. Paul. The ^{7}Be data did differ and is correlated to precipitation depth (R^2 = 0.44; Figure 3-12). The deposition data was based on the collected volumes from the samples and not what was recorded at the NADP gauge. The gauge data and the sampled data measured the same except for the first sample because the funnel and bottle ended up tilted and not parallel to the ground, thus affecting the quantity collected. When plotted using the precipitation depth based on the actual mass collected, precipitation and radionuclide activity were more strongly correlated (R^2 = 0.69). Besides being weakly correlated to precipitation depth, the NADP datasets did not show any strong correlations that could make the technique be used in a predictive sense. The principal components could probably be used to predict ^{7}Be deposition, but that methodology would still require sampling a suite of other aerosols to maintain the validity of the components rather than using one or two as hoped. Mann et al. (2011) and Igarashi (1998) showed strong correlation between sulfate and ^{7}Be but that relationship did not exist for the Marcell dataset. This relationship has been surmised because there are large sulfate reservoirs located in the lower stratosphere similarly to ^{7}Be, making sulfate influxes representative of stratosphere troposphere exchange. Similar to St. Paul, a linear pattern was observed when plotting the cumulative deposition of the Marcell dataset (Figure 3-13).

In spite of only being sampled for a year, the samples from the Marcell Experimental Forest provided a location and setting different than the St. Paul

weather station. Including samples from another mid-continental location that experiences similar climatic processes provided another check on regional patterns based on the literature (D. M. Koch et al., 1996; D. Koch & Rind, 1998). The precipitation and deposition patterns were similar between the two sites which provides some validation that existing transport models may be right in assuming similar behavior and depositional records across broad areas (D. M. Koch et al., 1996; D. Koch & Rind, 1998). Similar patterns have also been shown at different geographical locations in Europe (Kulan et al., 2006). Despite similar patterns observed at the St. Paul Weather Station and the Marcell Experimental Forest, long-term monitoring would be the best way to check if patterns remained the same or changed compared to the data collected in St. Paul. Capturing a full solar cycle or multiple solar cycles would provide a better means of comparison. Long term sampling would also be useful for $^{210}Pb_{ex}$ monitoring; it would be interesting to see if off gassing could be related to land use changes that disturb the soil upwind of the monitoring locations.

If sampling were to continue long-term there are a number of improvements that could be made to the sampling protocol. Weekly samples are more advantageous than event-based sampling for a variety of reasons. Time series statistics are easier to employ with a regular sampling interval. For my work, these statistics were not effective because of the storm-based sampling regime, data gaps during the winter of 2016 and 2017, and the sampling duration. Although four years is a long record from the perspective of the sediment fingerprinting community, it is not long enough to maximize time series

statistics. The statistics rely on data structured in a particular way, such as long-term and regularly sampled datasets. Gamma detection is time intensive and because it is a specialized niche within atmospheric sciences, geochronology, and sediment fingerprinting most labs are detector limited. At one point, procedural protocol modifications were made to speed up lab processing times to avoid ^{7}Be depletion due to an influx of additional samples from other projects that increased the time needed prior to gamma analysis. This modification helped alleviate pressure on the lab resources at the time of implementation, but success waned as the lab continued receiving more samples; when plotted the distribution of sample collection date to gamma analysis date remained unchanged. Weekly sampling would alleviate some of that pressure by reducing samples. The other main modifications would be to increase the counting times along with the funnel size. I presented a full dataset, however a large amount of samples were below the minimum detectable area (MDA) despite being counted for 48 h. Thus the dataset is still considered in its preliminary stages until it can be further reviewed. Increasing the counting time and funnel size should increase the gamma radiation measured by the detectors in order to capture low activities within samples. Lead-210 excess in particular was below the MDA for the majority of samples but because MDA is individually calculated, the MDAs for $^{210}Pb_{ex}$ require much larger activities compared to the MDAs that were calculated for ^{7}Be. Luckily, the 22 y half-life of lead means that the samples could be recounted for a longer timeframe to obtain new measurements. The longer count time should reduce the MDA. Initial ^{7}Be samples were also below the MDA,

however the second half of the dataset was above the MDA. I chose to work with the whole dataset because activity was still measured and patterns were still evident making the exercise and analysis still useful for future lab efforts.

5.0 Conclusion

Fallout radionuclide datasets are uncommon in the literature, especially in the sediment fingerprinting community. Detector availability and the need to count samples containing ^{7}Be on a short timeframes limit its broad use. Datasets also tend to be shorter based on the sediment study duration rather than with a goal of developing a long-term deposition dataset. I collected precipitation samples from 2016 through 2019 to measure ^{7}Be and $^{210}Pb_{ex}$ at a mid-continental location and assess any potential patterns in hopes of supporting the sediment fingerprinting community.

Samples were collected starting in the summer of 2016 and continuing through early winter of 2019. Between 2016 and the beginning of 2018 $^{210}Pb_{ex}$ had greater deposition than ^{7}Be but the relationship was reversed with ^{7}Be having the greatest deposition beginning in 2018 and continuing until the end of the sampling period in 2019. Seasonally, summer resulted in the greatest deposition and also coincided with the greatest number of precipitation events compared to other seasons. Autumn typically had the next greatest deposition and number of precipitation events, but spring deposition was within the variation observed in autumn. Neither ^{7}Be nor $^{210}Pb_{ex}$ were correlated with precipitation depth or each other which suggests important event based, seasonal, and annual differences in the vertical mixing dynamics of precipitation events.

Precipitation scavenging was observed, but did not occur during every event or series of precipitation events. During the summer and autumn of 2018 additional samples were collected at the Marcell Experimental Forest. Those samples showed similar patterns to the samples collected at the St. Paul weather station; only ^{7}Be was found in detectable levels. Beryllium-7 was compared to NADP data; the comparison showed slight correlation to sulfate and chloride but the correlation is not strong enough to be of predictive value. The cumulative deposition plots linearly through time with a number of inflection points that largely correspond to winter deposition. This linear relationship could be used to fill in data gaps, reduce the required number of samples, or possibly be used in a predictive manner for future projects that rely on radionuclide deposition datasets.

Illustrations and Tables

Table 1-1 Scores using % slope and hydrologic soils group to indicate areas for revegetation. Hydrologic soils group describes the infiltration capacity or water transmission rate of a soil and is denoted by letters A, B, C, and D going from well drained to very poorly drained soils. Combinations show what the drainage would be like in well drained versus poorly drained soils. Scores range from 2 to 9 with 9; a score of 6 and above is high priority; a score of 4 to 5 is mid-priority; and a score less than 4 is low priority.

% Slope	>25	15-25	7-15	4-7	2-4	< 2	Hydrologic Soil Group	C, D, C/D	B, B/D, A/D	A
Component Score	6	5	4	3	2	1		3	2	1

Table 1-2 Sub-watershed comparison of Total Phosphorus (TP) and Sediment export from modeled fields in Plum Creek and the Lower East River to U.S. Geological Survey gauge data Annual average modeled results are the summation of high priority, mid-priority, and tile drained field phosphorus and sediment export based on 35 y of simulations.

		Modeled				Measured		
Sub-watershed	Material Exported	Tiled	High Priority	Mid-Priority	Total	USGS Gage	Annual Mean	Range
Plum Creek	TP (Mg yr^{-1})	2.33	5.54x10^{-1}	3.36	6.23	04085119 (Sampled 2012-2017)	1.24x10^{1}	6.12-1.87x10^{1}
	Sediment (Mg yr^{-1})	2.23x10^{3}	1.19x10^{3}	4.63x10^{3}	8.05x10^{3}		6.61x10^{3}	3.16x10^{3}-1.16x10^{4}

		Modeled				Measured		
Sub-watershed	Material Exported	Tiled	High Priority	Mid-Priority	Total	USGS Gage	Annual Mean	Range
Lower East River	TP (Mg yr^{-1})	1.61	1.18		2.74	04085119 (Sampled 2004-2006)	$3.51x10^{1}$	$1.73x10^{1}$ - $6.26x10^{1}$
	Sediment (Mg yr^{-1})	$1.61x10^{3}$	$2.39x10^{3}$		$3.99x10^{3}$		$9.35x10^{3}$	$2.42x10^{3}$ - $2.06x10^{4}$

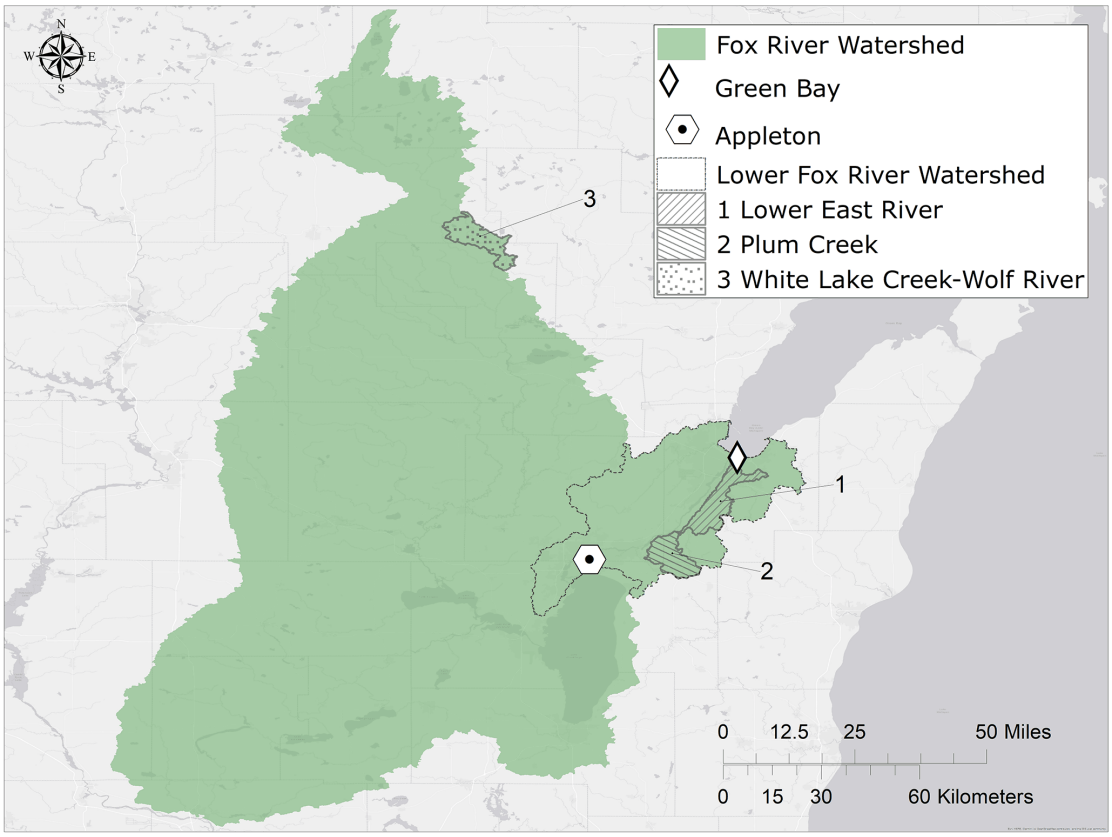

Figure 1-1 Fox River Watershed (FRW) and the Lower FRW. Three sub-watersheds are highlighted and include 1) the Lower East River (LER) 2) Plum Creek (PC) 3) White Lake Creek-Wolf River (WLCWR).

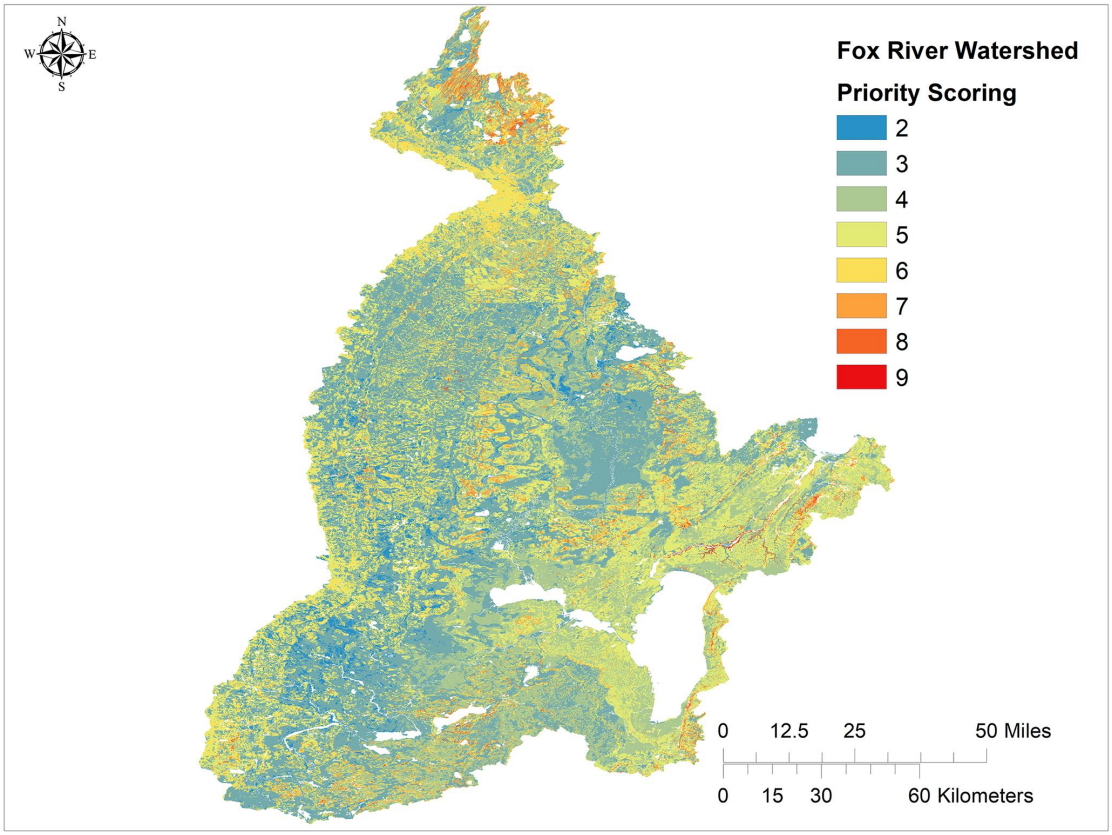

Figure 1-2 Priority Scoring Results for the FRW based on slope and soil hydrologic drainage class. Hydrologic soil group and slope were scored and the values assigned to 10-m grid cells. Grid cells with a score greater than 6 were classified as high priority; a score from 4 to 5 was classified as mid-priority; and scores less than 4 were classified as low priority.

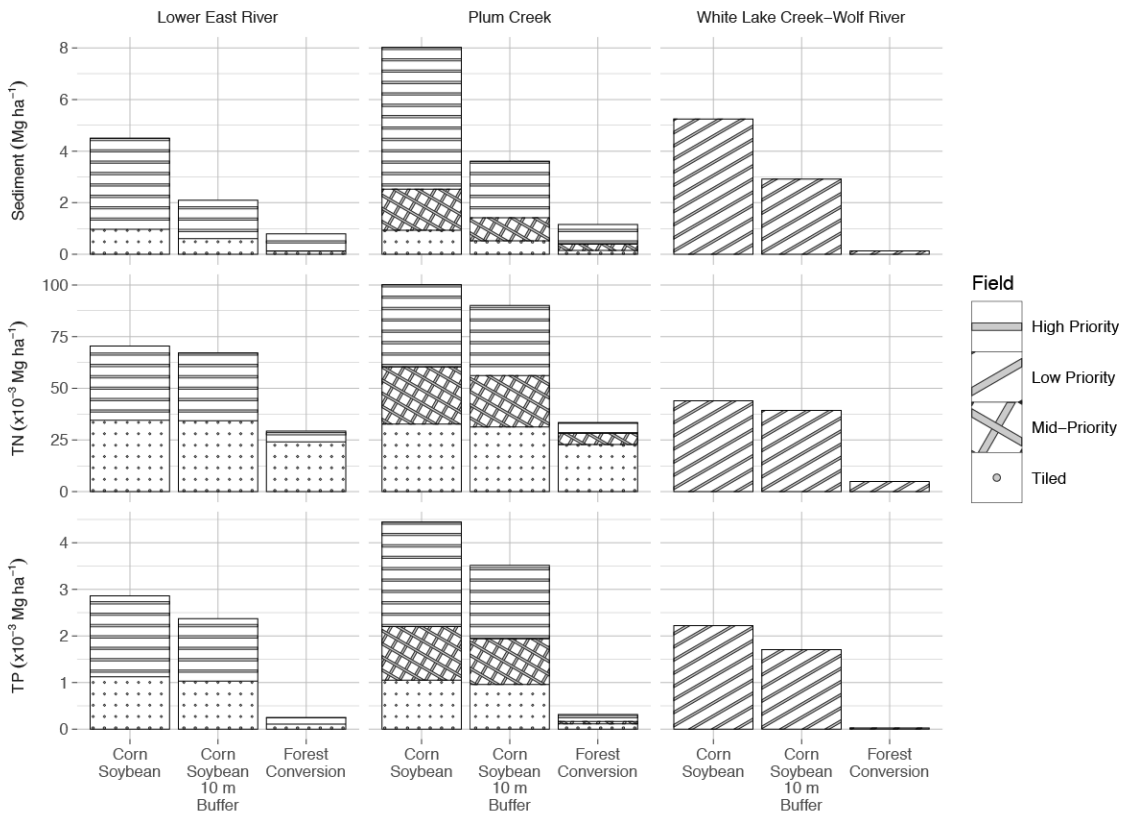

Figure 1-3 Nutrient Tracking Tool (NTT) modeling results for sediment, total nitrogen (TN), and total phosphorus (TP) in the Lower East River (LER), Plum Creek (PC), and White Lake Creek-Wolf River (WLCWR) for all, high priority, mid-priority, and tiled fields.

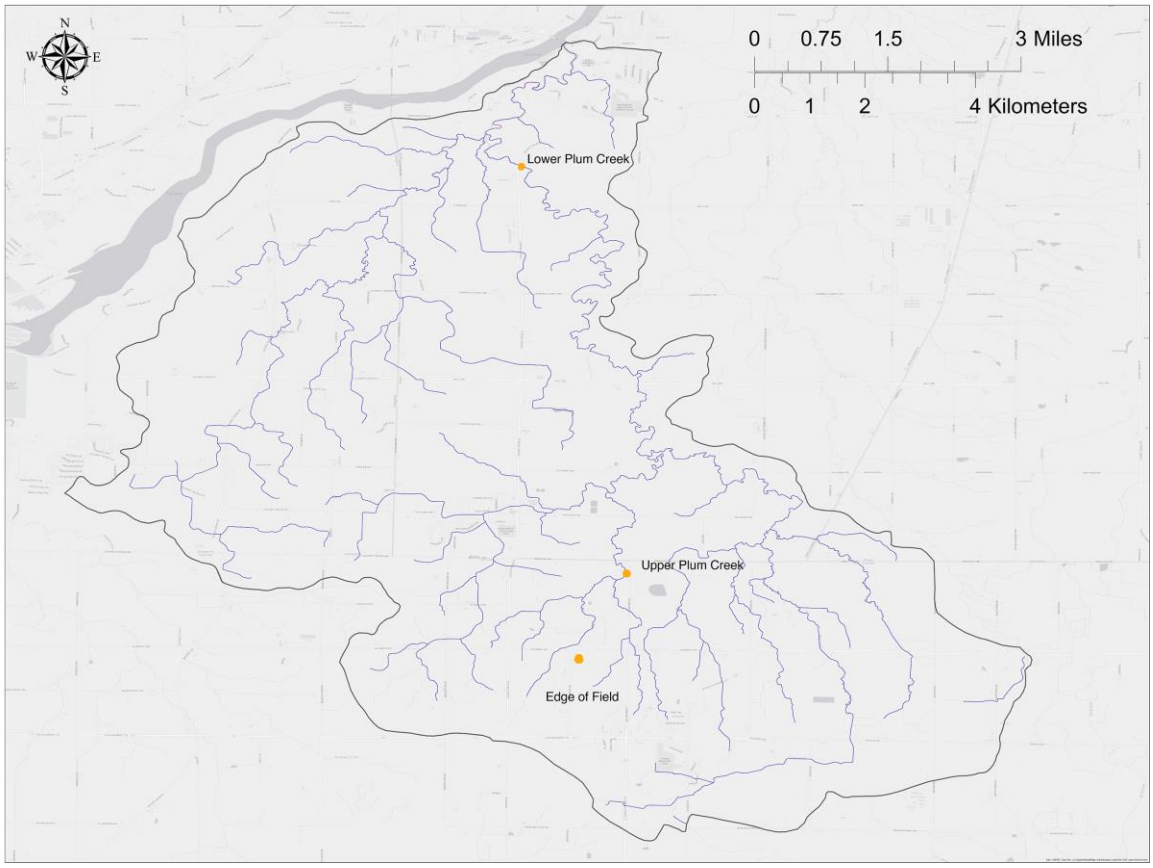

Figure 2-1 Plum Creek, WI with sites of field experiments and sample collection noted. Sediments were collected and tracer tests completed within reaches at the Lower and Upper Plum Creek locations. The Edge of Field location was the site of sediment sampling that was used to determine the equilibrium phosphorus concentration, phosphorus saturation index, and phosphorus exchange potential.

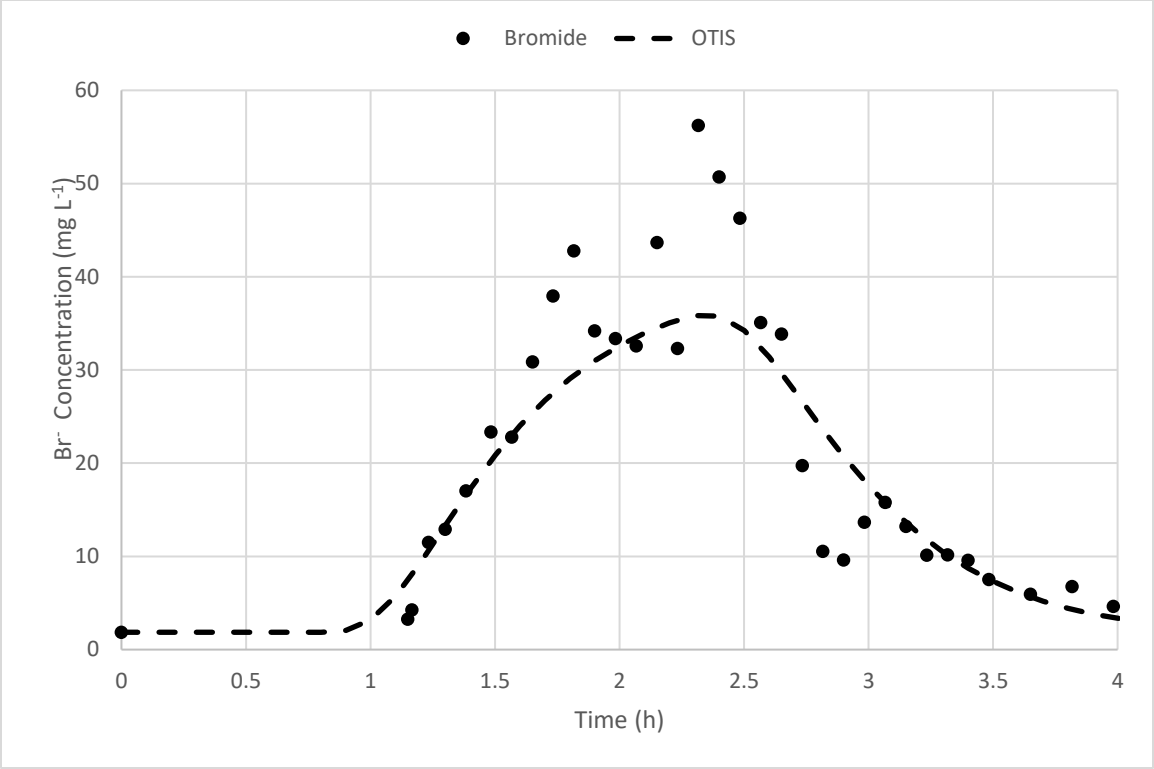

Figure 2-2a Break through curves for Lower Plum Creek. The figure depicts measured concentration data (mg/L) for bromide (Br^-) and the modeled OTIS values for the June 2019 tracer test.

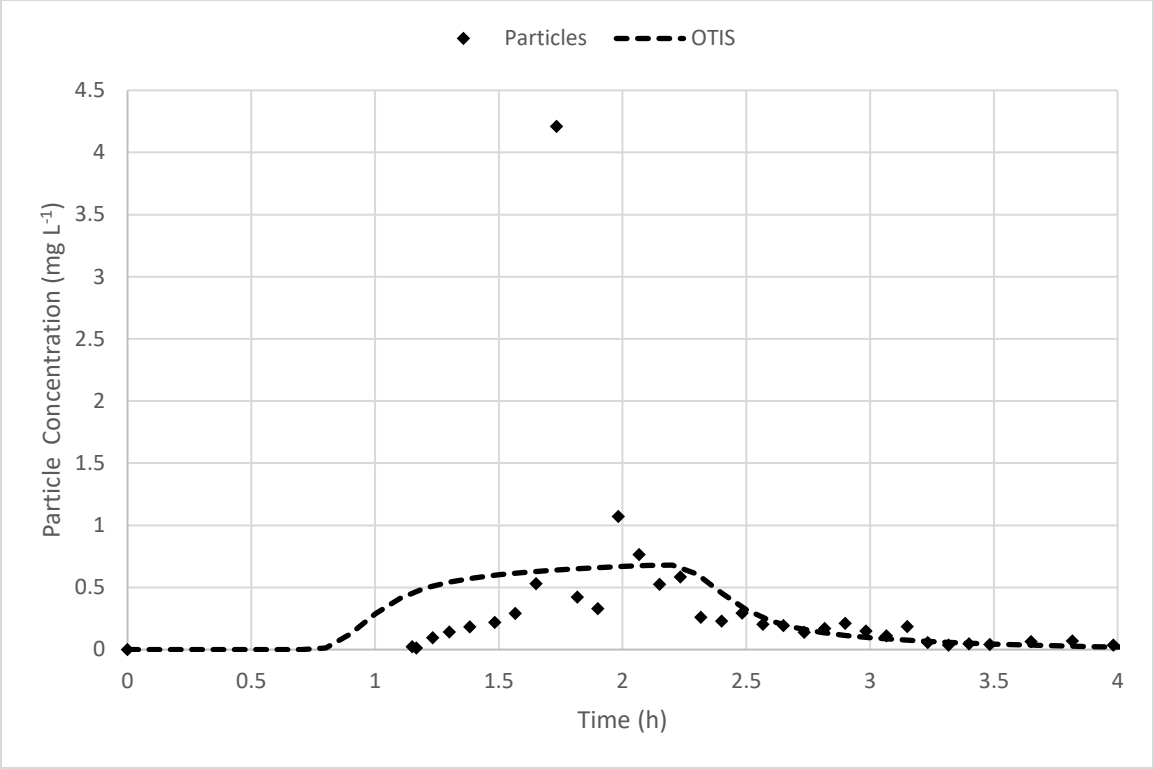

Figure 2-2b Break through curves for Lower Plum Creek. The figure depicts measured concentration data (mg L^{-1}) for particles and the modeled OTIS values for the June 2019 tracer test.

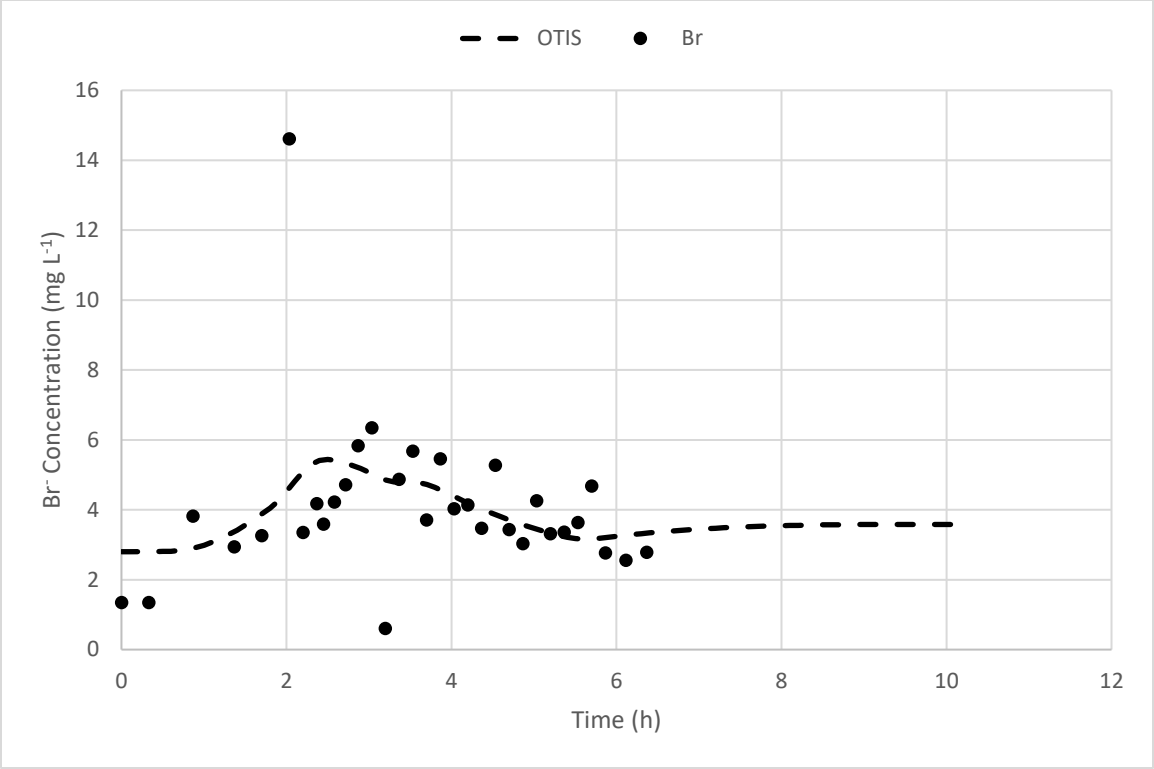

Figure 2-3a Break through curves for Upper Plum Creek. The figure depicts measured concentration data (mg L^{-1}) for bromide (Br^-) and the modeled OTIS values for the November 2019 tracer test.

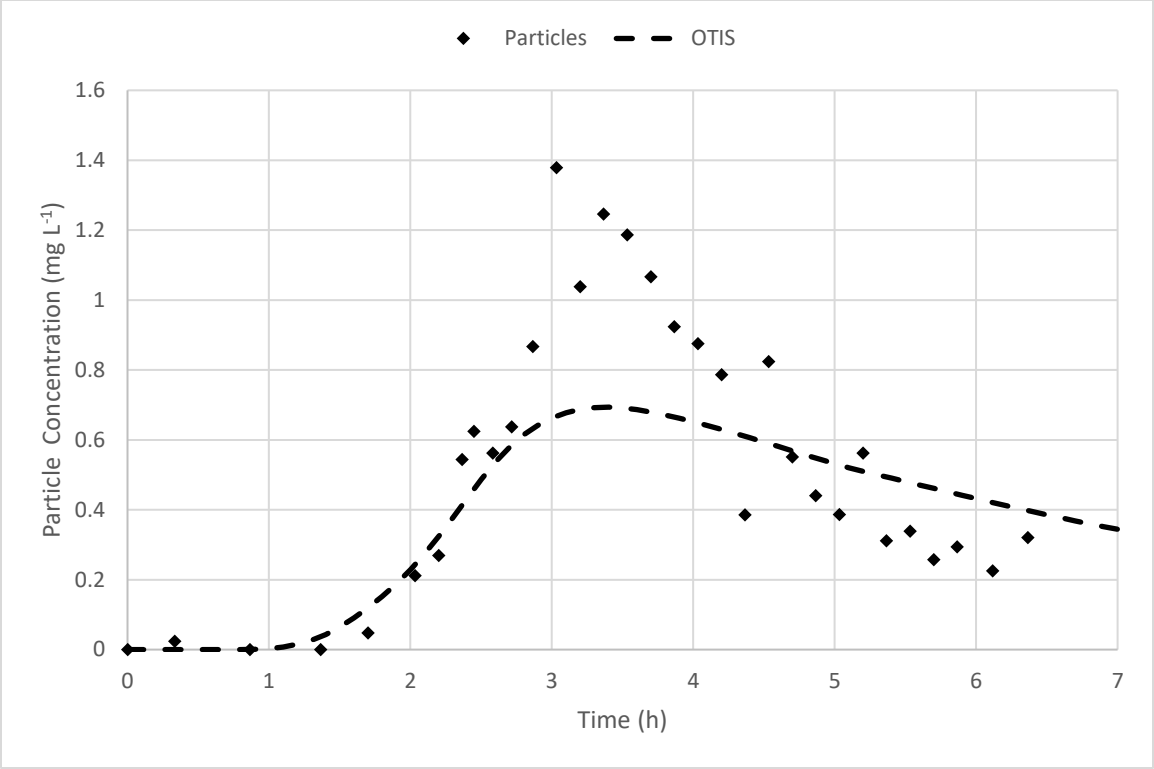

Figure 2-3b Break through curves for Upper Plum Creek. The figure depicts measured concentration data (mg L^{-1}) for particles and the modeled OTIS values for the November 2019 tracer test.

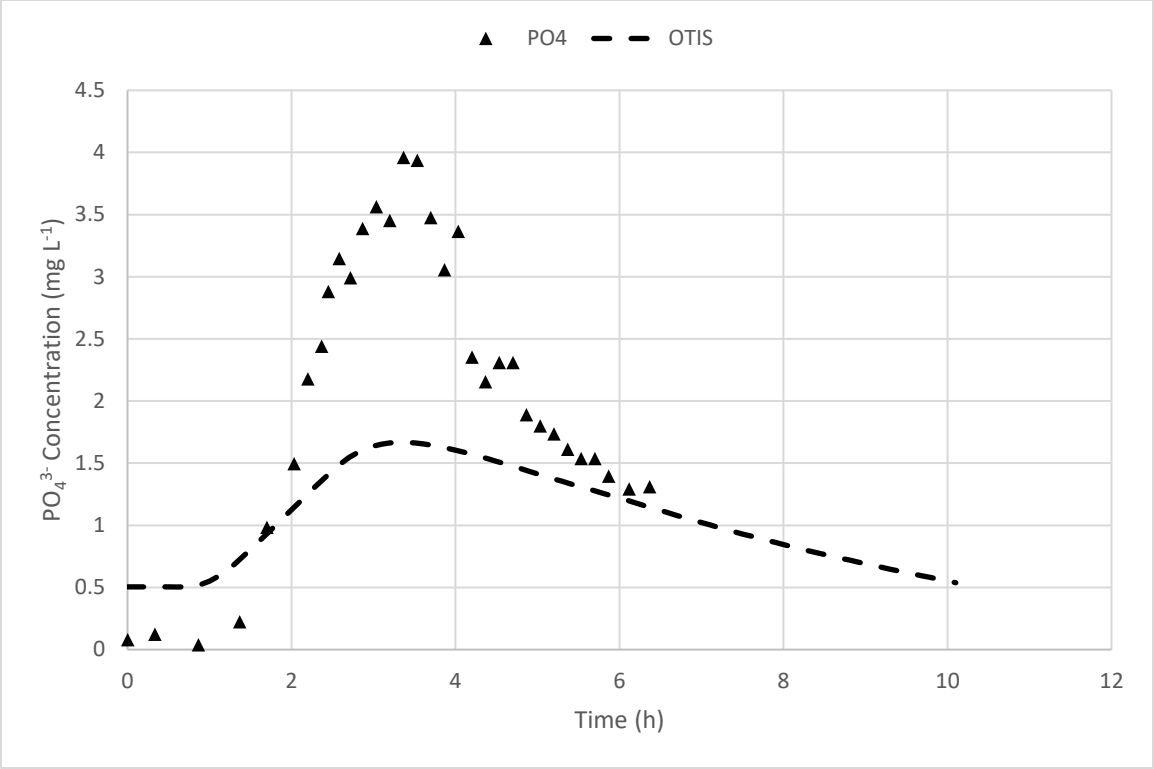

Figure 2-3c Break through curves for Upper Plum Creek. The figure depicts measured concentration data (mg L^{-1}) for phosphate (PO_4^{3-}; bottom) and the modeled OTIS values for the November 2019 tracer test.

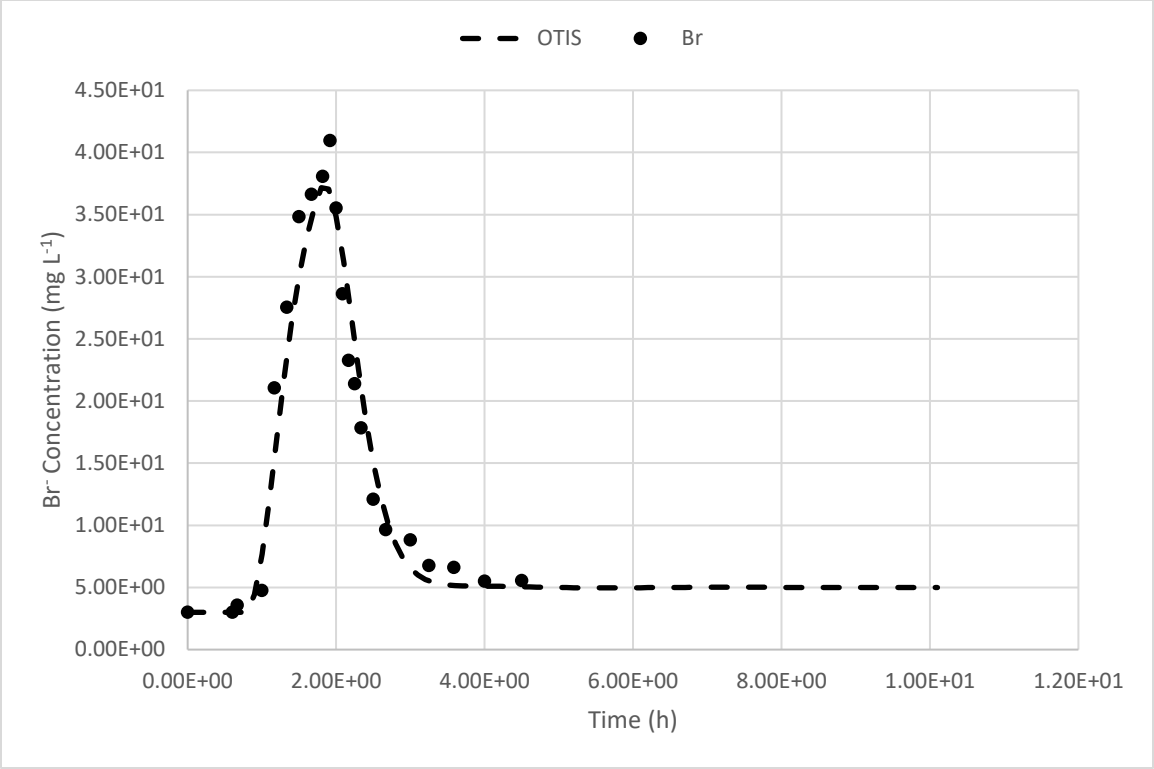

Figure 2-4a Break through curves for Lower Plum Creek. The figure depicts measured concentration data (mg L^{-1}) for bromide (Br^-) and the modeled OTIS values for the November 2019 tracer test.

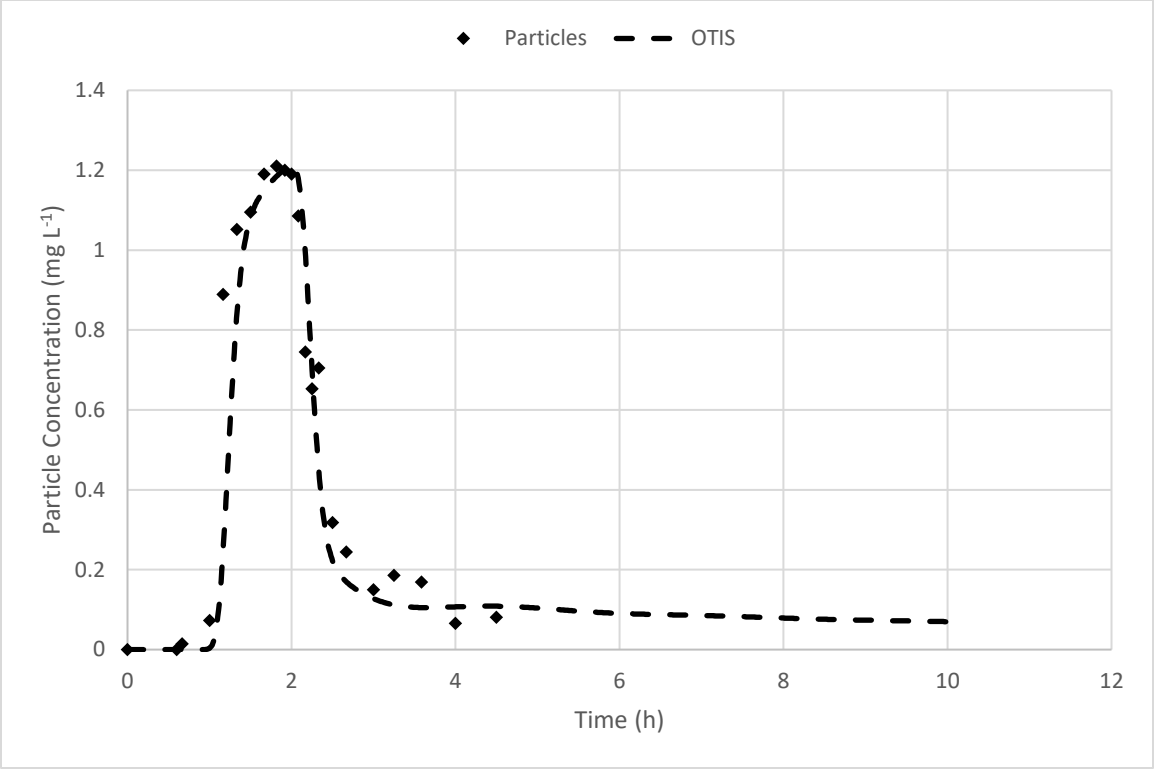

Figure 2-4b Break through curves for Lower Plum Creek. The figure depicts measured concentration data (mg L^{-1}) for particles and the modeled OTIS values for the November 2019 tracer test.

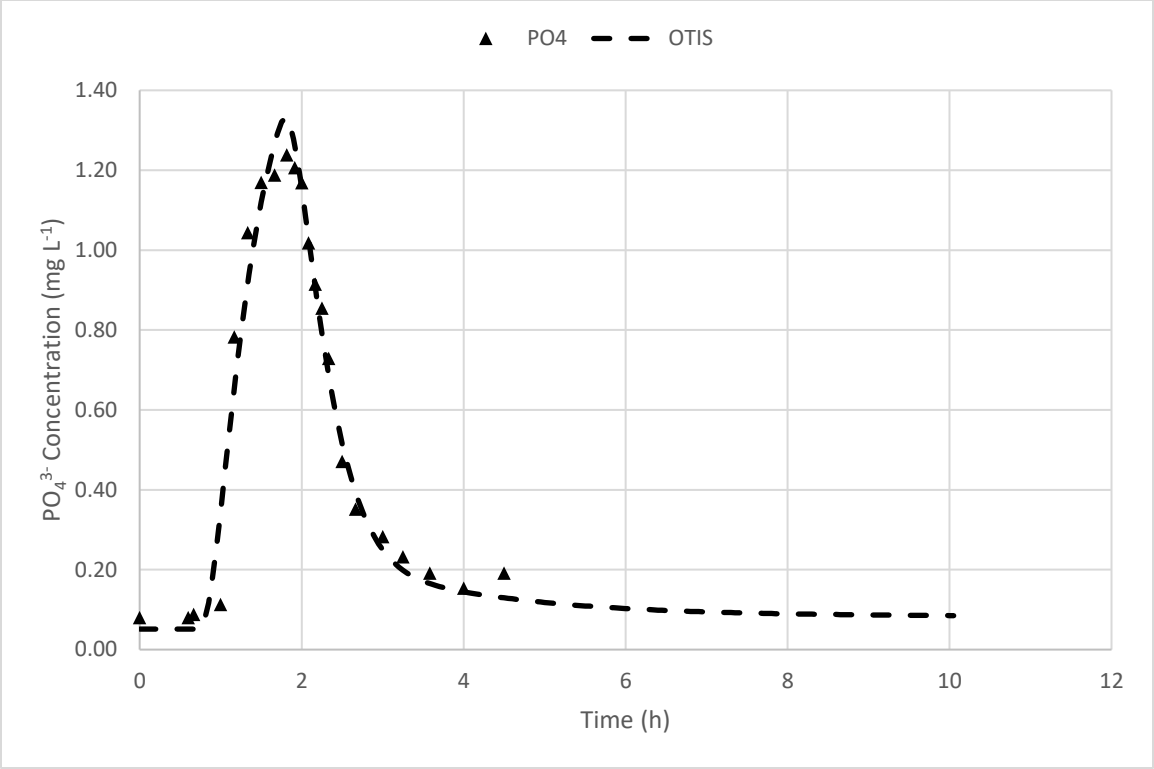

Figure 2-4c Break through curves for Lower Plum Creek. The figure depicts measured concentration data (mg L^{-1}) for phosphate (PO_4^{3-}) and the modeled OTIS values for the November 2019 tracer test.

Table 2-1 Parameters for completed OTIS models including Damkohler numbers.

	JUNE LOWER PLUM CREEK			NOVEMBER UPPER PLUM CREEK			NOVEMBER LOWER PLUM CREEK		
PARAMETER	Br	Particles	PO4	Br	Particles	PO4	Br	Particles	PO4
DISCHARGE (Q; M^3S^{-1})		$2.33x10^{-2}$			$4.34x10^{-4}$			$2.78x10^{-2}$	
AREA (A; M^2)	$6.00x10^{-1}$	$7.49x10^{-1}$		8.14	$8.75x10^{-1}$	1.66	$2.5x10^{-1}$	$6.7x10^{-1}$	1.03
DISPERSION COEFFICIENT (D)	$3.5x10^{-1}$	1.18		3.44	$3.70x10^{-1}$	$5.25x10^{-1}$	$1.14x10^{-2}$	$6.4x10^{-2}$	$6.37x10^{-1}$
STORAGE ZONE CROSS SECTIONAL AREA (AS; M^2)	$1.1x10^{-1}$	$2.97x10^{2}$		$2.67x10^{2}$	5.61	$1.57x10^{1}$	$5.17x10^{-1}$	1.79	$1.31x10^{1}$
STORAGE ZONE COEFFICIENT ALPHA	$6.0x10^{-3}$	$9.67x10^{-4}$		$1.20x10^{4}$	$1.35x10^{6}$	$1.20x10^{4}$	$5.25x10^{-3}$	$1.75x10^{-4}$	$1.02x10^{-4}$
MAIN CH DECAY RATE (LAMBDA; S^{-1})						$1.0x10^{-4}$			$1.411x10^{-4}$
STORAGE DECAY RATE (LAMBDA2; S^{-1})						0			$2.61x10^{3}$
MAIN CH SORPTION RATE COEFFICIENT (LAMBDA 3; S^{-1})									$1.85x10^{-4}$
STORAGE ZONE COEFFICIENT (LAMBDA 4; S^{-1})									$1.91x10^{6}$
MASS OF SED/VOLUME OF WATER (RHO)									$1.52x10^{3}$
DISTRIBUTION COEFFICIENT (KD)									$3.58x10^{-4}$
DAMKOHLER NUMBER	$9.97x10^{1}$	3.12		$8.78x10^{9}$	$1.19x10^{11}$	$1.92x10^{9}$	7.00	0.58	0.41

Table 2-2 Sediment and water column phosphorus metrics for tracer test reaches and an edge of field location.

Location	Deposit Type	Equilibrium Phosphorus Concentration (mg L^{-1})	Water SRP (mg L^{-1})	Phosphorus Exchange Potential	Phosphorus Sorption Index (mg kg^{-1})
Upper Plum Creek	Stream Bed	$8.47x10^{-3}$	$3.35x10^{-1}$	-1.60	$1.37x10^{3}$
	Stream Bar	$1.26x10^{-2}$	$3.35x10^{-1}$	-1.42	$1.32\ x10^{3}$
	Side Bank	$9.51x10^{-3}$	$3.35x10^{-1}$	-1.54	$1.02\ x10^{3}$
Lower Plum Creek	Upper Side Bank	$1.21x10^{-2}$	1.38	-2.06	$1.31\ x10^{3}$
	Stream Bed	$1.20x10^{-2}$	1.38	-2.06	$1.32\ x10^{3}$
	Lower Side Bank	$5.87x10^{-3}$	1.38	-2.37	$1.37\ x10^{3}$
Edge of Field	Ag. Field	$3.83x10^{-2}$	$3.35x10^{-1}$	-0.94	$1.33\ x10^{3}$

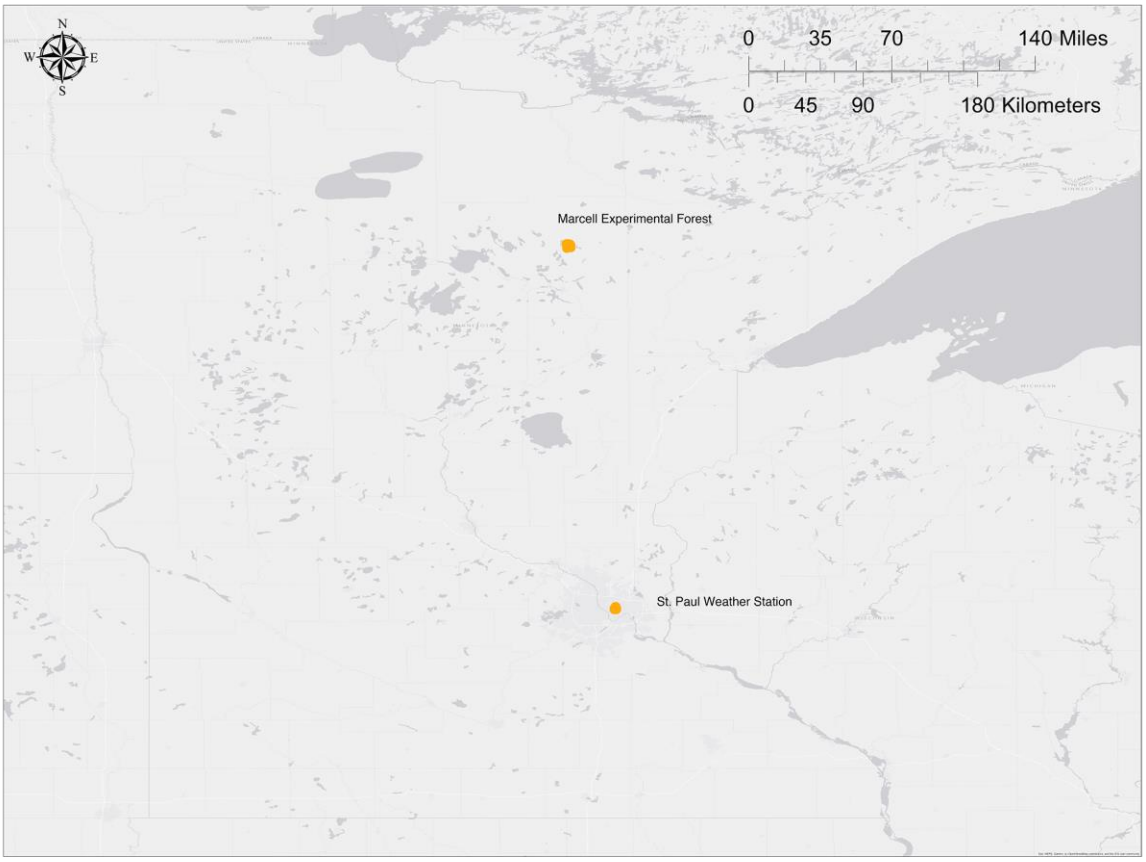

Figure 3-1 St. Paul Weather Station and the Marcell Experimental Forest.

Table 3-1 Summary Statistics for the St. Paul Weather Station and Marcell Experimental Forest Precipitation and Radionuclide Deposition.

Location	Season	Metric	Precipitation Depth (mm)	^{7}Be (Bq L^{-1})	^{7}Be (Bq L^{-1}) Uncertainty +-	^{7}Be (Bq m^{-2})	^{7}Be (Bq m^{-2}) Uncertainty +-	$^{210}Pb_{ex}$ (Bq L^{-1})	$^{210}Pb_{ex}$ (Bq L^{-1}) Uncertainty +-	$^{210}Pb_{ex}$ (Bq m^{-2})	$^{210}Pb_{ex}$ (Bq m^{-2}) Uncertainty +-
St. Paul Weather Station	*Summer*	Mean	16	1.42	0.31	15.48	1.68	1.50	1.09	15.45	6.22
		Std Dev	10	2.18	0.43	26.95	1.31	2.31	1.30	17.35	5.07
		Min	3	0.00	0.00	0.00	0.06	0.00	0.01	0.00	0.37
		Max	35	9.97	1.89	142.32	5.06	11.63	4.54	87.06	18.16
	Autumn	Mean	16	1.16	0.14	16.44	1.13	1.56	0.74	11.64	5.14
		Std Dev	13	1.24	0.21	19.29	1.09	2.47	1.17	13.13	7.27
		Min	3	0.00	0.01	0.00	0.22	0.00	0.02	0.00	0.65
		Max	56	5.27	0.88	77.84	5.33	10.53	4.01	38.51	24.64
	Winter	Mean	12	0.62	0.10	3.77	0.70	0.63	0.38	9.24	2.60
		Std Dev	8	0.78	0.26	4.67	0.96	0.88	0.89	13.99	3.38
		Min	1	0.00	0.00	0.00	0.09	0.00	0.01	0.00	0.59
		Max	31	2.76	0.88	15.40	3.45	2.81	2.90	35.09	11.35
	Spring	Mean	16	0.87	0.11	15.80	1.24	1.35	0.49	13.12	4.70
		Std Dev	11	1.26	0.15	25.21	0.87	2.31	0.77	15.16	4.53
		Min	3	0.00	0.00	0.00	0.12	0.00	0.00	0.00	0.43
		Max	46	4.58	0.51	87.32	3.42	9.72	2.93	40.20	16.62
	All Seasons	Mean	16	1.14	0.20	14.68	1.34	1.39	0.78	13.31	5.18
		Std Dev	11	1.68	0.33	23.67	1.18	2.27	1.15	15.65	5.44
		Min	1	0.00	0.00	0.00	0.06	0.00	0.00	0.00	0.37
		Max	56	9.97	1.89	142.32	5.33	11.63	4.54	87.06	24.64

Location	Season	Metric	Precipitation Depth (mm)	^{7}Be (Bq L^{-1})	^{7}Be (Bq L^{-1}) Uncertainty +-	^{7}Be (Bq m^{-2})	^{7}Be (Bq m^{-2}) Uncertainty +-	$^{210}Pb_{ex}$ (Bq L^{-1})	$^{210}Pb_{ex}$ (Bq L^{-1}) Uncertainty +-	$^{210}Pb_{ex}$ (Bq m^{-2})	$^{210}Pb_{ex}$ (Bq m^{-2}) Uncertainty +-
Marcell Experimental Forest	*Summer*	Mean	26	2.73	0.17	32.41	1.29	0.00	0.13	0.00	1.39
		SD	23	1.49	0.18	15.63	0.78	0.00	0.14	0.00	0.72
		Min	5	0.57	0.01	7.82	0.46	0.00	0.01	0.00	0.52
		Max	66	5.67	0.54	58.33	2.47	0.00	0.42	0.00	2.74
	Autumn	Mean	18	1.74	0.10	31.30	0.95	0.03	1.04	1.05	3.88
		SD	13	0.94	0.15	21.42	0.52	0.06	1.38	1.97	3.52
		Min	2	0.00	0.01	0.00	0.49	0.00	0.02	0.00	0.62
		Max	38	3.50	0.45	57.21	2.07	0.14	3.39	5.00	9.50
	All Seasons	Mean	22	2.20	0.14	31.82	1.13	0.02	0.59	0.56	2.63
		SD	19	1.33	0.17	18.93	0.69	0.04	1.08	1.53	2.83
		Min	2	0.00	0.01	0.00	0.46	0.00	0.01	0.00	0.52
		Max	66	5.67	0.54	58.33	2.47	0.14	3.39	5.00	9.50

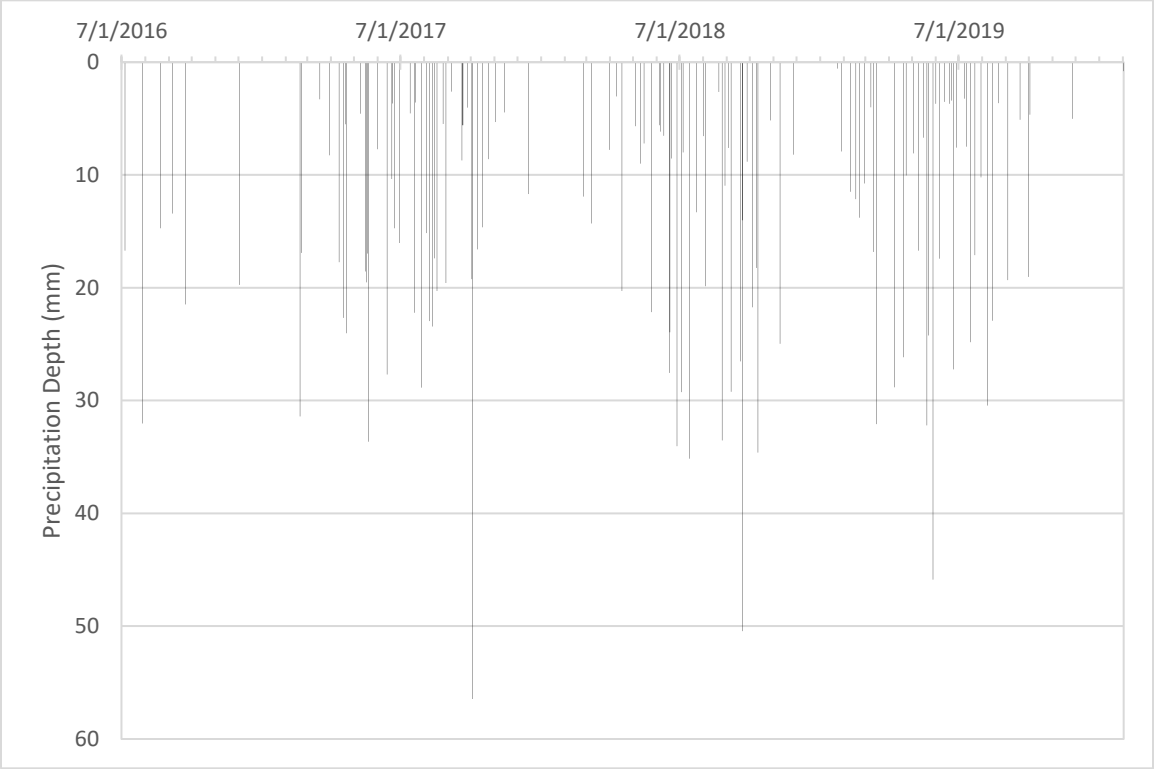

Figure 3-2a St. Paul Weather Station precipitation depth.

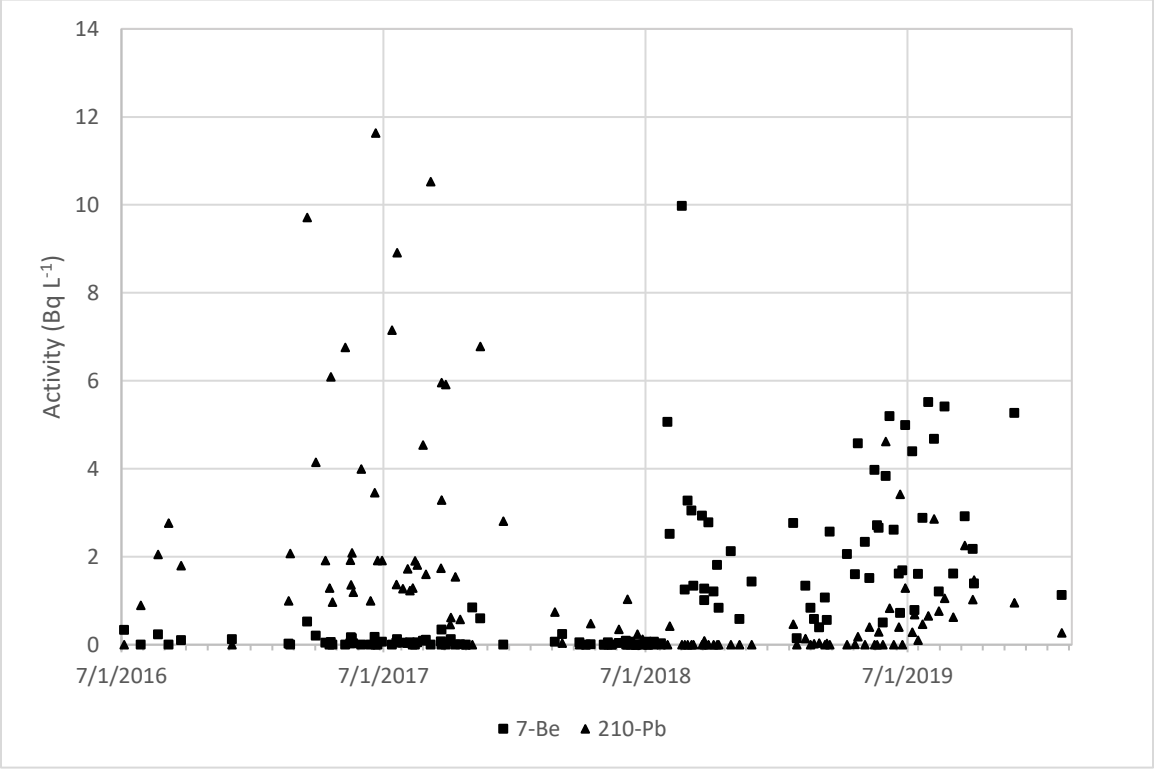

Figure 3-2b St. Paul Weather Station sampled radionuclide activity.

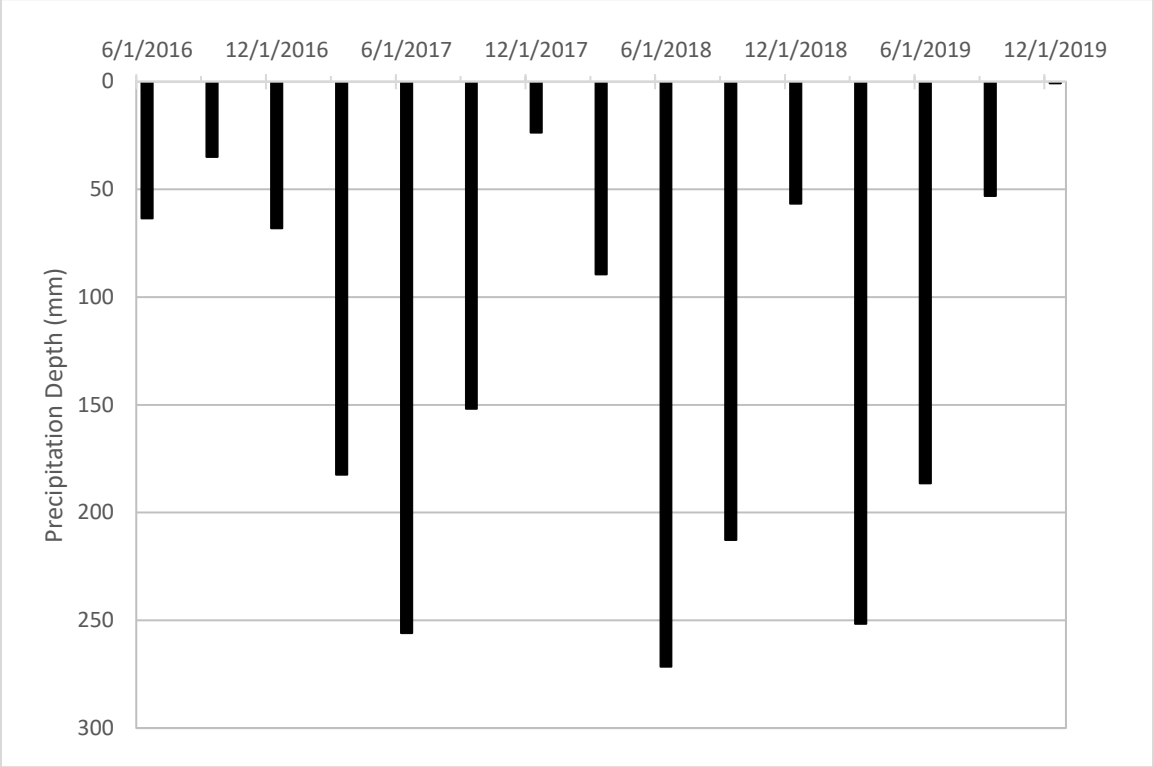

Figure 3-3a St. Paul Weather Station seasonal precipitation. Precipitation was aggregated for Summer (Jun-Aug), Autumn (Sept-Nov), Winter (Dec-Feb), and Spring (Mar-May).

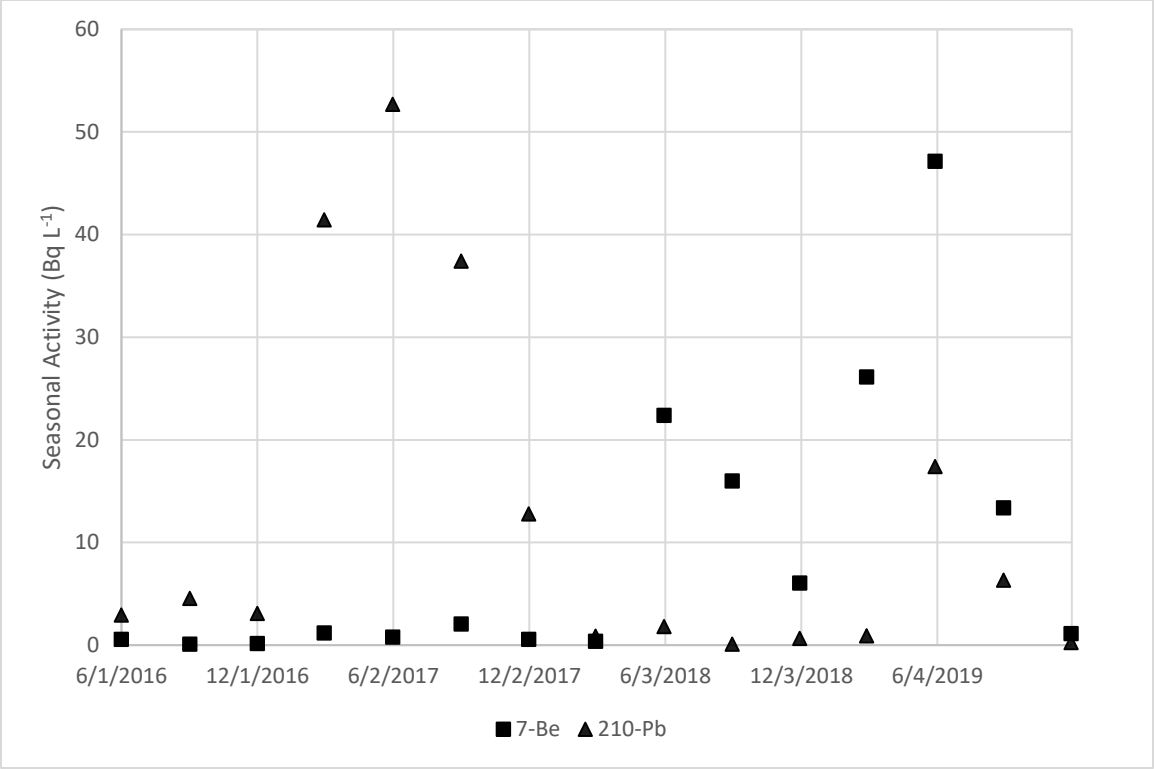

Figure 3-3b St. Paul Weather Station seasonal radionuclide activity. Activity was aggregated for Summer (Jun-Aug), Autumn (Sept-Nov), Winter (Dec-Feb), and Spring (Mar-May).

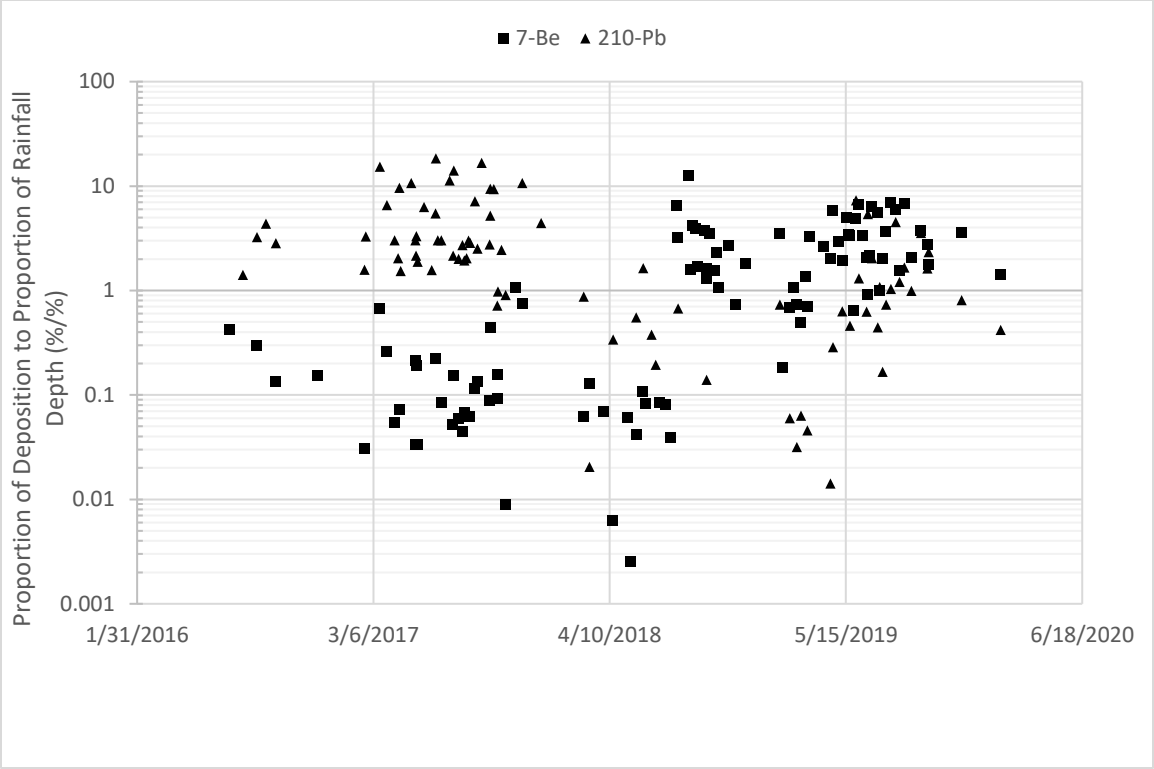

Figure 3-4 Plotted ratio of the proportion of fallout radionuclide (event to cumulative total) to the proportion of rainfall (event depth to cumulative depth).

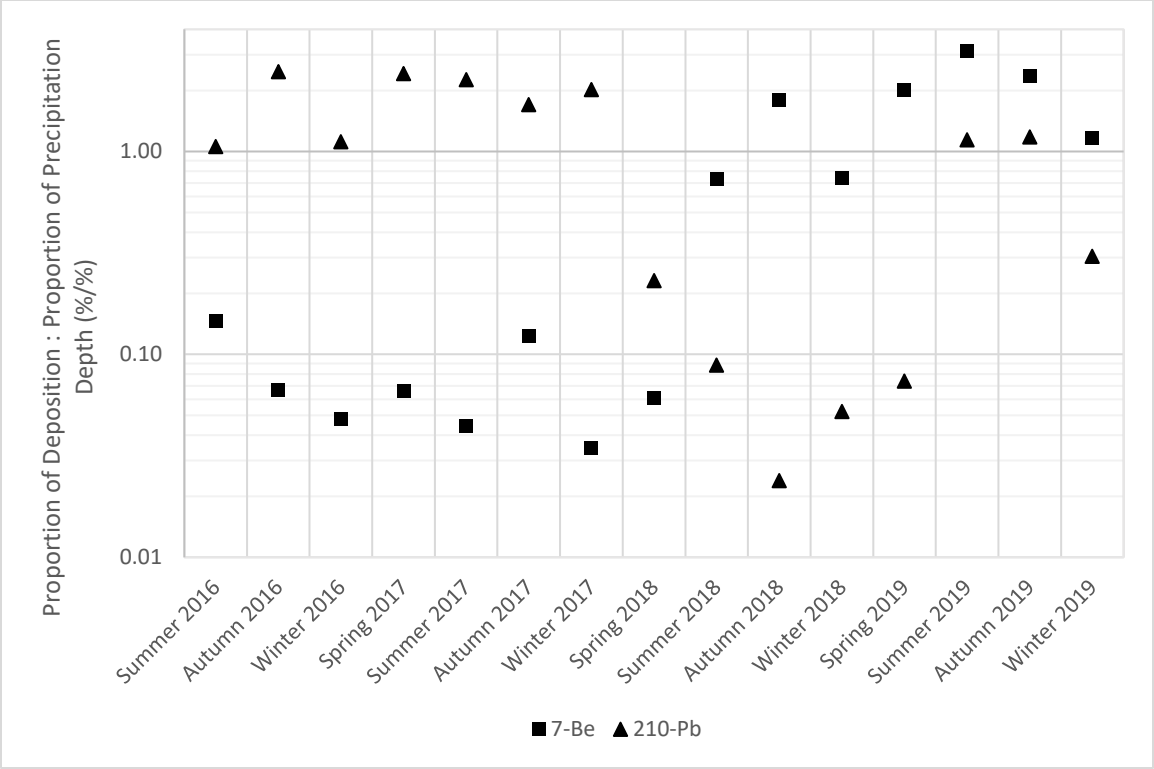

Figure 3-5 Plotted ratio of the proportion of fallout radionuclide (event to cumulative total) to the proportion of rainfall (event depth to cumulative depth) separated by season. Summer (Jun-Aug), Autumn (Sept-Nov), Winter (Dec-Feb), and Spring (Mar-May)

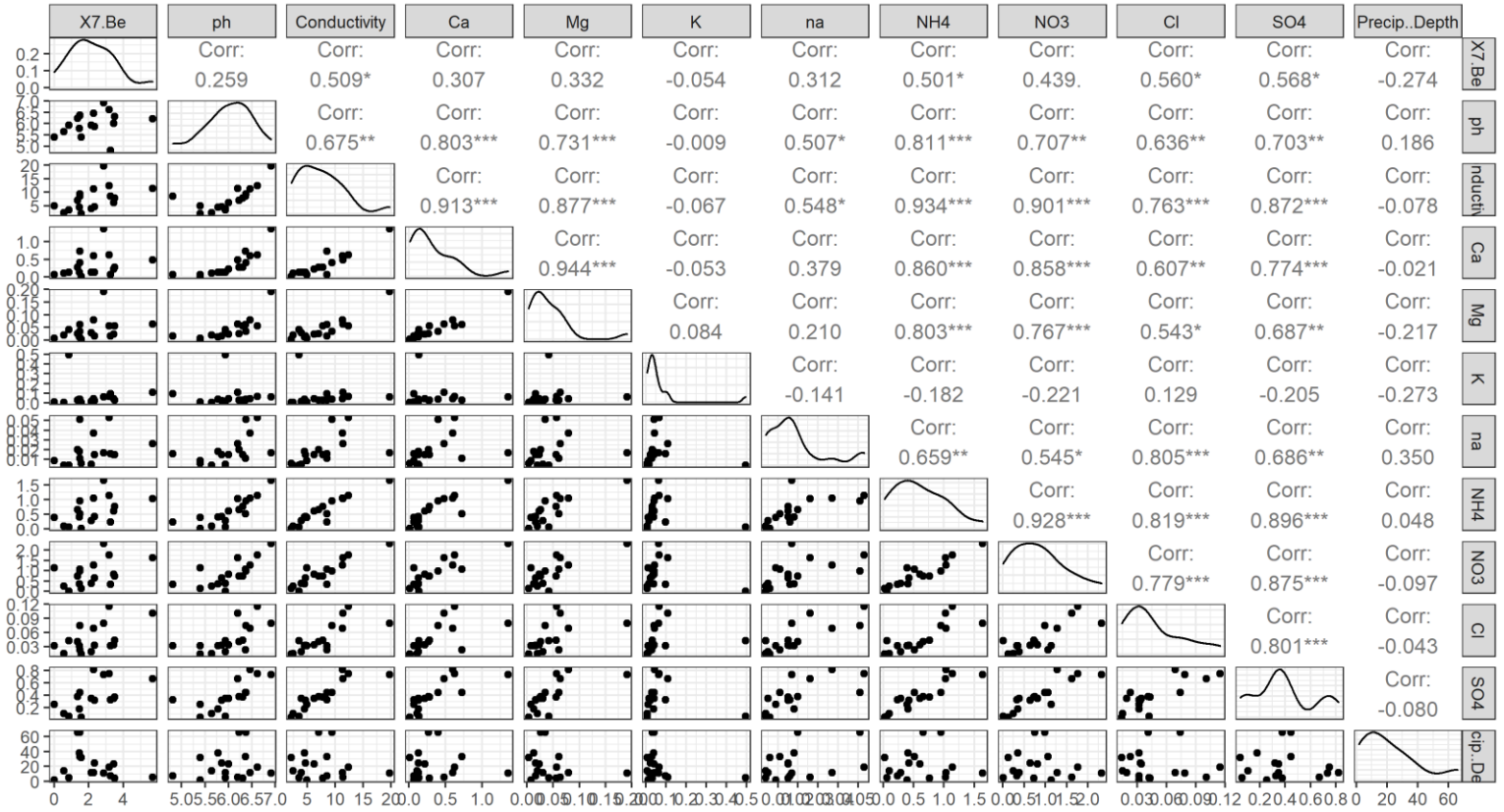

Figure 3-6 Pairwise plot of Beryllium-7 deposition with other deposited aerosols from the National Atmospheric Deposition Program. The numeric values are the Pearson correlation coefficients between the chemical species beryllium-7 (X7.Be), pH, conductivity, calcium (Ca), magnesium (Mg), potassium (K), sodium (na), ammonium (NH4), nitrate (NO3), chloride (Cl), sulfate (SO4), and precipitation depth.

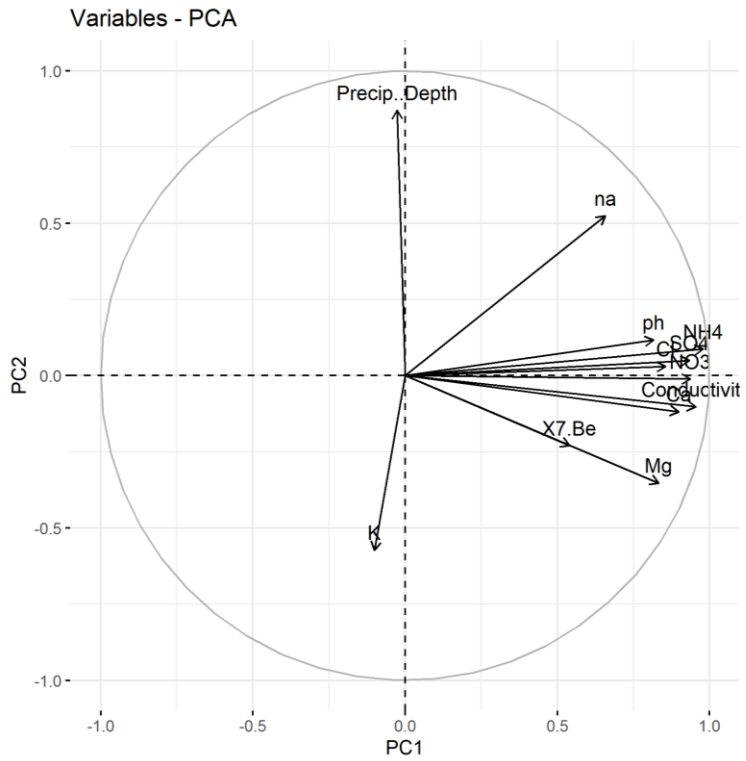

Figure 3-7a Contribution of beryllium-7 (X7.Be), pH, conductivity, calcium (Ca), magnesium (Mg), potassium (K), sodium (na), ammonium (NH4), nitrate (NO3), chloride (Cl), sulfate (SO4), and precipitation depth to principal components 1 and 2.

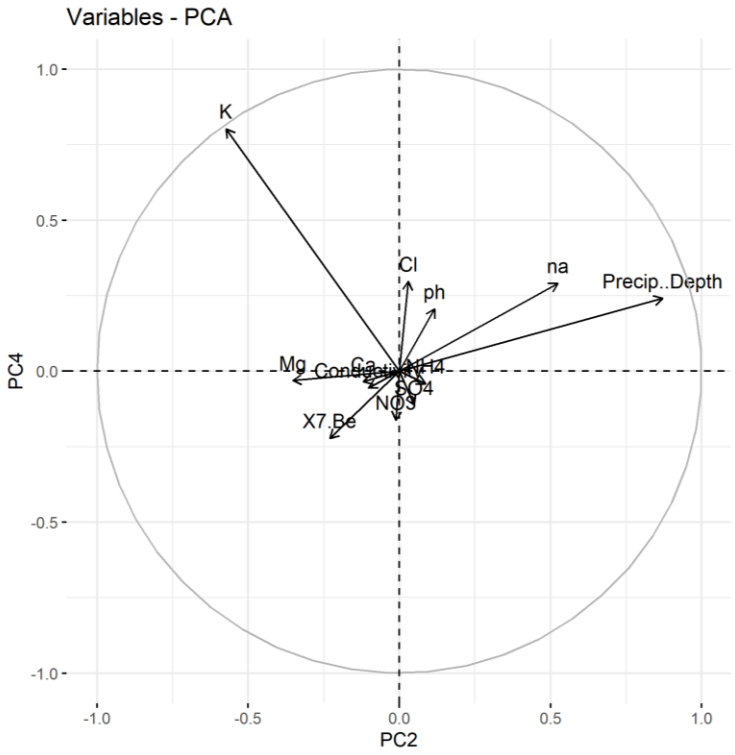

Figure 3-7b Contribution of beryllium-7 (X7.Be), pH, conductivity, calcium (Ca), magnesium (Mg), potassium (K), sodium (na), ammonium (NH4), nitrate (NO3), chloride (Cl), sulfate (SO4), and precipitation depth to principal components 3 and 4.

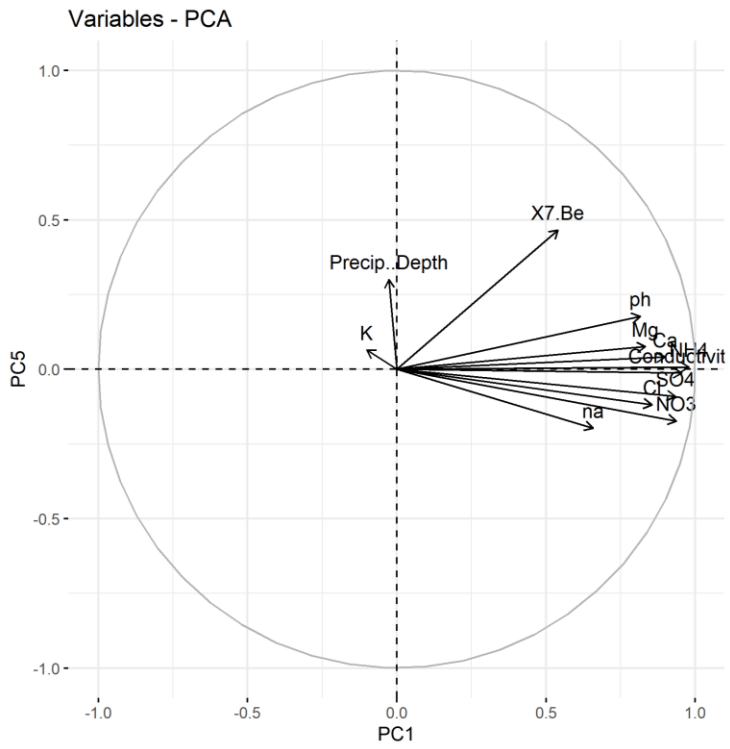

Figure 3-7c Contribution of beryllium-7 (X7.Be), pH, conductivity, calcium (Ca), magnesium (Mg), potassium (K), sodium (na), ammonium (NH4), nitrate (NO3), chloride (Cl), sulfate (SO4), and precipitation depth to principal components 1 and 5.

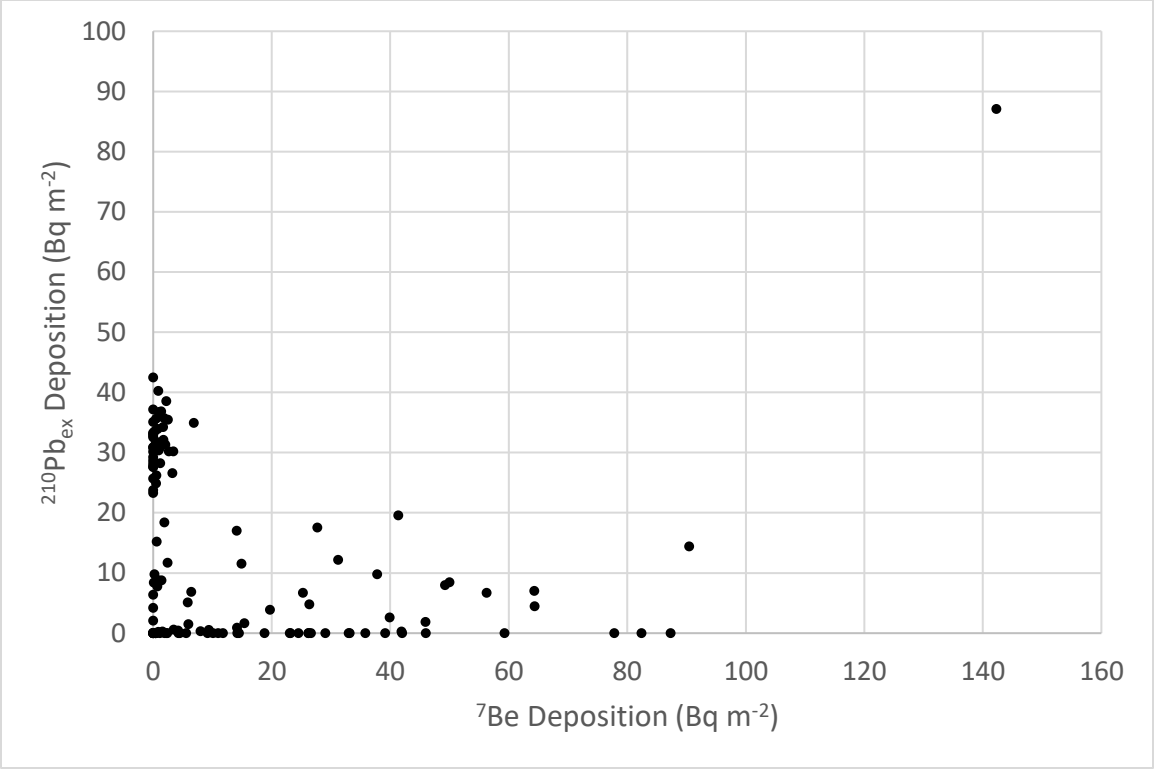

Figure 3-8 Plot of beryllium-7 to lead-210 activity for measured pairs of each recorded sample.

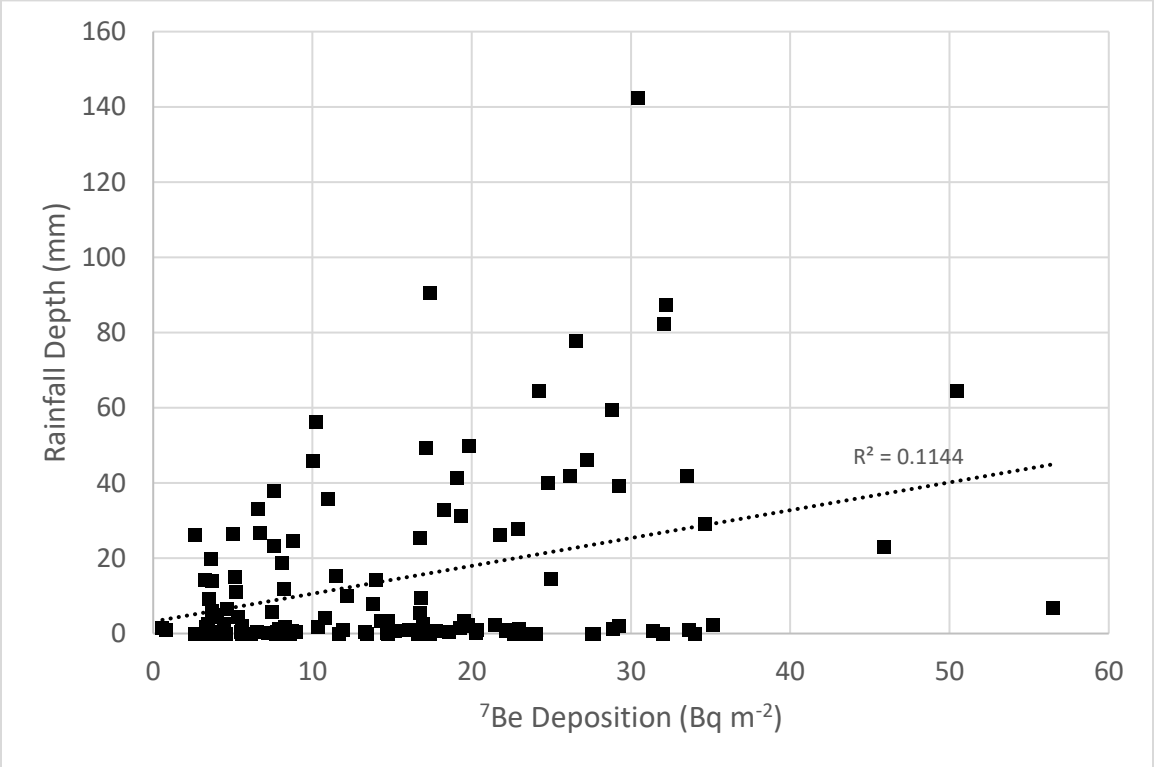

Figure 3-9 Beryllium-7 deposition plotted against rainfall depth.

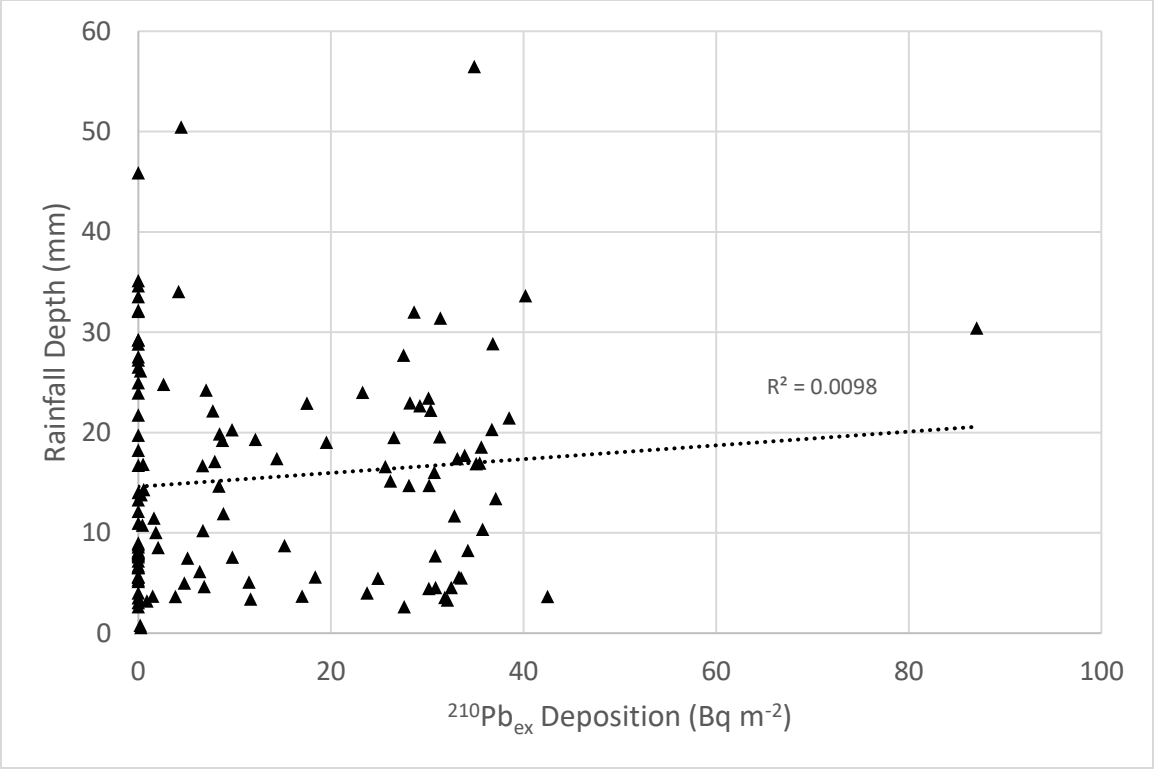

Figure 3-10 Lead-210 deposition plotted against rainfall depth.

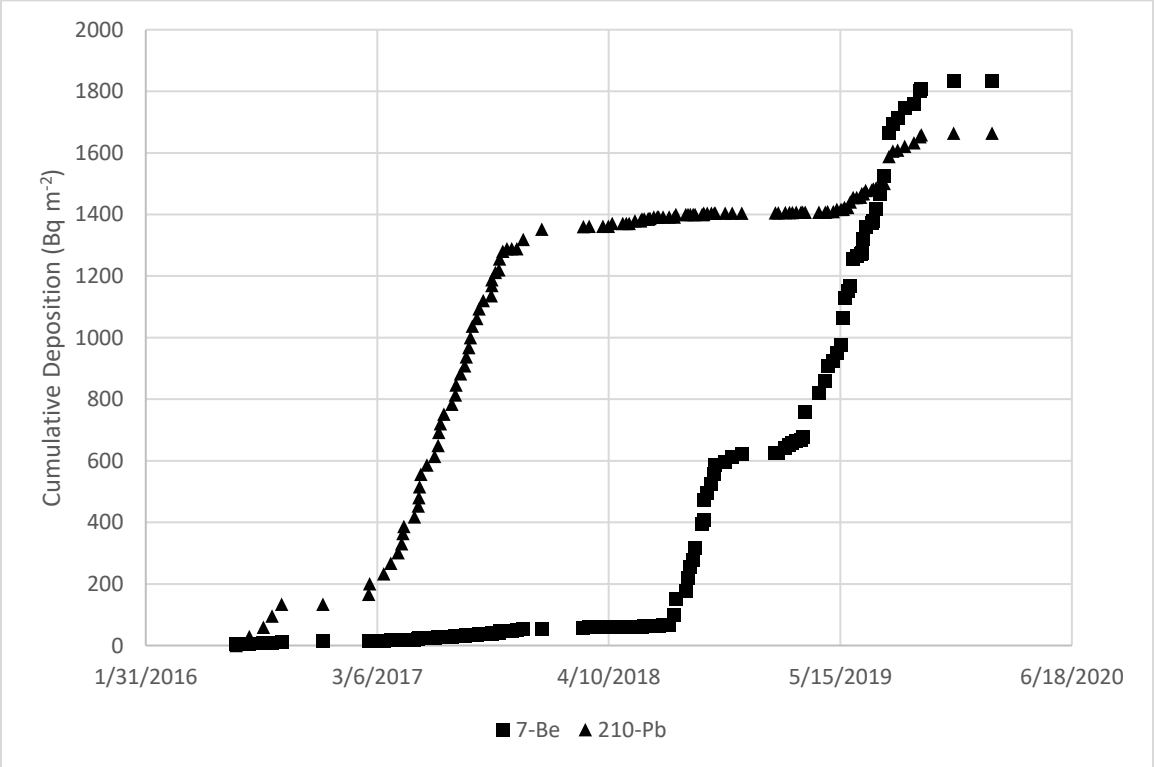

Figure 3-11 Cumulative deposition of beryllium-7 and lead-210 deposition at the St. Paul Weather Station.

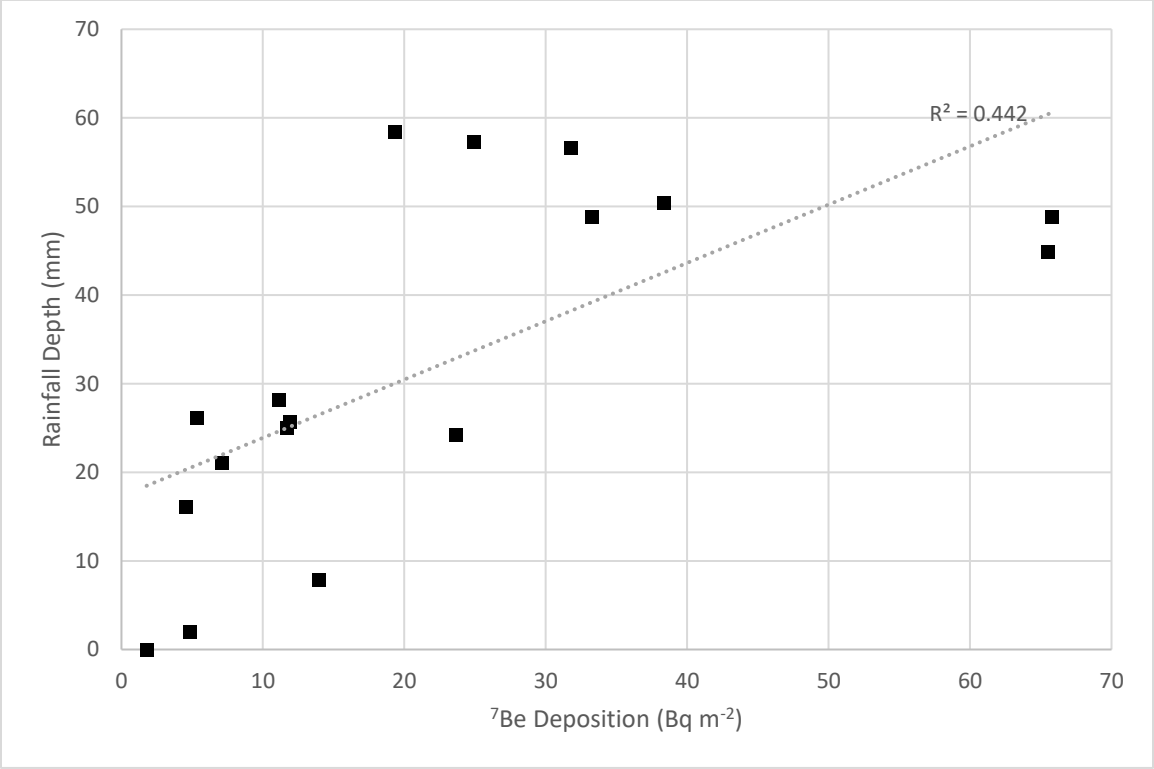

Figure 3-12 Beryllium-7 deposition plotted against rainfall depth at the Marcell Experimental Forest.

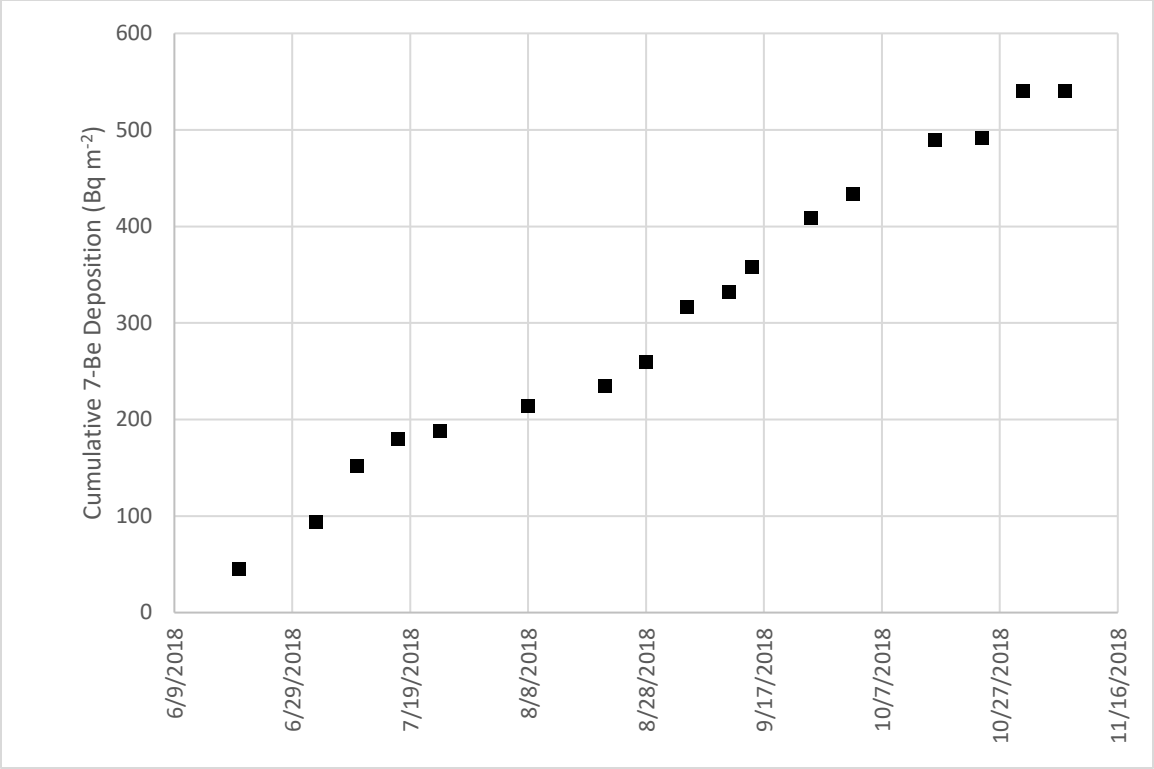

Figure 3-13 Cumulative deposition of beryllium-7 at the Marcell Experimental Forest.

Literature Cited

Agudelo, S. C., Nelson, N. O., Barnes, P. L., Keane, T. D., & Pierzynski, G. M. (2011). Phosphorus adsorption and desorption potential of stream sediments and field soils in agricultural watersheds. *Journal of Environmental Quality*, *40*(1), 144–152. https://doi.org/10.2134/jeq2010.0153

Alexander, R. B., Smith, R. A., Schwarz, G. E., Boyer, E. W., Nolan, J. V., & Brakebill, J. W. (2008). Differences in phosphorus and nitrogen delivery to the Gulf of Mexico from the Mississippi River Basin. *Environmental Science and Technology*, *42*(3), 822–830. https://doi.org/10.1021/es0716103

Ali, N., Khan, E. U., Akhter, P., Rana, M. A., Rajput, M. U., Khattak, N. U., Malik, F., & Hussain, S. (2011). Wet depositional fluxes of 210Pb- and 7Be-bearing aerosols at two different altitude cities of North Pakistan. *Atmospheric Environment*, *45*(32), 5699–5709. https://doi.org/10.1016/j.atmosenv.2011.07.032

Asbjornsen, H., Hernandez-Santana, V., Liebman, M., Bayala, J., Chen, J., Helmers, M. J., Ong, C. K., & Schulte, L. A. (2014). Targeting perennial vegetation in agricultural landscapes for enhancing ecosystem services. *Renewable Agriculture and Food Systems*, *29*(2), 101–125. https://doi.org/10.1017/S1742170512000385

Balkanski, Y. J., Jacob, D. J., Gardner, G. M., Graustein, W. C., & Turekian, K. K. (1993). Transport and residence times of tropospheric aerosols inferred from a global three-dimensional simulation of 210Pb. *Journal of Geophysical Research*, *98*(D11). https://doi.org/10.1029/93jd02456

Belmont, P., Willenbring, J. K., Schottler, S. P., Marquard, J., Kumarasamy, K., & Hemmis, J. M. (2014). Toward generalizable sediment fingerprinting with tracers that are conservative and nonconservative over sediment routing timescales. *Journal of Soils and Sediments*, *14*(8), 1479–1492. https://doi.org/10.1007/s11368-014-0913-5

Benefiel, R. (2022). *B ATCH E XPERIMENTS TO UNDERSTAND PHOSPHOROUS*. The Ohio State University.

Boano, F., Harvey, J. W., Marion, A., Packman, A. I., Revelli, R., Ridolfi, L., Wörman, A., & Boano F., Harvey J.W., Marion A., Packman A.I., Revelli R.m Ridolfi L., W. A. (2014). Hyophreic flow and transport processes. *Reviews of Geophysics*, *52*(4), 603–679. https://doi.org/10.1002/2012RG000417.Received

Boardman, E., Danesh-Yazdi, M., Foufoula-Georgiou, E., Dolph, C. L., & Finlay, J. C. (2019). Fertilizer, landscape features and climate regulate phosphorus retention and river export in diverse Midwestern watersheds. *Biogeochemistry*, *146*(3), 293–309. https://doi.org/10.1007/s10533-019-00623-z

Boedecker, A. R., Niewinski, D. N., Newell, S. E., Chaffin, J. D., & McCarthy, M. J. (2020). Evaluating sediments as an ecosystem service in western Lake Erie via quantification of nutrient cycling pathways and selected gene abundances. *Journal of Great Lakes Research*, *46*(4), 920–932. https://doi.org/10.1016/j.jglr.2020.04.010

Brady, N. C., & Weil, R. R. (2007). *The Nature and Properties of Soil* (14th ed.). Pearson.

Brant, G. (2003). *Barriers and Strategies Influencing the Adoption of Nutrient Management Practices*. https://www.nrcs.usda.gov/Internet/FSE_DOCUMENTS/stelprdb1045633.pdf

Cadmus Group, I. (2012). *Total maximum daily load and watershed man- agement plan for total phosphorus and total suspended solids in the lower Fox River basin and lower Green Bay*.

Canuel, E. A., Martens, C. S., & Benninger, L. K. (1990). Seasonal variations in 7Be activity in the sediments of Cape Lookout Bight, North Carolina. *Geochimica et Cosmochimica Acta*, *54*(1), 237–245. https://doi.org/10.1016/0016-7037(90)90211-3

Cappuyns, V., Swennen, R., & Devivier, A. (2006). Dredged river sediments: Potential chemical time bombs? A case study. *Water, Air, and Soil Pollution*, *171*(1–4), 49–66. https://doi.org/10.1007/s11270-005-9012-y

Carstensen, M. V., Hashemi, F., Hoffmann, C. C., Zak, D., Audet, J., & Kronvang, B. (2020). Efficiency of mitigation measures targeting nutrient losses from agricultural drainage systems: A review. *Ambio*, *49*(11), 1820–1837. https://doi.org/10.1007/s13280-020-01345-5

Casey, H., & Farr, I. S. (1982). The influence of within-stream disturbance on dissolved nutrient levels during spates. *Hydrobiologia*, *92*, 447–462.
Chate, D. M., & Devara, P. C. S. (2005). Parametric study of scavenging of atmospheric aerosols of various chemical species during thunderstorm and nonthunderstorm rain events. *Journal of Geophysical Research Atmospheres*, *110*(23), 1–14. https://doi.org/10.1029/2005JD006406
Chatfield, C. (2000). *Time-Series Forecasting*. Chapman & Hall/CRC.
Cheesman, A. W., Turner, B. L., & Reddy, K. R. (2014). Forms of organic phosphorus in wetland soils. *Biogeosciences*, *11*(23), 6697–6710. https://doi.org/10.5194/bg-11-6697-2014
Civan, A., Worrall, F., Jarvie, H. P., Howden, N. J. K., & Burt, T. P. (2018). Forty-year trends in the flux and concentration of phosphorus in British rivers. *Journal of Hydrology*, *558*, 314–327. https://doi.org/10.1016/j.jhydrol.2018.01.046
Climate Appleton- Wisconsin. (2020). U.S. Climate Data. https://www.usclimatedata.com/climate/appleton/wisconsin/united-states/uswi0020
Climate Green Bay, Wisconsin. (2021). U.S. Climate Data. https://www.usclimatedata.com/climate/green-bay/wisconsin/united-states/uswi0288
Collins, A. L., Pulley, S., Foster, I. D. L., Gellis, A., Porto, P., & Horowitz, A. J. (2017). Sediment source fingerprinting as an aid to catchment management: A review of the current state of knowledge and a methodological decision-tree for end-users. *Journal of Environmental Management*, *194*, 86–108. https://doi.org/10.1016/j.jenvman.2016.09.075
Davis, A. P., Shokouhian, M., Sharma, H., & Minami, C. (2006). Water Quality Improvement through Bioretention Media: Nitrogen and Phosphorus Removal. *Water Environment Research*, *78*(3), 284–293. https://doi.org/10.2175/106143005x94376
Dodd, R. J., & Sharpley, A. N. (2016). Conservation practice effectiveness and adoption: unintended consequences and implications for sustainable phosphorus management. *Nutrient Cycling in Agroecosystems*, *104*(3), 373–392. https://doi.org/10.1007/s10705-015-9748-8
Dodds, W. K., Bouska, W. W., Eitzmann, J. L., Pilger, T. J., Pitts, K. L., Riley, A. J., Schloesser, J. T., & Thornbrugh, D. J. (2009). Eutrophication of U. S. freshwaters: Analysis of potential economic damages. *Environmental Science and Technology*, *43*(1), 12–19. https://doi.org/10.1021/es801217q
Dolph, C. L., Boardman, E., Danesh-Yazdi, M., Finlay, J. C., Hansen, A. T., Baker, A. C., & Dalzell, B. (2019). Phosphorus Transport in Intensively Managed Watersheds. *Water Resources Research*, *55*(11), 9148–9172. https://doi.org/10.1029/2018WR024009
Dosskey, M. G., Helmers, M. J., Eisenhauer, D. E., Franti, T. G., & Hoagland, K. D. (2002). Assessment of concentrated flow through riparian buffers. *Journal of Soil and Water Conservation*, *57*(6), 336–343.
Drummond, J. D., Aubeneau, A. F., & Packman, A. I. (2014). Stochastic modeling of fine particulate organic carbon dynamics in rivers. *Water Resources Research*, *50*, 4341–4665. https://doi.org/10.1002/2013WR014665
Drummond, J. D., Bernal, S., Von Schiller, D., & Martí, E. (2016). Linking in-stream nutrient uptake to hydrologic retention in two headwater streams. *Freshwater Science*, *35*(4), 1176–1188. https://doi.org/10.1086/688599
Drummond, J. D., Larsen, L. G., González-Pinzón, R., Packman, A. I., & Harvey, J. W. (2018). Less Fine Particle Retention in a Restored Versus Unrestored Urban Stream: Balance Between Hyporheic Exchange, Resuspension, and Immobilization. *Journal of Geophysical Research: Biogeosciences*, *123*(4), 1425–1439. https://doi.org/10.1029/2017JG004212
Du Laing, G., Rinklebe, J., Vandecasteele, B., Meers, E., & Tack, F. M. G. (2009). Trace metal behaviour in estuarine and riverine floodplain soils and sediments: A review. *Science of the Total Environment*, *407*(13), 3972–3985. https://doi.org/10.1016/j.scitotenv.2008.07.025
Dunai, T. J., & Lifton, N. A. (2014). The nuts and bolts of cosmogenic nuclide production. *Elements*, *10*(5), 347–350. https://doi.org/10.2113/gselements.10.5.347
Fitzpatrick, F. A., Blount, J. D., Kammel, L. E., Francart, S. A., Gellis, A. C., & Eikenberry, B. C. (2019). Stream Corridor Sources of Suspended Sediment and Phosphorus from an Agricultural Tributary to the Great Lakes. *Proceedings of SEDHYD 2019*, *4*. https://www.sedhyd.org/2019/proceedings/SEDHYD_Proceedings_2019_Volume4.pdf

Froelich, P. N. (1988). Kinetic Control of Dissolved Phosphate in Natural Rivers and Estuaries : A Primer on the Phosphate Buffer Mechanism Author (s): Philip N . Froelich Source : Limnology and Oceanography , Vol . 33 , No . 4 , Part 2 : Comparative Ecology of Freshwater and. *Limnology and Oceanography*, *33*(4.2), 649–668.

Gassman, P. W., Williams, J. R., Wang, X., Saleh, A., Osei, E., Hauck, L. M., Izaurralde, R. C., & Flowers, J. D. (2009). The Agricultural Policy/Environmental eXtender (APEX) model: An emerging tool for landscape and watershed environmental analyses. In *Technical Report 09-TR-49*.

Gellis, A. C., Fitzpatrick, F., & Schubauer-Berigan, J. (2016). A Manual to Identify Sources of Fluvial Sediment. *U.S. Environmental Protection Agency, Washington, DC, EPA/600/R1*(September), 106.

Gettelman, a., Pan, L. L., Randel, W. J., Hoor, P., Birner, T., & Hegglin, M. I. (2011). the Extratropical Upper Troposphere and Lower Stratosphere. *Reviews of Geophysics*, *49*(3), 1–31. https://doi.org/10.1029/2011RG000355.1.INTRODUCTION

Gilmore, G. R. (2008). *Gamma-ray Spectrometry* (2nd ed.). John Wiley & Sons. https://onlinelibrary.wiley.com/doi/book/10.1002/9780470861981

Gordon, B. A., Lenhart, C., Peterson, H., Gamble, J., Nieber, J., Current, D., & Brenke, A. (2021). Reduction of nutrient loads from agricultural subsurface drainage water in a small, edge-of-field constructed treatment wetland. *Ecological Engineering*, *160*(October 2020), 106128. https://doi.org/10.1016/j.ecoleng.2020.106128

Graczyk, D. J., Robertson, D. M., Baumgart, P. D., & Fermanich, K. J. (2011). *Hydrology, phosphorus, and suspended solids in five agricultural streams in the Lower Fox River and Green Bay Watersheds, Wisconsin, Water Years 2004–06: Scientific Investigations Report 2011–5111*. http://pubs.usgs.gov/sir/2011/5111/

Grant, G. E., Lewis, S. L., Swanson, F. J., Cissel, J. H., & McDonnell, J. J. (2008). Effects of forest practices on peak flows and consequent channel response: A state-of-science report for western Oregon and Washington. *USDA Forest Service - General Technical Report PNW-GTR*, *760*, 1–82. https://doi.org/10.2737/PNW-GTR-760

Hadley, D. W., & Pelham, J. . (1976). *Glacial Deposits of Wisconsin: Sand and Gravel Resource Potential*. Wisconsin Geological and Natural History Survey. https://ngmdb.usgs.gov/ngm-bin/pdp/zui_viewer.pl?id=19927

Hanrahan, B. R., King, K. W., & Williams, M. R. (2021). Controls on subsurface nitrate and dissolved reactive phosphorus losses from agricultural fields during precipitation-driven events. *Science of the Total Environment*, *754*, 142047. https://doi.org/10.1016/j.scitotenv.2020.142047

Hansen, A. T., Campbell, T., Cho, S. J., Czuba, J. A., Dalzell, B. J., Dolph, C. L., Hawthorne, P. L., Rabotyagov, S., Lang, Z., Kumarasamy, K., Belmont, P., Finlay, J. C., Foufoula-Georgiou, E., Gran, K. B., Kling, C. L., & Wilcock, P. (2021). Integrated assessment modeling reveals near-channel management as cost-effective to improve water quality in agricultural watersheds. *Proceedings of the National Academy of Sciences of the United States of America*, *118*(28), 1–25. https://doi.org/10.1073/pnas.2024912118

Helmers, M. J., Eisenhauer, D. E., Dosskey, M. G., Franti, T. G., Brothers, J. M., & Mccullough, M. C. (2005). Flow Pathways and Sediment Trapping in a Field-Scale Vegetative Filter. *Transactions of the ASAE*, *48*(3), 955–968.

Helmers, M. J., Zhou, X., Asbjornsen, H., Kolka, R., Tomer, M. D., & Cruse, R. M. (2011). Sediment Removal by Prairie Filter Strips in Row-Cropped Ephemeral Watersheds. *Journal of Environmental Quality*, *41*(5), 1531–1539. https://doi.org/10.2134/jeq2011.0473

Hernandez-Santana, V., Zhou, X., Helmers, M. J., Asbjornsen, H., Kolka, R., & Tomer, M. (2013). Native prairie filter strips reduce runoff from hillslopes under annual row-crop systems in Iowa, USA. *Journal of Hydrology*, *477*, 94–103. https://doi.org/10.1016/j.jhydrol.2012.11.013

Ho, J. C., & Michalak, A. M. (2015). Challenges in tracking harmful algal blooms: A synthesis of evidence from Lake Erie. *Journal of Great Lakes Research*, *41*(2), 317–325. https://doi.org/10.1016/j.jglr.2015.01.001

House, W. A., & Denison, F. H. (2000). Factors influencing the measurement of equilibrium phosphate concentrations in river sediments. *Water Research*, *34*(4), 1187–1200. https://doi.org/10.1016/S0043-1354(99)00249-3

House, William A. (2003). Geochemical cycling of phosphorus in rivers. *Applied Geochemistry*, *18*(5), 739–748. https://doi.org/10.1016/S0883-2927(02)00158-0

Huisman, N. L. H., Karthikeyan, K. G., Lamba, J., Thompson, A. M., & Peaslee, G. (2013). Quantification of seasonal sediment and phosphorus transport dynamics in an agricultural watershed using radiometric fingerprinting techniques. *Journal of Soils and Sediments*, *13*(10), 1724–1734. https://doi.org/10.1007/s11368-013-0769-0

Igarashi, Y., Hirose, K., & Otsuji-Hatori, M. (1998). Beryllium-7 deposition and its relation to sulfate deposition. *Journal of Atmospheric Chemistry*, *29*(3), 217–231. https://doi.org/10.1023/A:1005921113496

Inamdar, S., Sienkiewicz, N., Lutgen, A., Jiang, G., & Kan, J. (2020). Streambank legacy sediments in surface waters: Phosphorus sources or sinks? *Soil Systems*, *4*(2), 1–20. https://doi.org/10.3390/soilsystems4020030

Ishikawa, Y. (2014). Precipitation scavenging studies of radionuclides in air using cosmogenic 7Be. *Journal of Environmental Radioactivity*, *26*(1), 19–36.

Jacobson, M. D. (2012). *Phosphorus and Sediment Runoff Loss: Management Challenges and Implications in a Northeast Wisconsin Agricultural Watershed*. University of Wisconsin-Green Bay.

Jaeglé, L., Wood, R., & Wargan, K. (2017). Multiyear Composite View of Ozone Enhancements and Stratosphere-to-Troposphere Transport in Dry Intrusions of Northern Hemisphere Extratropical Cyclones. *Journal of Geophysical Research: Atmospheres*, *122*(24), 13,436-13,457. https://doi.org/10.1002/2017JD027656

Jagercikova, M., Evrard, O., Balesdent, J., Lefèvre, I., & Cornu, S. (2014). Modeling the migration of fallout radionuclides to quantify the contemporary transfer of fine particles in Luvisol profiles under different land uses and farming practices. *Soil and Tillage Research*, *140*, 82–97. https://doi.org/10.1016/j.still.2014.02.013

Jarvie, H. P., Johnson, L. T., Sharpley, A. N., Smith, D. R., Baker, D. B., Bruulsema, T. W., & Confesor, R. (2017). Increased soluble phosphorus loads to lake erie: Unintended consequences of conservation practices? *Journal of Environmental Quality*, *46*(1), 123–132. https://doi.org/10.2134/jeq2016.07.0248

Jarvie, H. P., Sharpley, A. N., Flaten, D., Kleinman, P. J. A., Jenkins, A., & Simmons, T. (2015). The pivotal role of phosphorus in a resilient water-energy-food security nexus. *Journal of Environmental Quality*, *44*(4), 1049–1062. https://doi.org/10.2134/jeq2015.01.0030

Jarvie, H. P., Sharpley, A. N., Spears, B., Buda, A. R., May, L., & Kleinman, P. J. A. (2013). Water quality remediation faces unprecedented challenges from “legacy Phosphorus.” *Environmental Science and Technology*, *47*(16), 8997–8998. https://doi.org/10.1021/es403160a

Jarvie, H. P., Withers, J. A., & Neal, C. (2002). Review of robust measurement of phosphorus in river water: sampling, storage, fractionation and sensitivity. *Hydrology and Earth System Sciences*, *6*(1), 113–131. https://doi.org/10.5194/hess-6-113-2002

Jaynes, D. B., & Isenhart, T. M. (2014). Reconnecting Tile Drainage to Riparian Buffer Hydrology for Enhanced Nitrate Removal. *Journal of Environmental Quality*, *43*(2), 631–638. https://doi.org/10.2134/jeq2013.08.0331

Jefferson, A. J., Bhaskar, A. S., Hopkins, K. G., Fanelli, R., Avellaneda, P. M., & McMillan, S. K. (2017). Stormwater management network effectiveness and implications for urban watershed function: A critical review. *Hydrological Processes*, *31*(23), 4056–4080. https://doi.org/10.1002/hyp.11347

Jiang, F., Preisendanz, H. E., Veith, T. L., Cibin, R., & Drohan, P. J. (2020). Riparian buffer effectiveness as a function of buffer design and input loads. *Journal of Environmental Quality*, *49*(6), 1599–1611. https://doi.org/10.1002/jeq2.20149

Jollife, I. T., & Cadima, J. (2016). Principal component analysis: A review and recent developments. *Philosophical Transactions of the Royal Society A: Mathematical, Physical and Engineering Sciences*, *374*(2065). https://doi.org/10.1098/rsta.2015.0202

Jordan, P., Melland, A. R., Mellander, P. E., Shortle, G., & Wall, D. (2012). The seasonality of phosphorus transfers from land to water: Implications for trophic impacts and policy evaluation. *Science of the Total Environment*, *434*, 101–109. https://doi.org/10.1016/j.scitotenv.2011.12.070

Joung, Y. S., & Buie, C. R. (2015). Aerosol generation by raindrop impact on soil. *Nature Communications*, *6*(May 2014), 1–9. https://doi.org/10.1038/ncomms7083
Kalk, F. S. (2018). *Evaluation of the APEX Model to Simulate Runoff, Sediment, and Phosphorus Loss from Agricultural Fields in Northeast Wisconsin*. University of Wisconsin-Green Bay.
Karwan, D. L., Siegert, C. M., Levia, D. F., Pizzuto, J., Marquard, J., Aalto, R., & Aufdenkampe, A. K. (2016). Beryllium-7 wet deposition variation with storm height, synoptic classification, and tree canopy state in the mid-Atlantic USA. *Hydrological Processes*, *30*(1), 75–89. https://doi.org/10.1002/hyp.10571
Kaspar, T. C., & Singer, J. W. (2011). The Use of Cover Crops to Manage Soil. *Publications from USDA-ARS/UNL Faculty 1382*. https://doi.org/10.2136/2011.soilmanagement.c21
Kast, J. B., Apostel, A. M., Kalcic, M. M., Muenich, R. L., Dagnew, A., Long, C. M., Evenson, G., & Martin, J. F. (2021). Source contribution to phosphorus loads from the Maumee River watershed to Lake Erie. *Journal of Environmental Management*, *279*(May 2020), 111803. https://doi.org/10.1016/j.jenvman.2020.111803
Kaste, J. M., Norton, S. A., & Hess, C. T. (2002). Environmental chemistry of Beryllium-7. In E. S. Grew (Ed.), *Beryllium: Mineralogy, Petrology, and Geochemistry* (pp. 271–290). https://doi.org/10.2138/rmg.2002.50.6
Kelleher, C., Ward, A., Knapp, J. L. A., Blaen, P. J., Kurz, M. J., Drummond, J. D., Zarnetske, J. P., Hannah, D. M., Mendoza-Lera, C., Schmadel, N. M., Datry, T., Lewandowski, J., Milner, A. M., & Krause, S. (2019). Exploring Tracer Information and Model Framework Trade-Offs to Improve Estimation of Stream Transient Storage Processes. *Water Resources Research*, *55*(4), 3481–3501. https://doi.org/10.1029/2018WR023585
Keller, A. A., & Fox, J. (2019). Giving credit to reforestation for water quality benefits. *PLoS ONE*, *14*(6), 1–18. https://doi.org/10.1371/journal.pone.0217756
Kinsman-Costello, L. E., O'Brien, J., & Hamilton, S. K. (2014). Re-flooding a Historically Drained Wetland Leads to Rapid Sediment Phosphorus Release. *Ecosystems*, *17*(4), 641–656. https://doi.org/10.1007/s10021-014-9748-6
Klaiber, L. B., Kramer, S. R., & Young, E. O. (2020). Impacts of tile drainage on phosphorus losses from edge-of-field plots in the Lake Champlain Basin of New York. *Water (Switzerland)*, *12*(2), 1–15. https://doi.org/10.3390/w12020328
Kleinman, P. J. A., Sharpley, A. N., Buda, A. R., McDowell, R. W., & Allen, A. L. (2011). Soil controls of phosphorus in runoff: Management barriers and opportunities. *Canadian Journal of Soil Science*, *91*(3), 329–338. https://doi.org/10.4141/cjss09106
Koch, D. M., Jacob, D. J., & Graustein, W. C. (1996). Vertical transport of tropospheric aerosols as indicated by 7Be and 210Pb in a chemical tracer model. *Journal of Geophysical Research Atmospheres*, *101*(13), 18651–18666. https://doi.org/10.1029/96jd01176
Koch, D., & Rind, D. (1998). Beryllium 10/beryllium 7 as a tracer of stratospheric transport. *Journal of Geophysical Research Atmospheres*, *103*(D4), 3907–3917. https://doi.org/10.1029/97JD03117
Koiter, A. J., Owens, P. N., Petticrew, E. L., & Lobb, D. A. (2013). The behavioural characteristics of sediment properties and their implications for sediment fingerprinting as an approach for identifying sediment sources in river basins. *Earth-Science Reviews*, *125*, 24–42. https://doi.org/10.1016/j.earscirev.2013.05.009
Komiskey, M. J., Stuntebeck, T. D., Loken, L. C., Hood, K. A., Danz, M. E., Rachol, C. M., Toussant, C. A., Dobrowolski, E. G., Kowalczk, A. J., Ennis, R. P., Snarski, S. A., & Hardebeck, M. J. (2021). *Nutrient and sediment concentrations, loads, yields, and rainfall characteristics at USGS surface and subsurface-tile edge-of-field agricultural monitoring sites in Great Lakes States: U.S. Geological Survey data release*. https://doi.org/10.5066/P9LO8O70
Komura, K., Kuwahara, Y., Abe, T., Tanaka, K., Murata, Y., & Inoue, M. (2006). Measurements of short-lived cosmogenic nuclides in rain samples. *Journal of Radioanalytical and Nuclear Chemistry*, *269*(2), 511–516. https://doi.org/10.1007/s10967-006-0298-z
Kovacic, D. A., Twait, R. M., Wallace, M. P., & Bowling, J. M. (2006). Use of created wetlands to improve water quality in the Midwest-Lake Bloomington case study. *Ecological Engineering*, *28*(3 SPEC. ISS.), 258–270. https://doi.org/10.1016/j.ecoleng.2006.08.002
Kreiling, R. M., Bartsch, L. A., Perner, P. M., Hlavacek, E. J., & Christensen, V. G. (2021).

Riparian Forest Cover Modulates Phosphorus Storage and Nitrogen Cycling in Agricultural Stream Sediments. *Environmental Management*, *68*(2), 279–293. https://doi.org/10.1007/s00267-021-01484-9

Kulan, A., Aldahan, A., Possnert, G., & Vintersved, I. (2006). Distribution of 7Be in surface air of Europe. *Atmospheric Environment*, *40*(21), 3855–3868. https://doi.org/10.1016/j.atmosenv.2006.02.030

Lal, D., Malhotra, P. K., & Peters, B. (1958). On the production of radioisotopes in the atmosphere by cosmic radiation and their application to meteorology. *Journal of Atmospheric and Terrestrial Physics*, *12*(4), 306–328. https://doi.org/10.1016/0021-9169(58)90062-X

Land, C., & Feichter, J. (2003). Stratosphere-troposphere exchange in a changing climate simulated with the general circulation model MAECHAM4. *Journal of Geophysical Research*, *108*(D12), 8523. https://doi.org/10.1029/2002JD002543

Lannergård, E. E., Agstam-Norlin, O., Huser, B. J., Sandström, S., Rakovic, J., & Futter, M. N. (2020). New Insights Into Legacy Phosphorus From Fractionation of Streambed Sediment. *Journal of Geophysical Research: Biogeosciences*, *125*(9). https://doi.org/10.1029/2020JG005763

Lenhart, C. F., Smith, D. J., Lewandowski, A., Belmont, P., Gunderson, L., & Nieber, J. L. (2018). Assessment of stream restoration for reduction of sediment in a large agricultural watershed. *Journal of Water Resources Planning and Management*, *144*(7), 1–13. https://doi.org/10.1061/(ASCE)WR.1943-5452.0000908

Leppänen, A. P., Pacini, A. A., Usoskin, I. G., Aldahan, A., Echer, E., Evangelista, H., Klemola, S., Kovaltsov, G. A., Mursula, K., & Possnert, G. (2010). Cosmogenic 7Be in air: A complex mixture of production and transport. *Journal of Atmospheric and Solar-Terrestrial Physics*, *72*(13), 1036–1043. https://doi.org/10.1016/j.jastp.2010.06.006

Leppänen, Ari Pekka, & Paatero, J. (2013). 7Be in Finland during the 1999-2001 Solar maximum and 2007-2009 Solar minimum. *Journal of Atmospheric and Solar-Terrestrial Physics*, *97*, 1–10. https://doi.org/10.1016/j.jastp.2013.01.007

Li, H., Song, C. L., Cao, X. Y., & Zhou, Y. Y. (2016). The phosphorus release pathways and their mechanisms driven by organic carbon and nitrogen in sediments of eutrophic shallow lakes. *Science of the Total Environment*, *572*, 280–288. https://doi.org/10.1016/j.scitotenv.2016.07.221

Liu, R., Thomas, B. W., Shi, X., Zhang, X., Wang, Z., & Zhang, Y. (2021). Effects of ground cover management on improving water and soil conservation in tree crop systems: A meta-analysis. *Catena*, *199*(December 2020), 105085. https://doi.org/10.1016/j.catena.2020.105085

Lohani, S., Baffaut, C., Thompson, A. L., Aryal, N., Bingner, R. L., Bjorneberg, D. L., Bosch, D. D., Bryant, R. B., Buda, A., Dabney, S. M., Davis, A. R., Duriancik, L. F., James, D. E., King, K. W., Kleinman, P. J. A., Locke, M., McCarty, G. W., Pease, L. A., Reba, M. L., … Yasarer, L. M. W. (2020). Performance of the Soil Vulnerability Index with respect to slope, digital elevation model resolution, and hydrologic soil group. *Journal of Soil and Water Conservation*, *75*(1), 12–27. https://doi.org/10.2489/JSWC.75.1.12

Lü, C., He, J., Zuo, L., Vogt, R. D., Zhu, L., Zhou, B., Mohr, C. W., Guan, R., Wang, W., & Yan, D. (2016). Processes and their explanatory factors governing distribution of organic phosphorous pools in lake sediments. *Chemosphere*, *145*, 125–134. https://doi.org/10.1016/j.chemosphere.2015.11.038

Luczaj, J. A. (2011). Preliminary Geologic Map of the Buried Bedrock Surface, Brown County, Wisconsin (WOFR2011-02). *Wisconsin Geological and Natural History Survey Open-File Report 2011-02*, 1.

Luczaj, J. A. (2013). Geology of the Niagara Escarpment. *Geoscience Wisconsin*, *22*(September 2013).

Mabit, L., Benmansour, M., Abril, J. M., Walling, D. E., Meusburger, K., Iurian, A. R., Bernard, C., Tarján, S., Owens, P. N., Blake, W. H., & Alewell, C. (2014). Fallout 210Pb as a soil and sediment tracer in catchment sediment budget investigations: A review. *Earth-Science Reviews*, *138*, 335–351. https://doi.org/10.1016/j.earscirev.2014.06.007

Mann, M., Beer, J., Steinhilber, F., Abreu, J. A., Christl, M., & Kubik, P. W. (2011). Variations in

the depositional fluxes of cosmogenic beryllium on short time scales. *Atmospheric Environment*, *45*(17), 2836–2841. https://doi.org/10.1016/j.atmosenv.2011.03.005
Masarik, J., & Beer, J. (2009). An updated simulation of particle fluxes and cosmogenic nuclide production in the Earth's atmosphere. *Journal of Geophysical Research Atmospheres*, *114*(11), 1–9. https://doi.org/10.1029/2008JD010557
Massicotte, P. (2019). *{eemR}: {Tools} for {Pre}-{Processing} {Emission}-{Excitation}-{Matrix} ({EEM}) {Fluorescence} {Data}*. https://cran.r-project.org/package=eemR
McLaren, T. I., Smernik, R. J., McLaughlin, M. J., McBeath, T. M., Kirby, J. K., Simpson, R. J., Guppy, C. N., Doolette, A. L., & Richardson, A. E. (2015). Complex Forms of Soil Organic Phosphorus-A Major Component of Soil Phosphorus. *Environmental Science and Technology*, *49*(22), 13238–13245. https://doi.org/10.1021/acs.est.5b02948
Mendes, L. R. D. (2020). Edge-of-Field technologies for phosphorus retention from agricultural drainage discharge. *Applied Sciences (Switzerland)*, *10*(2). https://doi.org/10.3390/app10020634
Minneapolis/St. Paul Climate Data. (2022). https://www.dnr.state.mn.us/climate/twin_cities/listings.html
Minning, T., Lytle, D. A., Pham, M., & Kelty, K. (2015). Systematic evaluation of dissolved lead sorption losses to particulate syringe filter materials. *Environmental Monitoring and Assessment*, *187*(6). https://doi.org/10.1007/s10661-015-4610-7
Minshall, G. W., Thomas, S. A., Newbold, J. D., Monaghan, M. T., & Cushing, C. E. (2000). *Physical factors influencing fine organic particle transport and deposition in streams*. *19*(1), 1–16.
Mitsch, W. J., Zhang, L., Marois, D., & Song, K. (2015). Protecting the Florida Everglades wetlands with wetlands: Can stormwater phosphorus be reduced to oligotrophic conditions? *Ecological Engineering*, *80*, 8–19. https://doi.org/10.1016/j.ecoleng.2014.10.006
Mohan, M. P., D'Souza, R. S., Nayak, S. R., Kamath, S. S., Shetty, T., Kumara, K. S., Mayya, Y. S., & Karunakara, N. (2019). Influence of rainfall on atmospheric deposition fluxes of 7Be and 210Pb in Mangaluru (Mangalore) at the Southwest Coast of India. *Atmospheric Environment*, *202*(January), 281–295. https://doi.org/10.1016/j.atmosenv.2019.01.034
Moustafa, M. Z., White, J. R., Coghlan, C. C., & Reddy, K. R. (2012). Influence of hydropattern and vegetation on phosphorus reduction in a constructed wetland under high and low mass loading rates. *Ecological Engineering*, *42*, 134–145. https://doi.org/10.1016/j.ecoleng.2012.01.028
Multi-Resolution Land Characteristics Consortium, (U.S.). (2016). *National Land cover dataset (NLCD)*.
Myers, R., Weber, A., & Tellatin, S. (2019). Cover Crop Economics Opportunities to Improve Your Bottom Line in Row Crops. *SARE Technical Bulletin*, 1–24.
Naden, P. S. (2010). *The Fine-Sediment Cascade* (T. Burt & R. Allison (Eds.); pp. 271–306). John Wiley & Sons.
National Atmospheric Deposition Program (NRSP-3). (2022). NADP Program Office, Wisconsin State Laboratory of Hygiene.
Natural Resources Conservation Service. (2008a). *Rapid Watershed Assessment Lower Fox River Watershed* (Vol. 2600, Issue August). http://www.nrcs.usda.gov/Internet/FSE_DOCUMENTS/nrcs142p2_019949.pdf
Natural Resources Conservation Service. (2008b). *Rapid Watershed Assessment Wolf River Watershed* (Issue May).
Neitsch, S. I., Arnold, J. G., Kiniry, J. R., Srinivasan, R., & Williams, J. R. (2002). *Soil Water and Assessment Tool User's Manual*. https://swat.tamu.edu/media/1294/swatuserman.pdf
Newbold, J. D., Elwood, J. W., O'Neill, R. V., & Sheldon, A. . (1983). Phosphorus Dynamics in a Woodland Stream Ecosystem : A Study of Nutrient Spiralling. *Ecology*, *64*(5), 1249–1265.
Noller, J. S. (2000). *Lead-210 Geochronology*. *210*, 115–120.
Nonpoint Source Implementation Plan for the Plum and Kankapot Creek Watersheds. (2014). *Outagamie County Land Conservation Department*, 1–141.
Olsen, C. R. (1985). Atmospheric fluxes and marsh-soil inventories of 7Be and 210Pb. *Journal of Geophysical Research*, *90*(D6), 10487–10495. https://doi.org/10.1029/JD090iD06p10487
Ongley, E. (1996). Sediment Measurements. In J. Bartram & R. Ballance (Eds.), *Water Quality*

Monitoring - A Practical Guide to the Design and Implementation of Freshwater Quality Studies and Monitoring Programmes (pp. 1–15). United Nations Environment Programme and the World Health Organization. http://www.who.int/water_sanitation_health/resourcesquality/wqmchap13.pdf

Owens, P. N., Blake, W. H., Gaspar, L., Gateuille, D., Koiter, A. J., Lobb, D. A., Petticrew, E. L., Reiffarth, D. G., Smith, H. G., & Woodward, J. C. (2016). Fingerprinting and tracing the sources of soils and sediments: Earth and ocean science, geoarchaeological, forensic, and human health applications. *Earth-Science Reviews*, *162*, 1–23. https://doi.org/10.1016/j.earscirev.2016.08.012

Palmer-Felgate, E. J., Jarvie, H. P., Withers, P. J. A., Mortimer, R. J. G., & Krom, M. D. (2009). Stream-bed phosphorus in paired catchments with different agricultural land use intensity. *Agriculture, Ecosystems and Environment*, *134*(1–2), 53–66. https://doi.org/10.1016/j.agee.2009.05.014

Paludan, C., & Jensen, H. S. (1995). Sequential extraction of phosphorus in freshwater wetland and lake sediment: Significance of humic acids. *Wetlands*, *15*(4), 365–373. https://doi.org/10.1007/BF03160891

Papastefanou, C. (2009). Beryllium-7 aerosols in ambient air. *Aerosol and Air Quality Research*, *9*(2), 187–197. https://doi.org/10.4209/aaqr.2009.01.0004

Pawlowski, E. D., & Karwan, D. L. (2019). Assessment of lead and beryllium sorption to exposed stream channel sediment under varying freshwater channel conditions. *Journal of Soils and Sediments*, *19*(9), 3397–3410. https://doi.org/10.1007/s11368-019-02245-2

Pierzynski, G. M., McDowell, R. W., & Sims, J. T. (2005). Chemistry, Cycling, and Potential Movement of Inorganic Phosphorus in Soils. In J. T. Sims & A. N. Sharpley (Eds.), *Phosphorus: Agriculture and the envrionment* (Issue June, pp. 53–86). ASA, CSSA, and SSSA. https://doi.org/10.2134/agronmonogr46.c3

Pietro, K. C., & Ivanoff, D. (2015). Comparison of long-term phosphorus removal performance of two large-scale constructed wetlands in South Florida, U.S.A. *Ecological Engineering*, *79*, 143–157. https://doi.org/10.1016/j.ecoleng.2014.12.013

Poeplau, C., & Don, A. (2015). Carbon sequestration in agricultural soils via cultivation of cover crops - A meta-analysis. *Agriculture, Ecosystems and Environment*, *200*, 33–41. https://doi.org/10.1016/j.agee.2014.10.024

Ponce, V. M., & Hawkins, R. H. (1996). Runoff Curve Number: Has It Reached Maturity? In *Journal of Hydrologic Engineering* (Vol. 1, Issue 1, pp. 11–19). https://doi.org/10.1061/(asce)1084-0699(1996)1:1(11)

Porter, S. A., Tomer, M. D., James, D. E., & Boomer, K. M. B. (2016). *Agricultural Conservation Planning Framework ArcGIS® Toolbox User's Manual Version 2.2 Date of Release: 06/2017*. 82. http://northcentralwater.org/acpf/

Poulida, O., Dickerson, R. R., & Heymsfield, A. (1996). Stratosphere-troposphere exchange in a midlatitude mesoscale convective complex. *Journal of Geophysical Research*, *101*, 6823–6836.

Powers, S. M., Bruulsema, T. W., Burt, T. P., Chan, N. I., Elser, J. J., Haygarth, P. M., Howden, N. J. K., Jarvie, H. P., Lyu, Y., Peterson, H. M., Sharpley, A. N., Shen, J., Worrall, F., & Zhang, F. (2016). Long-term accumulation and transport of anthropogenic phosphorus in three river basins. *Nature Geoscience*, *9*(5), 353–356. https://doi.org/10.1038/ngeo2693

Powers, S. M., Johnson, R. A., & Stanley, E. H. (2012). Nutrient Retention and the Problem of Hydrologic Disconnection in Streams and Wetlands. *Ecosystems*, *15*(3), 435–449. https://doi.org/10.1007/s10021-012-9520-8

PRISM Climate Group. (2004). *No Title*. Oregon State University. http://prism.oregonstate.edu

Prosser, R. S., Hoekstra, P. F., Gene, S., Truman, C., White, M., & Hanson, M. L. (2020). A review of the effectiveness of vegetated buffers to mitigate pesticide and nutrient transport into surface waters from agricultural areas. *Journal of Environmental Management*, *261*(July 2019), 110210. https://doi.org/10.1016/j.jenvman.2020.110210

Provost, S., Hyatt, L., McLennan, R., Fix, S., & Al, E. (2001). *The State of the Upper Fox River Basin*.

Ramesh, R., Kalin, L., Hantush, M., & Chaudhary, A. (2021). A secondary assessment of sediment trapping effectiveness by vegetated buffers. *Ecological Engineering*,

159(November 2019), 106094. https://doi.org/10.1016/j.ecoleng.2020.106094
Reddy, K. R., Kadlec, R. H., Flaig, E., & Gale, P. M. (1999a). Phosphorus retention in streams and wetlands: A review. *Critical Reviews in Environmental Science and Technology*, *29*(1), 83–146. https://doi.org/10.1080/10643389991259182
Reddy, K. R., Kadlec, R. H., Flaig, E., & Gale, P. M. (1999b). Streams and Wetlands: A Review. *Critical Reviews in Environmental Science and Technology*, *29*(1), 83–146. https://doi.org/10.1080/10643389991259182
Reid, K., Schneider, K., & McConkey, B. (2018). Components of Phosphorus Loss From Agricultural Landscapes, and How to Incorporate Them Into Risk Assessment Tools. *Frontiers in Earth Science*, *6*(September), 1–15. https://doi.org/10.3389/feart.2018.00135
Revelli, R., & Ridolfi, L. (2003). Transport of reactive chemicals in sediment-laden streams. *Advances in Water Resources*, *26*(8), 815–831. https://doi.org/10.1016/S0309-1708(03)00077-0
Richards, R. P., Baker, D. B., & Crumrine, J. P. (2009). Improved water quality in Ohio tributaries to Lake Erie: A consequence of conservation practices. *Journal of Soil and Water Conservation*, *64*(3), 200–211. https://doi.org/10.2489/jswc.64.3.200
Richardson, A. E., & Simpson, R. J. (2011). Soil microorganisms mediating phosphorus availability. *Plant Physiology*, *156*(3), 989–996. https://doi.org/10.1104/pp.111.175448
Robinson, C. A., Ghaffarzadeh, M., & Cruse, R. M. (1996). Vegetative filter strip effects on sediment concentration in cropland runoff. *Journal of Soil and Water Conservation*, *51*(3), 227–230.
Rose, D. C., Sutherland, W. J., Amano, T., González-Varo, J. P., Robertson, R. J., Simmons, B. I., Wauchope, H. S., Kovacs, E., Durán, A. P., Vadrot, A. B. M., Wu, W., Dias, M. P., Di Fonzo, M. M. I., Ivory, S., Norris, L., Nunes, M. H., Nyumba, T. O., Steiner, N., Vickery, J., & Mukherjee, N. (2018). The major barriers to evidence-informed conservation policy and possible solutions. *Conservation Letters*, *11*(5), 1–12. https://doi.org/10.1111/conl.12564
Rose, L. A., & Karwan, D. L. (2021). Stormflow concentration–discharge dynamics of suspended sediment and dissolved phosphorus in an agricultural watershed. *Hydrological Processes*, *35*(12), 1–16. https://doi.org/10.1002/hyp.14455
Royer, T. V., David, M. B., & Gentry, L. E. (2006). Timing of riverine export of nitrate and phosphorus from agricultural watersheds in Illinois: Implications for reducing nutrient loading to the Mississippi River. *Environmental Science and Technology*, *40*(13), 4126–4131. https://doi.org/10.1021/es052573n
Ruban, V., López-Sánchez, J. F., Pardo, P., Rauret, G., Muntau, H., & Quevauviller, P. (2001). Development of a harmonised phosphorus extraction procedure and certification of a sediment reference material. *Journal of Environmental Monitoring*, *3*(1), 121–125. https://doi.org/10.1039/b005672n
Rubin, J. A., & Görres, J. H. (2021). Potential for mycorrhizae-assisted phytoremediation of phosphorus for improved water quality. *International Journal of Environmental Research and Public Health*, *18*(1), 1–24. https://doi.org/10.3390/ijerph18010007
Runkel, R. L. (1998). One-dimensional transport with inflow and storage (otis): a solute transport model for streams and rivers. In *Water-Resources Investigations Report 98-4018*.
Ryken, N., Al-Barri, B., Blake, W., Taylor, A., Tack, F., Bodé, S., Boeckx, P., & Verdoodt, A. (2018). Impact of soil hydrological properties on the 7Be depth distribution and the spatial variation of 7Be inventories across a small catchment. *Geoderma*, *318*(April 2017), 88–98. https://doi.org/10.1016/j.geoderma.2017.12.036
Saleh, A., Gallego, O., Osei, E., Lal, H., Gross, C., McKinney, S., & Cover, H. (2011). Nutrient Tracking Tool-a user-friendly tool for calculating nutrient reductions for water quality trading. *Journal of Soil and Water Conservation*, *66*(6), 400–410. https://doi.org/10.2489/jswc.66.6.400
Saleh, Ali, Gallego, O., & Osei, E. (2015). Evaluating nutrient tracking tool and simulated conservation practices. *Journal of Soil and Water Conservation*, *70*(5), 115–120. https://doi.org/10.2489/jswc.70.5.115A
Salemi, L. F., Groppo, J. D., Trevisan, R., Marcos de Moraes, J., de Paula Lima, W., & Martinelli, L. A. (2012). Riparian vegetation and water yield: A synthesis. *Journal of Hydrology*, *454–455*, 195–202. https://doi.org/10.1016/j.jhydrol.2012.05.061

Santy, K. L., Bougie, C., Lychwick, T., Nikolai, D., Rasman, T., Szymanski, S., Boronow, G., Mella, T., Garbisch, S., Woodbury, B., Young, J., Helmuth, L., Pike, J., O'Connor, K., Johnson, D., Chern, L., & Lindauer, A. (2001). *LOWER FOX RIVER BASIN INTEGRATED INTE GRATED MANAGEMENT PLAN*.

Schilling, K. E., & Jacobson, P. (2014). Effectiveness of natural riparian buffers to reduce subsurface nutrient losses to incised streams. *Catena*, *114*, 140–148. https://doi.org/10.1016/j.catena.2013.11.005

Schilling, K. E., Streeter, M. T., Vogelgesang, J., Jones, C. S., & Seeman, A. (2020). Subsurface nutrient export from a cropped field to an agricultural stream: Implications for targeting edge-of-field practices. *Agricultural Water Management*, *241*(January). https://doi.org/10.1016/j.agwat.2020.106339

Schulte, L. A., Niemi, J., Helmers, M. J., Liebman, M., Arbuckle, J. G., James, D. E., Kolka, R. K., O'Neal, M. E., Tomer, M. D., Tyndall, J. C., Asbjornsen, H., Drobney, P., Neal, J., Van Ryswyk, G., & Witte, C. (2017). Prairie strips improve biodiversity and the delivery of multiple ecosystem services from corn–soybean croplands. *Proceedings of the National Academy of Sciences of the United States of America*, *114*(42), 11247–11252. https://doi.org/10.1073/pnas.1620229114

Sebestyen, S. D., Lany, N. K., Roman, D. T., Burdick, J. M., Kyllander, R. L., Verry, E. S., & Kolka, R. K. (2021). Hydrological and meteorological data from research catchments at the Marcell Experimental Forest, Minnesota, USA. *Hydrological Processes*, *35*(3), 1–9. https://doi.org/10.1002/hyp.14092

Selman, M., Greenhalgh, S., Diaz, R., & Sugg, Z. (2008). Eutrophication and Hypoxia in Coastal Areas: A Global Assessment of the State of Knowledge. *Water Resources Institute*, *1*, 1–6.

Semertzidou, P., Piliposian, G. T., & Appleby, P. G. (2016). Atmospheric residence time of 210Pb determined from the activity ratios with its daughter radionuclides 210Bi and 210Po. *Journal of Environmental Radioactivity*, *160*, 42–53. https://doi.org/https://doi.org/10.1016/j.jenvrad.2016.04.019

Shapiro, M. A. (1980). Turbulent Mixing within Tropopause Folds as a Mechanism for the Exchange of Chemical Constituents between the Stratosphere and Troposphere. In *Journal of the Atmospheric Sciences* (Vol. 37, Issue 5, pp. 994–1004). https://doi.org/10.1175/1520-0469(1980)037<0994:tmwtfa>2.0.co;2

Sharpley, A. N., Kleinman, P. J. A., Jordan, P., Bergström, L., & Allen, A. L. (2009). Evaluating the success of phosphorus management from field to watershed. *Journal of Environmental Quality*, *38*(5), 1981–1988. https://doi.org/10.2134/jeq2008.0056

Sharpley, A., Richards, P., Herron, S., & Baker, D. (2012). Case study comparison between litigated and voluntary nutrient management strategies. *Journal of Soil and Water Conservation*, *67*(5), 442–450. https://doi.org/10.2489/jswc.67.5.442

Sharpley, Andrew, Jarvie, H., Flaten, D., & Kleinman, P. (2018). Celebrating the 350th anniversary of phosphorus discovery: A conundrum of deficiency and excess. *Journal of Environmental Quality*, *47*(4), 774–777. https://doi.org/10.2134/jeq2018.05.0170

Sharpley, Andrew, Jarvie, H. P., Buda, A., May, L., Spears, B., & Kleinman, P. (2013). Phosphorus legacy: Overcoming the effects of past management practices to mitigate future water quality impairment. *Journal of Environmental Quality*, *42*(5), 1308–1326. https://doi.org/10.2134/jeq2013.03.0098

Shore, M., Murphy, S., Mellander, P. E., Shortle, G., Melland, A. R., Crockford, L., O'Flaherty, V., Williams, L., Morgan, G., & Jordan, P. (2017). Influence of stormflow and baseflow phosphorus pressures on stream ecology in agricultural catchments. *Science of the Total Environment*, *590–591*, 469–483. https://doi.org/10.1016/j.scitotenv.2017.02.100

Simpson, Z. P., McDowell, R. W., Condron, L. M., McDaniel, M. D., Jarvie, H. P., & Abell, J. M. (2021). Sediment phosphorus buffering in streams at baseflow: A meta-analysis. *Journal of Environmental Quality*, *50*(2), 287–311. https://doi.org/10.1002/jeq2.20202

Soil Survey Staff. (2020). *Web Soil Survey*. Natural Resources Conservation Service, United States Department of Agriculture. https://websoilsurvey.sc.egov.usda.gov/

Sprenger, M., Wernli, H., & Bourqui, M. (2007). Stratosphere-troposphere exchange and its relation to potential vorticity streamers and cutoffs near the extratropical tropopause. *Journal of the Atmospheric Sciences*, *64*(5), 1587–1602. https://doi.org/10.1175/JAS3911.1

Stoddard, J. L., Van Sickle, J., Herlihy, A. T., Brahney, J., Paulsen, S., Peck, D. V., Mitchell, R., & Pollard, A. I. (2016). Continental-Scale Increase in Lake and Stream Phosphorus: Are Oligotrophic Systems Disappearing in the United States? *Environmental Science and Technology*, *50*(7), 3409–3415. https://doi.org/10.1021/acs.est.5b05950

Stohl, A., Bonasoni, P., Cristofanelli, P., Collins, W., Feichter, J., Frank, A., Forster, C., Gerasopoulos, E., Gäggeler, H., James, P., Kentarchos, T., Kromp-Kolb, H., Krüger, B., Land, C., Meloen, J., Papayannis, A., Priller, A., Seibert, P., Sprenger, M., … Zerefos, C. (2003). Stratosphere-troposphere exchange: A review, and what we have learned from STACCATO. *Journal of Geophysical Research Atmospheres*, *108*(12). https://doi.org/10.1029/2002jd002490

Stutter, M. I., Langan, S. J., & Lumsdon, D. G. (2009). Vegetated buffer strips can lead to increased release of phosphorus to waters: A biogeochemical assessment of the mechanisms. *Environmental Science and Technology*, *43*(6), 1858–1863. https://doi.org/10.1021/es8030193

Taylor, A., Blake, W. H., Couldrick, L., & Keith-Roach, M. J. (2012). Sorption behaviour of beryllium-7 and implications for its use as a sediment tracer. *Geoderma*, *187–188*, 16–23. https://doi.org/10.1016/j.geoderma.2012.04.013

Taylor, A., Blake, W. H., Smith, H. G., Mabit, L., & Keith-Roach, M. J. (2013). Assumptions and challenges in the use of fallout beryllium-7 as a soil and sediment tracer in river basins. *Earth-Science Reviews*, *126*, 85–95. https://doi.org/10.1016/j.earscirev.2013.08.002

Taylor, A., Keith-Roach, M. J., Iurian, A. R., Mabit, L., & Blake, W. H. (2016). Temporal variability of beryllium-7 fallout in southwest UK. *Journal of Environmental Radioactivity*, *160*, 80–86. https://doi.org/10.1016/j.jenvrad.2016.04.025

Texas A&M AgriLife Research. (2017). *APEX - Agricultural Policy/Environmental eXtender Model*. Texas A&M AgriLife Research.

Thalmann, L. E. (2021). *Phosphorus and nitrogen losses in runoff from fields with and without tile drainage* [University of Vermont]. https://scholarworks.uvm.edu/graddis/1355

Thompson, S. E., Basu, N. B., Lascurain, J., Aubeneau, A., & Rao, P. S. C. (2011). Relative dominance of hydrologic versus biogeochemical factors on solute export across impact gradients. *Water Resources Research*, *47*(7), 1–20. https://doi.org/10.1029/2010WR009605

Tilman, D., Balzer, C., Hill, J., & Befort, B. L. (2011). Global food demand and the sustainable intensification of agriculture. *Proceedings of the National Academy of Sciences of the United States of America*, *108*(50), 20260–20264. https://doi.org/10.1073/pnas.1116437108

Tilman, D., Cassman, K. G., Matson, P. A., Naylor, R., & Polasky, S. (2002). Agricultural sustainability and intensive production practices. *Nature*, *418*(August), 671–677.

Tomer, M. D., & Locke, M. A. (2011). The challenge of documenting water quality benefits of conservation practices: A review of USDA-ARS's conservation effects assessment project watershed studies. *Water Science and Technology*, *64*(1), 300–310. https://doi.org/10.2166/wst.2011.555

Tye, A. M., Rawlins, B. G., Rushton, J. C., & Price, R. (2016). Understanding the controls on sediment-P interactions and dynamics along a non-tidal river system in a rural-urban catchment: The River Nene. *Applied Geochemistry*, *66*, 219–233. https://doi.org/10.1016/j.apgeochem.2015.12.014

Tye, A. M., Young, S., Crout, N. M. J., Zhang, H., Preston, S., Zhao, F. J., & McGrath, S. P. (2004). Speciation and solubility of Cu, Ni and Pb in contaminated soils. *European Journal of Soil Science*, *55*(3), 579–590. https://doi.org/10.1111/j.1365-2389.2004.00627.x

U.S. Environmental Protection Agency. (1978). Phosphorous, all Forms (colorimetric, ascorbic acid, two reagent). *Method 365.3*, *National P*, 3–7. https://doi.org/10.1159/000330408

U.S. Geological Survey. (2016a). *National Water Information System data available on the World Wide Web (USGS Water Data for the Nation)*. https://waterdata.usgs.gov/nwis/uv?site_no=040851378

U.S. Geological Survey. (2016b). *National Water Information System data available on the World Wide Web (USGS Water Data for the Nation)*. https://waterdata.usgs.gov/wi/nwis/uv/?site_no=04084911&PARAmeter_cd=00065,00060

U.S. Geological Survey. (2018). *USGS NED 1/3 arc-second n40w098 1 x 1 degree IMG*. U.S. Geological Survey.

US Environmental Protection Agency. (2018). *Nutrient and Sediment Estimation Tools for Watershed Protection. Report EPA 841-K-18-002.*
USDA ARS Grassland Soil and Water Research, L., & Texas A&M AgriLife Research. (2018). *SWAT- Soil and Water Assessment Tool*. https://swat.tamu.edu/
Vanrobaeys, J. A., Owens, P. N., Lobb, D. A., Kieta, K. A., & Campbell, J. M. (2019). Seasonal Efficacy of Vegetated Filter Strips for Phosphorus Reduction in Surface Runoff. *Journal of Environmental Quality*, *48*(4), 880–888. https://doi.org/10.2134/jeq2018.12.0452
Verhoff, F. H., Melfi, D. A., & Yaksich, S. M. (1979). Storm travel distance calculations for total phosphorus and suspended materials in rivers. *Water Resources Research*, *15*(6), 1354–1360. https://doi.org/10.1029/WR015i006p01354
Wagner, B. J., & Harvey, J. W. (1997). Experimental design for estimating parameters of rate-limited mass transfer: Analysis of stream tracer studies. *Water Resources Research*, *33*(7), 1731–1741. https://doi.org/10.1029/97WR01067
Walling, D. E. (2005). Tracing suspended sediment sources in catchments and river systems. *Science of the Total Environment*, *344*(1-3 SPEC. ISS.), 159–184. https://doi.org/10.1016/j.scitotenv.2005.02.011
Walling, D. E. (2013). The evolution of sediment source fingerprinting investigations in fluvial systems. *Journal of Soils and Sediments*, *13*(10), 1658–1675. https://doi.org/10.1007/s11368-013-0767-2
Walsh, J. C., Dicks, L. V., Raymond, C. M., & Sutherland, W. J. (2019). A typology of barriers and enablers of scientific evidence use in conservation practice. *Journal of Environmental Management*, *250*(August), 109481. https://doi.org/10.1016/j.jenvman.2019.109481
Wang, C., Zhang, Y., Li, H., & Morrison, R. J. (2013). Sequential extraction procedures for the determination of phosphorus forms in sediment. *Limnology*, *14*(2), 147–157. https://doi.org/10.1007/s10201-012-0397-1
Wang, X., Kannan, N., Santhi, C., Potter, S. R., Williams, J. R., & Arnold, J. G. (2011). Integrating APEX output for cultivated cropland with SWAT simulation for regional modeling. *Transactions of the ASABE*, *54*(4), 1281–1298.
Ward, A. S., Kelleher, C. A., Mason, S. J. K., Wagener, T., McIntyre, N., McGlynn, B., Runkel, R. L., & Payn, R. A. (2017). A software tool to assess uncertainty in transient-storage model parameters using Monte Carlo simulations. *Freshwater Science*, *36*(1), 195–217. https://doi.org/10.1086/690444
Williams, M. R., King, K. W., Baker, D. B., Johnson, L. T., Smith, D. R., & Fausey, N. R. (2016). Hydrologic and biogeochemical controls on phosphorus export from Western Lake Erie tributaries. *Journal of Great Lakes Research*, *42*(6), 1403–1411. https://doi.org/10.1016/j.jglr.2016.09.009
Williams, M. R., King, K. W., Ford, W., Buda, A. R., & Kennedy, C. D. (2016). Effect of tillage on macropore flow and phosphorus transport to tile drains. *Water Resources Research*, *52*, 2868–2882. https://doi.org/10.1002/2015WR017650
Winston, R. J., Dorsey, J. D., & Hunt, W. F. (2016). Quantifying volume reduction and peak flow mitigation for three bioretention cells in clay soils in northeast Ohio. *Science of the Total Environment*, *553*, 83–95. https://doi.org/10.1016/j.scitotenv.2016.02.081
Withers, P. J. A., & Jarvie, H. P. (2008). Delivery and cycling of phosphorus in rivers: A review. *Science of the Total Environment*, *400*(1–3), 379–395. https://doi.org/10.1016/j.scitotenv.2008.08.002
Wood, P. J., & Armitage, P. D. (1997). Biological effects of fine sediment in the lotic environment. *Environmental Management*, *21*(2), 203–217. https://doi.org/10.1007/s002679900019
Yang, W., Guo, L., Chuang, C. Y., Santschi, P. H., Schumann, D., & Ayranov, M. (2015). Influence of organic matter on the adsorption of 210Pb, 210Po and 7Be and their fractionation on nanoparticles in seawater. *Earth and Planetary Science Letters*, *423*, 193–201. https://doi.org/10.1016/j.epsl.2015.05.007
Zhang, T., Wang, Y., Tan, C. S., & Welacky, T. (2020). An 11-Year Agronomic, Economic, and Phosphorus Loss Potential Evaluation of Legacy Phosphorus Utilization in a Clay Loam Soil of the Lake Erie Basin. *Frontiers in Earth Science*, *8*(May), 1–8. https://doi.org/10.3389/feart.2020.00115
Zhang, X. C., Friedrich, J. M., Nearing, M. A., & Norton, L. D. (2001). Potential use of rare earth

oxides as tracers for soil erosion and aggregation studies. *Soil Science Society of America Journal*, *65*(5), 1508–1515. https://doi.org/10.2136/sssaj2001.6551508x

Zhou, X., Helmers, M. J., Asbjornsen, H., Kolka, R., Tomer, M. D., & Cruse, R. M. (2014). Nutrient removal by prairie filter strips in agricultural landscapes. *Journal of Soil and Water Conservation*, *69*(1), 54–64. https://doi.org/10.2489/jswc.69.1.54

Zhu, X., Liu, W., Chen, J., Bruijnzeel, L. A., Mao, Z., Yang, X., Cardinael, R., Meng, F. R., Sidle, R. C., Seitz, S., Nair, V. D., Nanko, K., Zou, X., Chen, C., & Jiang, X. J. (2020). Reductions in water, soil and nutrient losses and pesticide pollution in agroforestry practices: a review of evidence and processes. In *Plant and Soil* (Vol. 453, Issues 1–2). Plant and Soil. https://doi.org/10.1007/s11104-019-04377-3

Zierl, B., & Wirth, V. (1997). The influence of radiation on tropopause behavior and stratosphere-troposphere exchange in an upper tropospheric anticyclone. *Journal of Geophysical Research*, *102*, 23,883-23,894.